DEVELOPMENT OF A MATLAB BASED SOFTWARE PACKAGE
FOR IONOSPHERE MODELING

A THESIS SUBMITTED TO
THE GRADUATE SCHOOL OF NATURAL AND APPLIED SCIENCES
OF
THE MIDDLE EAST TECHNICAL UNIVERSITY

BY

METİN NOHUTCU

IN PARTIAL FULFILLMENT OF THE REQUIREMENTS
FOR
THE DEGREE OF DOCTOR OF PHILOSOPHY
IN
CIVIL ENGINEERING

SEPTEMBER 2009

Approval of the thesis:

**DEVELOPMENT OF A MATLAB BASED SOFTWARE PACKAGE
FOR IONOSPHERE MODELING**

submitted by **METİN NOHUTCU** in partial fulfillment of the requirements for the degree of **Doctor of Philosophy in Civil Engineering Department, Middle East Technical University** by,

Prof. Dr. Canan Özgen   _____
Dean, Graduate School of **Natural and Applied Sciences**

Prof. Dr. Güney Özcebe   _____
Head of Department, **Civil Engineering**

Assoc. Prof. Dr. Mahmut Onur Karslıoğlu   _____
Supervisor, **Civil Engineering Dept., METU**

Examining Committee Members:

Prof. Dr. Gülbin Dural   _____
Electrical and Electronics Engineering Dept., METU

Assoc. Prof. Dr. Mahmut Onur Karslıoğlu   _____
Civil Engineering Dept., METU

Assoc. Prof. Dr. İsmail Yücel   _____
Civil Engineering Dept., METU

Assoc. Prof. Dr. Mehmet Lütfi Süzen   _____
Geological Engineering Dept., METU

Assoc. Prof. Dr. Bahadır Aktuğ   _____
General Command of Mapping

                              Date: 23 / 09 / 2009

I hereby declare that all information in this document has been obtained and presented in accordance with academic rules and ethical conduct. I also declare that, as required by these rules and conduct, I have fully cited and referenced all material and results that are not original to this work.

Name, Last name: Metin Nohutcu

Signature   :

ABSTRACT

DEVELOPMENT OF A MATLAB BASED SOFTWARE PACKAGE FOR IONOSPHERE MODELING

Nohutcu, Metin

Ph. D., Department of Civil Engineering

Supervisor: Assoc. Prof. Dr. Mahmut Onur Karslıoğlu

September 2009, 115 Pages

Modeling of the ionosphere has been a highly interesting subject within the scientific community due to its effects on the propagation of electromagnetic waves. The development of the Global Positioning System (GPS) and creation of extensive ground-based GPS networks started a new period in observation of the ionosphere, which resulted in several studies on GPS-based modeling of the ionosphere. However, software studies on the subject that are open to the scientific community have not progressed in a similar manner and the options for the research community to reach ionospheric modeling results are still limited. Being aware of this need, a new MATLAB® based ionosphere modeling software, i.e. TECmapper is developed within the study. The software uses three different algorithms for the modeling of the Vertical Total Electron Content (VTEC) of the ionosphere, namely, 2D B-spline, 3D B-spline and spherical harmonic models. The study includes modifications for the original forms of the B-spline and the spherical harmonic approaches. In order to decrease the effect of outliers in the

data a robust regression algorithm is utilized as an alternative to the least squares estimation. Besides, two regularization methods are employed to stabilize the ill-conditioned problems in parameter estimation stage. The software and models are tested on a real data set from ground-based GPS receivers over Turkey. Results indicate that the B-spline models are more successful for the local or regional modeling of the VTEC. However, spherical harmonics should be preferred for global applications since the B-spline approach is based on Euclidean theory.

Keywords: Ionosphere Modeling, GPS, B-splines, Spherical Harmonics, MATLAB

ÖZ

İYONOSFER MODELLEMESİ İÇİN MATLAB TABANLI BİR YAZILIM PAKETİNİN GELİŞTİRİLMESİ

Nohutcu, Metin

Doktora, İnşaat Mühendisliği Bölümü

Tez Yöneticisi: Doç. Dr. Mahmut Onur Karslıoğlu

Eylül 2009, 115 Sayfa

İyonosfer modellemesi, iyonosferin elektromanyetik dalgaların yayılımı üzerindeki etkileri nedeniyle bilim camiasında fazlaca ilgi çeken bir konu olmuştur. Global Konumlama Sistemi'nin (GPS) geliştirilmesi ve yaygın yersel GPS ağlarının kurulması iyonosferin gözlenmesinde yeni bir dönem başlatmış ve bu da iyonosferin GPS-bazlı modellenmesi konusunda birçok çalışma ile sonuçlanmıştır. Ancak, konu ile ilgili ve bilim camiasına açık yazılım çalışmaları benzer bir çizgi izlememiştir ve araştırmacıların iyonosfer modellemesi sonuçlarına erişimi için seçenekler hala kısıtlıdır. Bu gereksinimin farkında olarak, bu çalışmada MATLAB® tabanlı ve yeni bir iyonosfer modelleme yazılımı olan TECmapper geliştirilmiştir. Yazılım iyonosferin Dik Toplam Elektron İçeriği'nin (VTEC) modellenmesi için 2D B-spline, 3D B-spline ve küresel harmonik modelleri olmak üzere üç ayrı algoritma kullanmaktadır. Çalışmada B-spline ve küresel

harmonik yaklaşımlarının orijinal hallerine çeşitli değişiklikler getirilmiştir. Verideki kaba hataların etkilerini azaltmak için en küçük kareler yöntemine alternatif olarak bir sağlam regresyon algoritmasına yer verilmiştir. Ayrıca, parametre kestirimi aşamasında kötü-durumlu problemlerin stabilize edilmesi için iki ayrı düzenleme (regülarizasyon) metodu kullanılmıştır. Yazılım ve modeller Türkiye üzerinden toplanan gerçek yersel GPS verileri ile test edilmiştir. Sonuçlar lokal ve bölgesel VTEC modellemelerinde B-spline modellerinin daha başarılı olduğunu göstermektedir. Ancak, B-spline yaklaşımı Öklid teorisine dayandığı için global uygulamalarda küresel harmonikler tercih edilmelidir.

Anahtar Kelimeler: İyonosfer Modellemesi, GPS, B-Spline, Küresel Harmonikler, MATLAB

To my daughter, *Beyza*

For my inattentive period towards her due to this tiring study

ACKNOWLEDGMENTS

TABLE OF CONTENTS

LIST OF TABLES

TABLES

LIST OF FIGURES

FIGURES

CHAPTER 1

INTRODUCTION

1.1 Background and Motivation

The ionosphere is that region of the upper atmosphere, starting at height of about 50 km and extending to heights 1000 km and more, where the free electron density affects the propagation of radio frequency electromagnetic waves. Free electrons are mainly produced by ionizing radiation which primarily depends on solar ultraviolet and X-ray emissions (Langrey, 1998). The effect of ionosphere on radio wave propagation interests various study areas including space-based observation systems as well as communication systems and space weather studies (Liu and Gao, 2004). For example, the radio channel selection for HF (High Frequency) communication must consider the ionospheric condition (Zeng and Zhang, 1999); single frequency altimetry measurements should be corrected for ionospheric delays which may reach to 20 cm or above (Leigh et al., 1988; Schreiner et al., 1997; Komjathy and Born, 1999); possible mitigation techniques must be investigated for the adverse effects of the ionosphere on synthetic aperture radar (SAR) imaging, such as image shift in the range, and degradations of the range resolution, azimuthal resolution, and/or the resolution in height, which will distort the SAR image (Xu et al., 2004); and the massive solar flares can cause ionospheric disruptions which can interfere with or even destroy communication systems, Earth satellites and power grids on the Earth (Brunini et al., 2004). Global Navigation Satellite Systems (GNSS), such as the Global Positioning System

(GPS), are also severely affected by the ionosphere, which is a dispersive medium for GNSS signals between the satellites and the receivers. The largest error source for the GPS is due to the ionosphere after selective availability (SA) was turned off on May 1, 2000 (Kunches and Klobuchar, 2001). The delay in the received signal that is created by the ionosphere can range from several meters to more than one hundred meters (Parkinson, 1994).

The widespread effect of the ionosphere on various areas made ionosphere modeling a popular subject starting with the early 1970s. Theoretical, semi-empirical or empirical models such as the Bent ionospheric model (Llewellyn and Bent, 1973), Raytrace, Ionospheric Bent, Gallagher (RIBG; Reilly, 1993), the Parameterized Ionospheric Model (PIM; Daniel et al., 1995), the NeQuick Model (Hochegger et al., 2000) or the International Reference Ionosphere (IRI; Bilitza, 2001) are well-known global ionosphere models used as referent in many ionospheric researches. They produce ionospheric information for any location and any time without nearby measurements but they only provide monthly averages of ionosphere behavior for magnetically quite conditions. However, electron content of the ionosphere is highly variable that its day-to-day variability can reach up to 20 to 25% root-mean-square (RMS) in a month. (Doherty et al., 1999; Klobuchar and Kunches, 2000).

Since its full operation in 1993, GPS applications have rapidly expanded far beyond its initial purpose which was primarily for military applications (Parkinson, 1994). The development of the GPS and creation of extensive ground-based GPS networks that provide worldwide data availability through the internet opened up a new era in remote sensing of the ionosphere (Afraimovich et al., 2002). Dual-frequency GPS receivers can be used to determine the number of electrons in the ionosphere in a column of 1 m^2 cross-section and extending along the ray-path of the signal between the satellite and the receiver, which is called the Slant Total Electron Content (STEC). STEC data obtained from accurate GPS observations resulted in numerous GPS-based ionosphere modeling studies. A

comprehensive description of GPS applications on ionospheric research can be found in Manucci et al. (1999).

GPS-based ionospheric models can be spatially classified as 3-dimensional (3D) and 2-dimensional (2D). In 3D studies, STEC measurements are inverted into electron density distribution by use of tomographic approaches, depending on latitude, longitude and height. Although the ground-based GPS receivers provide relatively accurate and low-cost STEC, these data do not supply good vertical resolution for ionospheric tomography as they scan the ionosphere by vertical or near-vertical paths (Kleusberg, 1998; García-Fernández et al., 2003). In order to overcome the low sensitivity of ground-based GPS measurements to the vertical structure of the ionosphere, additional data sources, such as ionosondes, satellite altimetry or GPS receivers on Low-Earth-Orbiting (LEO) satellites was considered in several 3D studies (Rius et al., 1997; Meza, 1999; Hernández-Pajares et al., 1999; García-Fernández et al., 2003; Stolle et al., 2003; Schmidt et al., 2007b, Zeilhofer, 2008). However, as these additional sources have, spatially or temporarily, limited coverage, they can be applied only where or when available.

Owing to the problems in 3D modeling that are mentioned in the previous paragraph, majority of the GPS-based studies headed towards 2D modeling. Works proposed by Wild (1994), Wilson et al. (1995), Brunini (1998), Gao et al. (2002), Wielgosz et al. (2003), Mautz et al. (2005) and Schmidt (2007) are only a few of them. In 2D approach the ionosphere is often represented by a spherical layer of infinitesimal thickness in which all the electrons are concentrated. The height of this idealized layer approximately corresponds to the altitude of the maximum electron density and it is usually set to values between 350 and 450 kilometers (Wild, 1994; Schaer, 1999). Accordingly, STEC is transformed into the Vertical Total Electron Content (VTEC), which is spatially a two-dimensional function depending on longitude and latitude.

The most concrete and continuous results on GPS-based VTEC modeling are produced by the analysis centers of the International GNSS Service (IGS). The IGS Working Group on Ionosphere was created in 1998 (Feltens and Schaer, 1998). Since then, four analysis centers, namely CODE (Center for Orbit Determination in Europe), ESA (European Space Agency), JPL (Jet Propulsion Laboratory) and UPC (Technical University of Catalonia), have been producing Global Ionosphere Maps (GIMs) in IONEX format (IONosphere map Exchange format) with a resolution of 2 hr, 5º and 2.5º in time, longitude and latitude respectively (Hernández-Pajares et al., 2009). Corresponding details of their modeling techniques can be seen in Schaer (1999), Feltens (1998), Mannucci et al. (1998) and Hernández-Pajares et al. (1999), respectively. Although IGS supports the scientific community with quality GPS products, the resolution of GIMs might not be sufficient to reproduce local, short-lasting processes in the ionosphere (Wielgosz, 2003).

The main difficulty for the practical use of the GPS-based models mentioned is that in general they are not supported with related software accessible to scientific community. Thus, a researcher who wants to apply these models to ground-based GPS data should need to prepare the software codes required. However, this task is not an easy one as it is required to include related units to process the GPS data in order to extract ionospheric information and to accomplish parameter estimation etc. in the software, which demands heavy work.

An exception to the above state is the Bernese GPS Software which was developed by Astronomical Institute of University of Bern (AIUB). The Bernese GPS Software is a highly sophisticated tool which has wide application areas including ionosphere modeling (Dach et al., 2007). Considerable price of the software besides its complexity should be mentioned here. The ionosphere modeling tasks of the CODE analysis center are accomplished by the Bernese Software which uses spherical harmonic expansion to represent VTEC globally or regionally (Schaer et al., 1996).

Spherical harmonics is the most widely used method in GPS-based ionospheric modeling. Spherical harmonics can be effectively used to represent the target function as long as the modeled area covers the whole sphere and the data is distributed regularly. However, the drawbacks of this method for regional applications or data of heterogeneous density have been widely discussed. (Chambodut et al., 2005; Mautz et al., 2005; Schmidt et al., 2007a).

Considering the above information, the main alternatives to acquire knowledge about the ionospheric electron content can be listed as follows:

- One of the state-of-the-art models, such as IRI, can be employed to produce electron density at any location and time, but enduring the low accuracy,

- IGS GIMs can be utilized as source of VTEC data with their low resolution both spatially and temporarily,

- The Bernese GPS Software can be used to process GPS data with spherical harmonics. However, the price and complexity of the software must be taken into account.

This study aims to add a new and powerful alternative to the above list.

1.2 Objectives of the Study

The effects of the ionosphere on the propagation of radio frequency electromagnetic waves concerns variety of study areas. GPS has become an important and widely-used tool to acquire ionospheric information especially in the last fifteen years which resulted in several studies on GPS-based modeling of the ionosphere. However, software studies on the subject have not progressed in a similar manner and the options for the research community to reach ionospheric modeling results are still limited.

5

The main objective of this study is to develop a user-friendly software package to model the VTEC of the ionosphere by processing ground-based GPS observations. The software should have both regional and global modeling abilities. Thus, selection of the appropriate model(s) and, if required, offering modifications and/or improvements for it (them) are also in the scope of the study.

Another objective of the study is to investigate the performance of the software to be developed on real (not simulated) ground-based GPS observations.

1.3 Overview of the Study

The software, which is developed and named as TECmapper is coded in MATLAB$^®$ environment. Its interactive environment for programming and debugging, language flexibility, rich set of graphing capabilities and graphical user interface development environment makes MATLAB a well-suited tool for this study. Capabilities of TECmapper can be listed as:

- Processing ground-based GPS observations to extract ionospheric data,

- Saving STEC and VTEC data in a text file for each observation file,

- Modeling VTEC by three methods in regional or global scales,

- Option to use a robust regression algorithm for parameter estimation to decrease the effect of outliers,

- Carrying out regularization processes for ill-conditioned systems,

- Generating 2D VTEC maps for specified epochs,

- Option to save VTEC values at user specified grid points and differential code bias values (DCBs) for the receivers in text files,

- Generating VTEC maps and saving VTEC values at user specified grid points from ionosphere models which are produced by the Bernese GPS Software, including the Global Ionosphere Models of CODE.

The only external data necessary for the software, besides GPS observation files, are precise orbit files and DCB values for the GPS satellites, which are freely available by IGS analysis centers through the internet with high accuracy.

One of the most important steps for the theory of an ionosphere modeling software is the selection of the appropriate models. For global modeling tasks spherical harmonics are well-suited methods with their global support. They form an orthonormal basis and have been widely used by many disciplines and studies including the gravity field and the magnetic field modeling of the Earth as well as the ionosphere modeling. However, this method has drawbacks for regional applications and irregular data distribution. Advantages and disadvantages of spherical harmonics modeling are described in detail by Chambodut et al. (2005). In order to represent the variations in the ionosphere in local or regional scales B-splines are suitable tools with respect to their compact support. They have been frequently utilized as basis functions due to their properties concerning continuity, smoothness and computational efficiency (Fok and Ramsay, 2006).

The fundamentals of the first model used in this study are presented by Schmidt (2007). Schmidt proposed to split the VTEC or the electron density of the ionosphere into a reference part, which can be computed from a given model like IRI, and an unknown correction term to be modeled by a series expansion in terms of B-spline base functions in an Earth-fixed reference frame. The theory of Schmidt was later used by Schmidt et al. (2007b), Schmidt et al. (2008), Zeilhofer (2008), Nohutcu et al. (2008) and Zeilhofer et al. (2009) for different dimensions, application regions and data sources.

In this study, two main modifications are implemented for B-spline model of Schmidt. Firstly, instead of using a given model like IRI, the reference part of the model is computed with the low-level solutions of the B-spline model. This prevents the software to be dependent on the results of another model, and the reference part will probably be closer to the final solution due to the accuracy levels of the models like IRI, as described before. Secondly, B-spline model is adapted to be used in a Sun-fixed reference frame for the first time. Consequently, two B-spline based models are made available for the software: a 3D model in an Earth-fixed frame depending on geodetic latitude, geodetic longitude and time, and a 2D model in a Sun-fixed frame depending on geodetic latitude and Sun-fixed longitude.

Since the B-spline approach is based on Euclidean theory, its implementation is restricted to local and regional areas. In order to expand the capabilities of the software to global scale, an additional model which is based on spherical harmonics is added for VTEC representation as described by Schaer et al. (1995) or Schaer (1999). Spherical harmonics are widely-used to represent scalar or vector fields in many areas including the ionosphere modeling. Modifications are also proposed and implemented in the study for spherical harmonic representation. VTEC is split into reference and correction terms and reference part is computed by low degree and order of spherical harmonic functions, as proposed in the B-spline approach.

A robust regression algorithm, namely Iteratively Re-weighted Least Squares (IRLS) with a bi-square weighting function, is given place in the software as an alternative to least squares estimation for the calculation of the unknown model coefficients in order to reduce the effects of outliers. Two alternative methods, i.e. Tikhonov and LSQR, are also included in parameter estimation stage to regularize the ill-conditioned systems. For the selection of the regularization parameter for Tikhonov's method, L-curve and generalizes cross validation (GCV) techniques

are employed in the software. Note that MATLAB codes of Hansen (1994) are utilized extensively for coding LSQR, L-curve and GCV methods.

1.4 Thesis Outline:

This thesis consists of 7 chapters. Background and motivation, objectives and an overview for the study are given in Chapter 1.

Brief overviews for the ionosphere and the GPS are provided in Chapter 2 and Chapter 3, respectively. Note that both subjects are very extensive but only the brief theory related to the study are presented in these chapters.

The main theoretical background for the software is presented in Chapter 4, while the main functions and graphical user interface of it are described in Chapter 5.

Chapter 6 is the application part of the study where the performances of the software and the models are tested on real ground-based GPS observations over Turkey.

The thesis is concluded with Chapter 7 which contains summary, discussion and potential future works for the study.

CHAPTER 2

THE IONOSPHERE

2.1 Structure of the Ionosphere

The ionosphere is one of the several layers of the Earth's atmosphere. There are not clearly defined boundaries for this plasma. However it is generally accepted that ionosphere begins at approximately 50 km from the Earth surface, after the neutral atmosphere layer, and extends to 1000 km or more where the protonosphere starts. The ultraviolet and X radiation emitted by the Sun are the main reasons for the ionization of several molecular species, the most important of which is the atomic oxygen (O, ionized to O^+) (García-Fernández, 2004).

The ionosphere's vertical structure is generally considered to be divided into four layers as D, E, F1 and F2 (Fig. 2.1). D layer lies between about 50 km and 90 km. Ions in this layer are mainly produced by the X-ray radiation. Due to the recombination of ions and electrons, this region is not present at night. E layer ranges in height from 90 km to 150 km above the Earth's surface with lower electron density than F1 and F2 layers. This region has irregular structure at high latitudes. The highest region of the ionosphere is divided into F1 and F2 sub-layers. F1 layer also principally vanishes at night. F2 layer is the densest part of the ionosphere and has the highest electron density at approximately 350 km in altitude. This height of the peak of the electron density highly depends on the diurnal and seasonal motion of the Earth and the solar cycle (El-Gizawy, 2003).
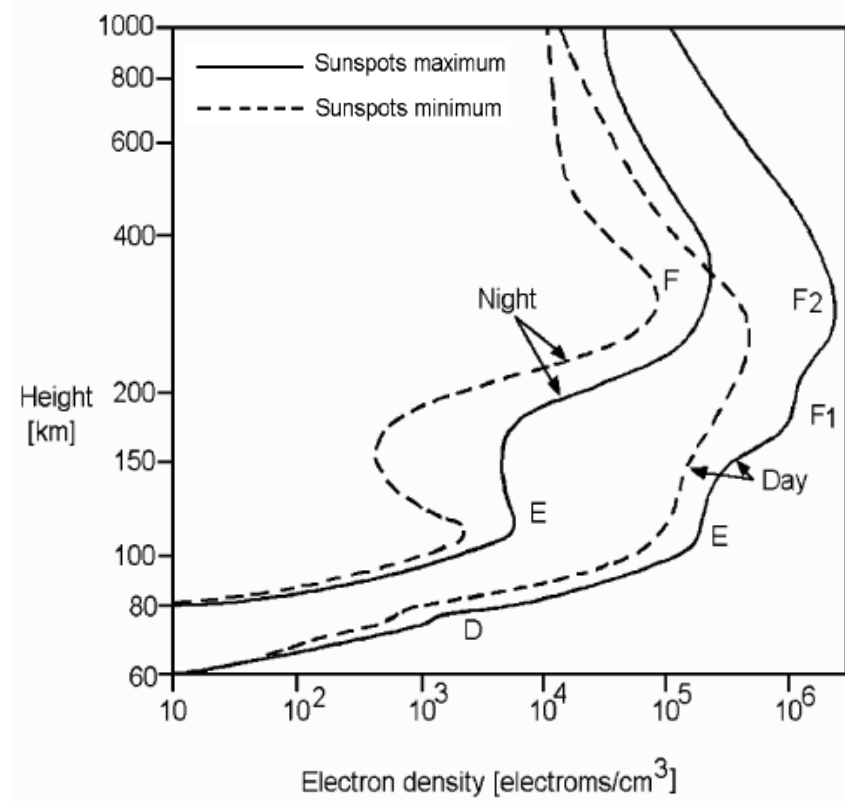
Figure 2.1: Vertical profile of the ionosphere (after Hargreaves, 1992)

2.2 Variations in the Ionosphere

The variability of the ionosphere can be characterized as spatially and temporally. Spatial variations are mainly latitude dependent. Roughly the ionosphere can be divided into three geographical regions with quite different behaviors. The region from about +30º to −30º of the geomagnetic latitude is the equatorial or low latitude region where the highest electron content values and large gradients in the spatial distribution of the electron density present. The geomagnetic anomaly that produces two peaks of electron content at about 20º to north and south of the geomagnetic equator occurs in this region. The variations in the ionosphere are more regular in the mid-latitude regions between about ±30º to ±60º of

geomagnetic latitude. However, sudden changes up to about 20% or more of the total electron content can take place in these regions due to ionospheric storms. The ionospheric variations in the polar or high latitude regions are rather unpredictable which are dominated by the geomagnetic field (Brunini et al., 2004).

Since the solar radiation is the main source for ionization, temporal variations in the ionosphere are closely connected to the activities of the Sun. Electron density in the ionosphere is undergoing variations on mainly three time scales. One of the major temporal variations of the ionosphere is due to the number of sunspots which are visibly dark patches on the surface of the Sun. Sunspots are indicators of intense magnetic activity of the Sun which result in enhanced solar radiation. Figure 2.2 shows the sunspot variation between 1954 and 2009. As it is depicted in the figure, sunspot numbers follow up a cycle of approximately 11 years. In addition to this 11-year cycle, ionospheric electron content varies seasonally due the annual motion of the Earth around the Sun. During the summer months the Sun is at its highest elevation angles. However, rather unexpectedly the electron density levels in the winter are typically higher than in the summer. The third main ionospheric activity cycle results from the diurnal rotation of the Earth, having therefore a period of a solar day. Following the solar radiation with some delay, the electron density reaches its maximum in the early afternoon and has the minimum values after the midnight (Kleusberg, 1998).

Besides these somewhat predictable variations, ionosphere is subjected to strong and unpredictable short-scale disturbances which are called as ionospheric irregularities. Ionospheric storms are important irregularities which are often coupled with severe disturbances in the magnetic field and strong solar eruptions (Schaer, 1999). Storms may last from hours to several days and may take place at global or regional scales. Traveling ionospheric disturbances (TIDs) are wave-like irregularities. Although little is known about them, they are thought to be related to perturbations of the neutral atmosphere, and can be classified according to their horizontal wavelengths, speeds and periods (García-Fernández, 2004).
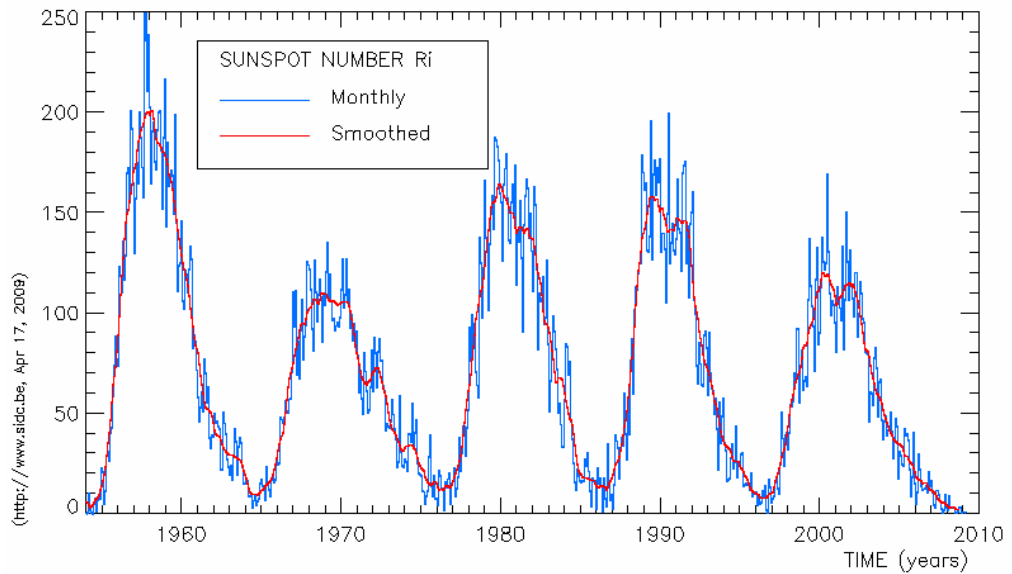
Figure 2.2: Monthly and monthly smoothed sunspot numbers since 1954 (SIDC: Sunspot data, http://sidc.oma.be/html/wolfmms.html, April 2009)

2.3 Ionospheric Effects on Electromagnetic Waves

The propagation speed for an electromagnetic signal in a vacuum is the speed of light which is equal to 299,792,458 m/s. However, in case of propagation in the ionosphere, the signals interact with the constituent charged particles with the result that their speed and direction of propagation are changed, i.e. the signals are refracted. The propagation of a signal through a medium is characterized by the refractive index of the medium, n:

$$ n = \frac{c}{v}, \tag{2.1} $$

where c is the speed of propagation in a vacuum, i.e. the speed of light and v is the signal speed in the medium (Langrey, 1998).

13

For electromagnetic waves the ionosphere is a dispersive medium, i.e. in the ionosphere the propagation velocity of electromagnetic waves depends on their frequency (Seeber, 2003). The refractive index of the ionosphere has been derived by Appleton and Hartree (Davies, 1989) and can be expressed as:

$$n^2 = 1 - \frac{X}{1 - iZ - \frac{Y_T^2}{2(1-X-iZ)} \pm \left[\frac{Y_T^4}{4(1-X-iZ)^2} + Y_L^2 \right]^{1/2}} \tag{2.2}$$

where $X = N_e e^2 / \varepsilon_0 m\omega^2 = f_n^2 / f^2$,

$Y_L = eB_L / m\omega = f_H \cos\theta / f$,

$Y_T = eB_T / m\omega = f_H \sin\theta / f$,

$Z = v / \omega$,

$\omega = 2\pi f$,

with f: the signal frequency,

f_H: the electron gyro frequency,

f_n: the electron plasma frequency,

N_e: electron density,

e: electron charge = -1.602*10^{-19} coulomb,

ε_0: permittivity of free space = 8.854*10^{-12} farad/m,

m: mass of an electron = 9.107*10^{-31} kg,

θ: the angle of the ray with respect to the Earth's magnetic field,

v: the electron-neutral collision frequency,

$B_{T,L}$: transverse and longitudinal components of earth's magnetic field.

14

Neglecting the higher order terms, to an accuracy of better than 1%, the refractive index of the ionosphere for the carrier phase of the signal, n_p, can be approximated to the first order as (Seeber, 2003):

$$n_p = 1 - 40.3 \frac{N_e}{f^2},$$ (2.3)

where the units for the electron density (N_e) and the signal frequency (f) are el/m^3 and 1/s, respectively. The ionospheric effect on code propagation (group delay) in terms of refractive index n_g is of the same size as the carrier phase propagation but has the opposite sign:

$$n_g = 1 + 40.3 \frac{N_e}{f^2}.$$ (2.4)

The range error on the signal caused by the ionospheric refraction can be derived as described, e.g., by Hofmann-Wellenhof et al. (2008). The measured range of the signal between the emitter (Tr) and the receiver (Rc), S, is defined by the integral of the refractive index along the signal path ds:

$$S = \int_{Tr}^{Rc} n \, ds .$$ (2.5)

The geometrical range S_0, i.e. the straight line, between the emitter and receiver can be obtained by setting $n = 1$:

$$S_0 = \int_{Tr}^{Rc} ds_0 .$$ (2.6)

The path length difference between measured and geometric ranges is called the ionospheric refraction and is given by:

15

$$\Delta S^{ION} = S - S_0 = \int_{Tr}^{Rc} n \, ds - \int_{Tr}^{Rc} ds_0 \ . \tag{2.7}$$

With Eq. (2.3) the phase delay, ΔS_p^{ION}, is

$$\Delta S_p^{ION} = \int_{Tr}^{Rc} (1 - \frac{40.3 N_e}{f^2}) \, ds - \int_{Tr}^{Rc} ds_0 \ , \tag{2.8}$$

and with Eq. (2.4) the group delay, ΔS_g^{ION}, is

$$\Delta S_g^{ION} = \int_{Tr}^{Rc} (1 + \frac{40.3 N_e}{f^2}) \, ds - \int_{Tr}^{Rc} ds_0 \ . \tag{2.9}$$

Since the delays will be small, Eqs. (2.8) and (2.9) can be simplified by integrating the first terms along geometric path, i.e. letting $ds = ds_0$,

$$\Delta S_p^{ION} = -\frac{40.3}{f^2} \int_{Tr}^{Rc} N_e \, ds_0 \ , \tag{2.10}$$

and

$$\Delta S_g^{ION} = \frac{40.3}{f^2} \int_{Tr}^{Rc} N_e \, ds_0 \ . \tag{2.11}$$

Defining the Total Electron Content (TEC) as the integration of electrons along the signal path,

$$TEC = \int_{Tr}^{Rc} N_e \, ds_0 \ , \tag{2.12}$$

16

the phase and group delays become:

$$\Delta S_p^{ION} = -I = -\frac{40.3}{f^2} TEC, \quad \Delta S_g^{ION} = I = \frac{40.3}{f^2} TEC,$$

(2.13)

where the TEC is measured in units of 10^{16} electrons per m^2.

CHAPTER 3

THE GLOBAL POSITIONING SYSTEM

3.1 GPS Overview

The NAVigation Satellite Timing And Ranging (NAVSTAR) GPS is a satellite-based navigation system providing position, navigation and time information. The system has been under development by United States Department of Defense since 1973 to fulfill primarily the military needs and as a by-product, to serve the civilian community. GPS has been fully operational since 1995 on a world-wide basis and provides continuous services independent of the meteorological conditions (Seeber, 2003).

GPS is composed of space, control and user segments. The space segment consists of 24 or more active satellites which are dispersed in six orbits. The orbital inclination is 55 degrees relative to the equator and the orbital periods are one-half of the sidereal day ($\approx$11.967 h). The orbits are nearly circular with radii of 26,560 km which corresponds to orbital heights of about 20,200 km above the Earth's surface. The GPS satellites transmit two L-band signals: L1 signal with carrier frequency 1575.42 MHz and L2 signal with carrier frequency 1227.60 MHz. The L1 signal is modulated by two pseudorandom noise codes which are designated as Coarse/Acquisition code (C/A code) and Precise code (P-code) with chipping rates of 1.023 MHz and 10.23 MHz, respectively. The L2 signal is also modulated by the P-code but does not comprise the C/A code. The corresponding wavelengths

for L1 carrier, L2 carrier, C/A code and P-code are approximately 19.0 cm, 24.4 cm, 300 m and 30 m, respectively. In addition to the pseudorandom codes, both signals are modulated by a navigation massage which contains information concerning the satellite orbit, satellite clock, ionospheric corrections and satellite health status (Mohinder et al., 2007). Table 3.1 gives a summary for the components of the satellite signal.

Table 3.1: Components of the GPS satellite signal (Dach et al., 2007)

Component	**Frequency** [MHz]	
Fundamental frequency	f_0	= 10.23
Carrier L_1	$f_1 = 154\,f_0$	= 1575.42 (λ_1 = 19.0 cm)
Carrier L_2	$f_2 = 120\,f_0$	= 1227.60 (λ_2 = 24.4 cm)
P-code $P(t)$	f_0	= 10.23
C/A code $C(t)$	$f_0 / 10$	= 1.023
Navigation message $D(t)$	$f_0 / 204600$	= 50 · 10^{-6}

The control segment of the GPS consists of a master control station, monitor stations and ground antennas. The main responsibilities of the control segment are to monitor and control the satellites, to determine and predict the satellite orbits and clock behaviors and to periodically upload navigation massage to the satellites (Hofmann-Wellenhof et al., 2008).

The user segment includes antennas and receivers to acquire and process the satellite signals. Single frequency GPS receivers can only output observations on L1 frequency, while dual frequency receivers can provide observations on both L1 and L2 frequencies.

The reference frame used by the GPS is the World Geodetic System 1984 (WGS84) which is a geocentric Earth-fixed system. Broadcast ephemeris of GPS satellites are provided in the WGS84 (Seeber, 2003).

3.2 GPS Observables

The basic observables of the Global Positioning System are the pseudorange and the carrier phase. A less-used third observable, namely Doppler measurement which represents the difference between the nominal and received frequencies of the signal due to the Doppler effect, is not described as it is not used in the study.

The observables for each receiver type are provided in the internal format of the receiver, which makes processing data of different receiver types difficult. In order to overcome this difficulty, a common data format, namely the Receiver Independent Exchange Format (RINEX), was accepted for data exchange in 1989. Several revisions and modifications for RINEX have been introduced (Seeber, 2003). A detailed document, e.g. for version 2.11, is available via the IGS server (Gurtner, 2004).

3.2.1 Pseudorange

The GPS receivers use the C/A and P codes to determine the pseudorange, which is a measure of the distance between the satellite and the receiver. The receiver replicates the code being generated by the satellite and determines the elapsed time for the propagation of the signal from the satellite to the receiver by correlating the transmitted code and the code replica. As the electromagnetic signal travels at the speed of light, the pseudorange can be computed by simply multiplying the time offset by the speed of light. This range measurement is called a pseudorange because it is biased by the lack of synchronization between the atomic clock governing the generation of the satellite signal and the crystal clock governing the generation of code replica in the receiver (Langrey, 1998). If this bias was zero,

i.e. the satellite and receiver clocks were synchronized, three pseudorange measurements from different satellites with known positions would be sufficient to compute three Cartesian coordinates of the receiver. However, in the presence of synchronization bias, at least four pseudorange measurements are required to determine the position of the receiver.

The pseudorange also comprises several other errors including ionospheric and tropospheric delays, multipath, hardware delays and measurement noise. Following equations for the pseudorange observables relates the measurements and various biases:

$$P1 = \rho + c(dt - dT) + c(\tau_{P1}^{S} + \tau_{P1}^{R}) + I_1 + d_{trop} + \varepsilon_{P1}, \tag{3.1}$$

$$P2 = \rho + c(dt - dT) + c(\tau_{P2}^{S} + \tau_{P2}^{R}) + I_2 + d_{trop} + \varepsilon_{P2}, \tag{3.2}$$

where $P1$ and $P2$ are the measured pseudoranges using P-code on $L1$ and $L2$, respectively, ρ is the geometric range from the receiver to the satellite, c is the speed of light, dt and dT are the offsets of the satellite and receiver clocks from GPS time, τ^{S} and τ^{R} are frequency dependent biases on pseudoranges due to the satellite and receiver hardware, I_1 and I_2 are ionospheric delays on $L1$ and $L2$ pseudoranges, d_{trop} is the delay due to the troposphere and ε_{P1} and ε_{P2} represent the effect of multipath and measurement noise on $L1$ and $L2$ pseudoranges, respectively.

A very similar observation equation can be written for C/A code:

$$C1 = \rho + c(dt - dT) + c(\tau_{C1}^{S} + \tau_{C1}^{R}) + I_1 + d_{trop} + \varepsilon_{C1}, \tag{3.3}$$

which only differs from $P1$ equation with multipath and noise term (ε_{C1}) and hardware delays (τ^S and τ^R), as these biases are not identical for P and C/A codes. Remember that C/A code is available only on $L1$ signal.

The precision for the pseudorange measurements has been traditionally about 1% of their chip lengths, which corresponds to a precision of roughly 3 m for C/A code measurements and 0.3 m for P-code measurements (Hofmann-Wellenhof et al., 2008). Therefore, if they are simultaneously provided by the receiver, $P1$ is commonly preferred over $C1$ observation.

3.2.2 Carrier Phase

The wavelengths of the carrier waves are very short compared to the code chip lengths. The phase of an electromagnetic wave can be measured to 0.01 cycles or better which corresponds to millimeter precision for carrier waves of the GPS signals (Hofmann-Wellenhof et al., 2008). However, the information for the transmission time of the signal cannot be imprinted on the carriers as it is done on the codes. Therefore, a GPS receiver can measure the phase of the carrier wave and track the changes in the phase but the whole number of carrier cycles that lie between the satellite and the receiver is initially unknown. In order to use the carrier phase as an observable for positioning, this unknown number of cycles or ambiguity, N, has to be determined with appropriate methods (Langrey, 1998).

If the measured carrier phases in cycles are multiplied by the wavelengths of the signals, the carrier phase observation equations can be expressed in distance units as:

$$\Phi 1 = \rho + c(dt - dT) + c(T_1^S + T_1^R) + \lambda_1 N_1 - I_1 + d_{trop} + \varepsilon_{L1}, \tag{3.4}$$

$$\Phi 2 = \rho + c(dt - dT) + c(T_2^S + T_2^R) + \lambda_2 N_2 - I_2 + d_{trop} + \varepsilon_{L2}, \tag{3.5}$$

where $\Phi 1$ and $\Phi 2$ are the carrier phase measurements in length units for $L1$ and $L2$, λ_1 and λ_2 are the wavelengths of the $L1$ and $L2$ carriers, T^S and T^R are frequency dependent biases on carrier phases due to the satellite and receiver hardware and ε_{L1} and ε_{L2} represent the effect of multipath and measurement noise on $L1$ and $L2$ carriers, respectively. Remember from Section 2.3 that the ionospheric delays on the carrier phase (the phase delay) and code (the group delay) are equal in amount but have opposite signs. Eqs. (3.4) and (3.5) are very similar to the observation equations for the pseudoranges, where the major difference is the presence of the ambiguity terms N_1 and N_2 for $L1$ and $L2$, respectively.

3.3 GPS Observable Error Sources

As indicated in previous sections, the GPS measurements are subject to various error sources, which reduce the accuracy of GPS positioning. These error sources can be grouped into three categories as satellite related, receiver related and signal propagation errors. The satellite related errors are orbital errors, satellite clock errors and frequency dependent delays due to the satellite's hardware. The receiver related errors consist of receiver clock errors, receiver hardware delays and measurement noise. The signal propagation errors include ionospheric and tropospheric delays and multipath. These error sources are briefly reviewed below.

3.3.1 Ionospheric Delay

The ionospheric delay is the largest error source for GPS observables after selective availability (SA) was turned off on May 1, 2000 (Kunches and Klobuchar, 2001). The delay due to ionosphere can vary from a few meters to tens of meters in the zenith direction, while near the horizon this effect can be three times higher than the vertical value. For electromagnetic waves the ionosphere is a dispersive medium, i.e. its refractive index depends on the signal frequency.

Therefore dual-frequency GPS receivers can determine the ionospheric effects on the signal by comparing the observables of two distinct frequencies (Klobuchar, 1996). The ionospheric effects on GPS are discussed in Section 3.4, while the theory to extract ionospheric information from GPS observations is presented in Chapter 4 in detail.

3.3.2 Tropospheric Delay

The troposphere is the lower part of the atmosphere and extends from the Earth's surface up to about 50 km height. This medium is non-dispersive for GPS signals, i.e. tropospheric delay is independent of the signal frequency, and is equal for code and carrier phase observables. The refractive index of the troposphere is larger than unity, which causes the speed of the signal to decrease below its free space (vacuum) value. The resulting delay is a function of temperature, atmospheric pressure, and water vapor pressure and consists of dry and wet components. The dry component constitutes approximately 90% of the total tropospheric error and depends primarily on atmospheric pressure and temperature. The dry delay is approximately 2.3 m in zenith direction and it can be modeled successfully since its temporal variability is low. On the other hand, the wet component, which corresponds to approximately 10% of the total delay, shows high spatial and temporal variations. The wet delay depends on the water vapor and varies between 1 and 80 cm in the zenith direction (Spilker, 1996).

3.3.3 Orbital Error

The position and the velocity information for GPS satellites can be determined by means of almanac data, broadcast ephemerides (orbits) and precise ephemerides.

The almanac data, which are low-accuracy orbit data for all available satellites, are transmitted as part of the navigation message of the GPS signal. The purpose of the almanac data is to provide adequate information for faster lock-on of the

receivers to satellite signals and for planning tasks such as the computation of visibility charts. The accuracy of the almanac data is about several kilometers depending on the age of the data (Hofmann-Wellenhof et al., 2008).

The broadcast ephemerides are computed and uploaded to the GPS satellites by the master station of the control segment depending on observations at the monitor stations. The orbital information is broadcast in real-time as a part of the navigation message in the form of Keplerian parameters. These orbital data could be accurate to approximately 1 m (Hofmann-Wellenhof et al., 2008).

The precise ephemerides contain satellite positions and velocities with epoch interval of 15 minutes, which are provided by the IGS. There are several types of precise orbit data depending on the delay for their availability. The IGS Final Orbits are the most accurate orbital information, which are made available 13 days after the observations. Slightly less accurate ephemerides are provided as IGS Rapid Orbits and IGS Ultra Rapid Orbits with delays of 17 hours and 3 hours, respectively. The accuracy of the precise ephemerides is at the level of 5 cm or even better. The precise ephemerides are provided in files of SP3 (Standard Product 3) format with file extensions of sp3, EPH or PRE (Dach et al., 2007).

3.3.4 Clock Errors

The GPS system uses GPS time as its time scale. GPS time is an atomic time scale and is referenced to Universal Time Coordinated (UTC). Clock errors in GPS observables are due to the deviations of satellite and receiver oscillators from GPS time.

The GPS satellites are equipped with rubidium and/or cesium oscillators. Although these atomic clocks are highly accurate and stable, satellite clock errors, which are typically less than 1 ms, are still large enough to require correction. The deviation of each satellite clock from GPS time is monitored, modeled and broadcast as a

component of the navigation message by the control segment. After the corrections have been applied, the residual satellite clock errors are typically less than a few nanoseconds (Mohinder et al., 2007).

In general, receivers use less expensive quartz crystal oscillators. Although receiver clock errors are much higher as compared to satellite clock errors, they can be estimated as unknowns along with the receiver position or eliminated by differencing approaches.

3.3.5 Multipath

Multipath is the arrival of a signal at the receiver antenna via two or more different paths. It is usually stemmed from the reflection of the signal from surfaces such as buildings, streets and vehicles. The multipath affects both code and carrier phase measurements in a GPS receiver. The effect on P-code measurements can reach to decimeters to meters while the range error on C/A code measurements is at the order of several meters. The maximum error due to multipath is about 5 cm for carrier phase observations. Multipath can be eliminated or reduced by careful selection of site locations to avoid reflections, using carefully designed antennas, utilizing absorbing materials near the antenna and employing receivers with related software to detect multipath effects (Seeber, 2003).

3.3.6 Hardware Delays

Delays in hardware of satellites and receivers result in frequency dependent biases on both pseudorange and carrier phase measurements. These biases are not accessible in absolute sense; hence in general they are not given in observation equations and modeled with clock errors. However, they should be taken into account for the combinations of observations in some situations, e.g. geometry linear combination for ionosphere modeling (Dach et al., 2007).

3.3.7 Measurement Noise

Measurement noise in GPS observables results from some random influences such as the disturbances in the antenna, cables, amplifiers and the receiver. Typically, the observation resolution for GPS receivers is about 1% of the signal wavelength, which corresponds to approximate measurement noises of 3 m for C/A code, 30 cm for P-code and 2 mm for carrier phase observations (Seeber, 2003).

3.4 Ionospheric Effects on GPS

The ionosphere can cause two primary effects on the GPS signal. The first is a combination of group delay and carrier phase advance and the second is ionospheric scintillation.

3.4.1 Group Delay and Carrier Phase Advance

The largest effect of the ionosphere is on the speed of the signal, and hence the ionosphere primarily affects the measured range. The speed of a signal in ionosphere is a function of the signal frequency and electron density as described in Chapter 2. The speed of the carrier waves (the phase velocity) is increased, or advanced, but the speed of the codes (the so-called group velocity) is decreased due to ionospheric effects. Therefore, the code pseudoranges are measured longer and the ranges from the carrier phase observations are measured shorter than the true geometric distance between the satellite and the receiver.

3.4.2 Ionospheric Scintillation

Irregularities in the electron content of the ionosphere can cause short-term variations in the amplitude and phase of the received signal. Fluctuations due to either effect are known as ionospheric scintillations. Phase scintillations are rapid

changes in the phase of the carrier between consecutive epochs due to fast variations in the number of electrons along the signal path. During such incidents, amplitude scintillations can also occur due to signal fading. Scintillations may result in tracking losses and phase discontinuities (or cycle slips), which corrupt the carrier phase measurement. The region from +30º to –30º of the geomagnetic latitude and the auroral and polar cap regions are the zones in which ionospheric scintillations often occur (Langrey, 1998).

CHAPTER 4

THEORETICAL BACKGROUND

4.1 The Reference Frames Used

4.1.1 Earth-Fixed Reference Frame

In an Earth-fixed reference frame the origin of the coordinate system is the geocenter which is defined as the center of mass of the Earth, including oceans and the atmosphere. The X axis lies in the Greenwich meridian plane. The Z axis is identical to the mean position of the rotation axis of the Earth, i.e. in the direction of the terrestrial pole. The X-Y plane coincides with the conventional equatorial plane of the Earth and the Y axis completes the right-handed system (McCarthy, 2000).

GPS uses the WGS84 as the reference frame. A geocentric equipotential ellipsoid of revolution is associated with the WGS84. The position of a point in the Earth-fixed system can be represented by Cartesian coordinates X, Y, Z as well as by ellipsoidal geographic coordinates geodetic latitude (φ), geodetic longitude (λ) and geodetic height above the reference ellipsoid (h). Transformation between Cartesian and ellipsoidal coordinates can be found in, e.g., Hofmann-Wellenhof et al. (2008). Relationship between Cartesian and ellipsoidal coordinates is given in Fig. 4.1.
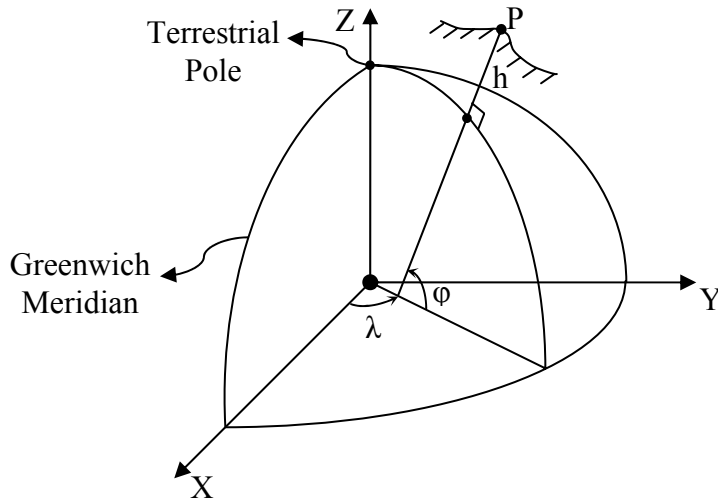
Figure 4.1: Cartesian and ellipsoidal coordinates in an Earth-fixed reference frame

4.1.2 Geographic Sun-Fixed Reference Frame

In the geographic Sun-fixed reference frame the origin of the coordinate system is the geocenter and the Z axis passes through the terrestrial pole as in the Earth-fixed frame. Hence, the latitude concept is identical for both frames. However, X axis of the geographic Sun-fixed frame is towards the fictitious mean Sun, which moves in the plane of the equator with constant velocity. Accordingly, the ellipsoidal coordinates of a point are described by ellipsoidal geographic (geodetic) latitude (φ) and Sun-fixed longitude (s). s is related to the geodetic longitude (λ) by

$$s \approx UT + \lambda - \pi,\tag{4.1}$$

where UT is the universal time (Schaer, 1999).

4.1.3 Geomagnetic Reference Frame

Geomagnetic reference frame is also a geocentric Sun-fixed frame, i.e. the X axis of the frame is in the direction of the fictitious mean Sun. The Z axis passes through the geomagnetic North Pole, and Y axis completes the right-handed system. Accordingly, the ellipsoidal coordinates of a point are described by geomagnetic latitude (φ_m) and Sun-fixed longitude (s). Representation of the geomagnetic reference frame is given in Fig. 4.2. Geomagnetic latitude of a point is computed by:

$$\varphi_m = \arcsin(\sin\varphi\sin\varphi_0 + \cos\varphi\cos\varphi_0\cos(\lambda - \lambda_0)), \tag{4.2}$$

where φ_0 and λ_0 are geodetic latitude and geodetic longitude of the geomagnetic North Pole, and φ and λ are geodetic latitude and geodetic longitude of the point under consideration (Dettmering, 2003).
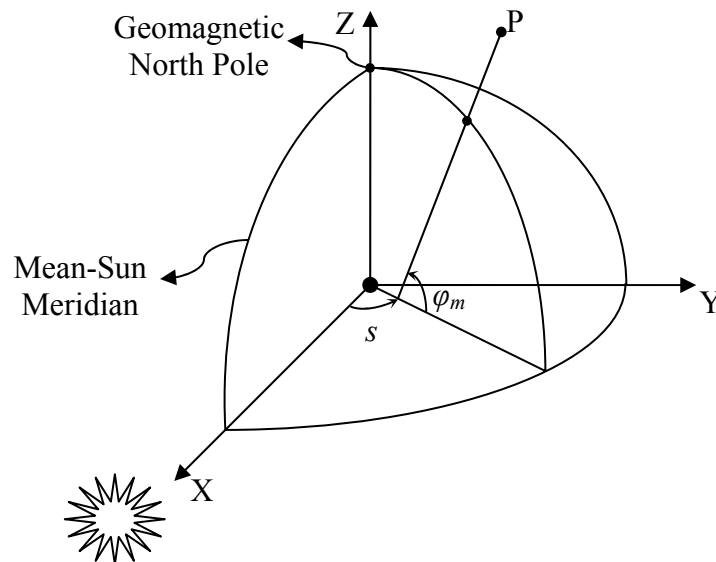
Figure 4.2: Geomagnetic reference frame

31

4.1.4 Local Ellipsoidal Reference Frame

Local reference systems are generally associated with an instrument such as a GPS receiver, a VLBI (Very Long Base-line Interferometry) antenna or a camera. The origin of the frame is at the observation point. Z axis is in the direction of the ellipsoidal vertical (normal) while X axis is directed to the north (geodetic meridian) and Y axis is directed to the east, completing a left-handed system. The location of a target point is generally defined via the angles ellipsoidal azimuth (α) and ellipsoidal zenith (ζ) and slant range (s) instead of local Cartesian coordinates. The transformations between the global Cartesian coordinates (Earth-fixed coordinates), local Cartesian coordinates and local ellipsoidal coordinates can be found in, e.g., Seeber (2003). Representation of the local ellipsoidal reference frame related to the Earth-fixed reference frame is described in Fig. 4.3.
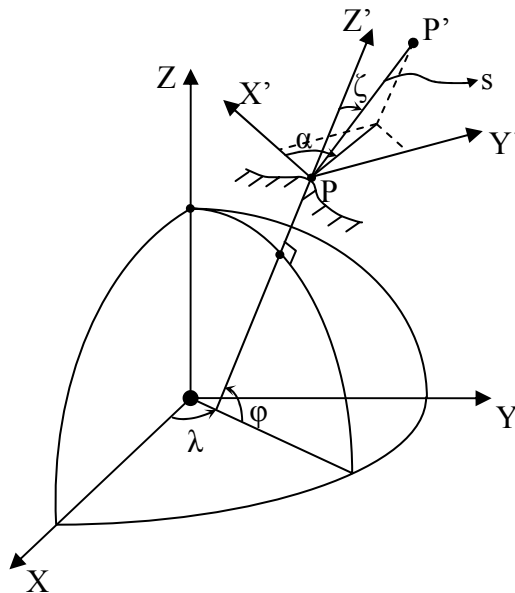
Figure 4.3: Local ellipsoidal reference frame defined at point P and local ellipsoidal coordinates of a target point P'

4.2 Extracting Ionospheric Information from GPS Observations

4.2.1 The Geometry-Free Linear Combination of GPS Observables

The geometry-free linear combination of GPS observations, which is also called the ionospheric observable, is classically used for ionospheric investigations and it is obtained by subtracting simultaneous pseudorange (P1-P2 or C1-P2) or carrier phase observations (Φ1-Φ2). With this combination, the satellite - receiver geometrical range and all frequency independent biases are removed (Ciraolo et al., 2007). Subtracting Eq. (3.2) from Eq. (3.1) the geometry-free linear combination of the pseudorange measurements is obtained:

$$P_4 = P_1 - P_2 = I_1 - I_2 + c(\tau_{P1}^R - \tau_{P2}^R) + c(\tau_{P1}^S - \tau_{P2}^S) + \varepsilon_p, \tag{4.3}$$

where I_1 and I_2 are ionospheric delays on L1 and L2 pseudoranges, τ^S and τ^R are frequency dependent biases on pseudoranges due to the satellite and receiver hardware and ε_p is the combination of multipath and measurement noises in P_1 and P_2. Defining the so-called inter-frequency biases (IFBs) for the pseudorange measurements due to hardware delays of the receiver and the satellite as $br = c(\tau_{P1}^R - \tau_{P2}^R)$ and $bs = c(\tau_{P1}^S - \tau_{P2}^S)$, respectively, and substituting the ionospheric delays (Eq. 2.13) in Eq. (4.3), P_4 is re-written as:

$$P_4 = 40.3\, STEC \left(\frac{f_2^2 - f_1^2}{f_1 f_2} \right) + br + bs + \varepsilon_p, \tag{4.4}$$

where STEC is the number of electrons in the ionosphere in a column of 1 m^2 cross-section and extending along the ray-path of the signal between the satellite and the receiver, as defined before.

The geometry-free linear combination for carrier phase observations can be written with Eqs. (3.4) and (3.5) as follows:

$$\Phi_4 = \Phi_1 - \Phi_2 = I_2 - I_1 + \lambda_1 N_1 - \lambda_2 N_2 + c(T_1^R - T_2^R) + c(T_1^S - T_2^S) + \varepsilon_L,$$

(4.5)

where λ_1 and λ_2 are the wavelengths of the $L1$ and $L2$ carriers, N_1 and N_2 are ambiguity terms for $L1$ and $L2$, T^S and T^R are frequency dependent biases on carrier phases due to the satellite and receiver hardware and ε_L is the combination of multipath and measurement noise in $L1$ and $L2$. Similarly, defining the inter-frequency biases (IFBs) for the carrier-phase measurements due to hardware delays of the receiver and the satellite as $Br = c(T_1^R - T_2^R)$ and $Bs = c(T_1^S - T_2^S)$, and substituting the ionospheric delays, Φ_4 is re-written as:

$$\Phi_4 = -40.3\, STEC \left(\frac{f_2^2 - f_1^2}{f_1 f_2} \right) + \lambda_1 N_1 - \lambda_2 N_2 + Br + Bs + \varepsilon_L.$$

(4.6)

4.2.2 Leveling the GPS Observations

STEC can be obtained from pseudorange or carrier-phase observations by extracting it from Eq. (4.4) or Eq. (4.6), respectively. The noise level of carrier phase measurements is significantly lower than those for pseudorange ones. However, carrier phase measurements possess ambiguity terms, which are the unknown number of whole cycles of the carrier signal between the satellite and the receiver and should be estimated within a preprocessing step. In order to take the advantage of both unambiguous pseudoranges and precise carrier phase measurements, several methods have been proposed to smooth pseudorange measurements with carrier phases. Among them, the works suggested by Hatch (1982), Lachapelle (1986) and Springer (2000) involves smoothing each

pseudorange by its corresponding carrier phase observation individually. However, as STEC is obtained from the geometry-linear combination of GPS observations, an algorithm to smooth the pseudorange ionospheric observable (Eq. 4.3) should be more appropriate for ionosphere modeling studies. For this purpose, a smoothing method, which is known as "carrier to code leveling process" is applied in this study. The related algorithm is followed from Ciraolo et al. (2007) with some small modifications and explained below.

By combining Eqs. (4.3) and (4.5) for simultaneous observations, following equation can be obtained:

$$P_4 + \Phi_4 = \lambda_1 N_1 - \lambda_2 N_2 + Br + Bs + br + bs + \varepsilon_P . \tag{4.7}$$

Note that noise and multipath term for carrier-phase observation (ε_L) has been neglected, as it is much lower than the one for the pseudorange observation (ε_P). In Eq. (4.7), P_4 and Φ_4 are available from GPS observations. The ambiguity terms N_1 and N_2 remain constant for every continuous arc which is defined as the group of consecutive carrier-phase observations without discontinuities, e.g. due to cycle slips. Besides, the IFB terms are stable for periods of days to months so they can be treated as constants for a continuous arc (Gao et al.; 1994, Sardon and Zarraoa, 1997; Schaer, 1999). Thus, Eq. (4.7) should provide constant or very stable results and an average value $\langle P_4 + \Phi_4 \rangle_{arc}$ can be computed for a continuous arc:

$$\langle P_4 + \Phi_4 \rangle_{arc} = \frac{1}{n} \sum_{i=1}^{n} (P_4 + \Phi_4)_i ,$$
$$= \langle \lambda_1 N_1 - \lambda_2 N_2 \rangle_{arc} + Br + Bs + br + bs + \langle \varepsilon_P \rangle_{arc}, \tag{4.8}$$

where n is the number of measurements in the continuous arc.

Subtracting Eq. (4.5) from Eq. (4.8), the ambiguity terms can be eliminated

$$\widetilde{P}_4 = \left\langle P_4 + \Phi_4 \right\rangle_{arc} - \Phi_4 \approx I_1 - I_2 + br + bs + \left\langle \varepsilon_P \right\rangle_{arc} - \varepsilon_L , \qquad (4.9)$$

where $\widetilde{P}_4$ is the pseudorange ionospheric observable smoothed with the carrier-phase ionospheric observable.

The smoothing effect of the leveling algorithm is presented in Fig. 4.4 for the first 200 observations of a ground-based GPS receiver that is used in this study. Note that the observation interval for the receiver is 30 sec.
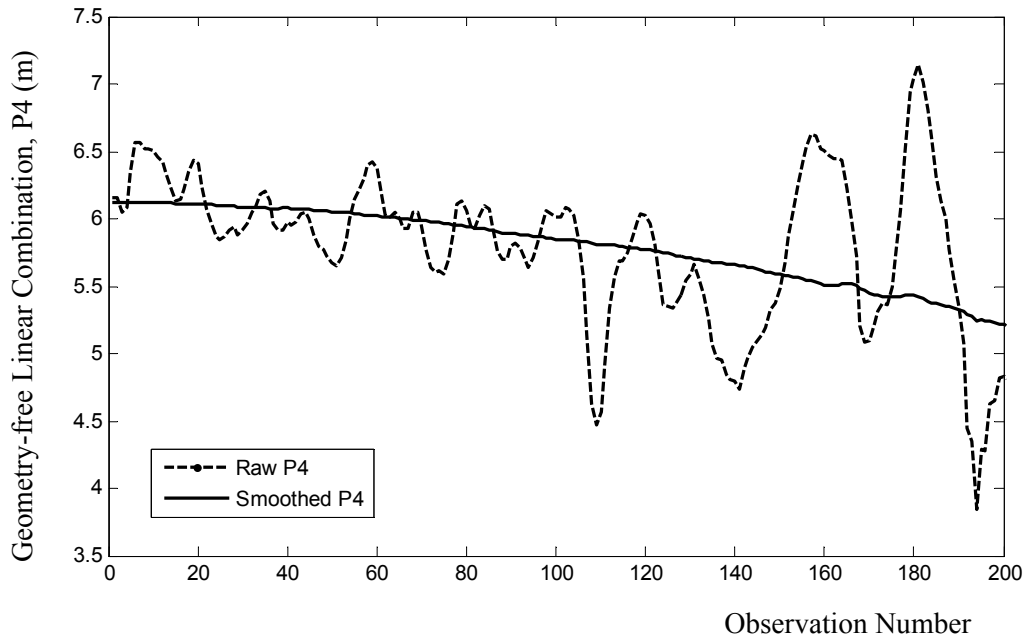
Figure 4.4: Raw and smoothed ionospheric observables of AFYN station for GPS satellite PRN01

36

In order to extract STEC from smoothed ionospheric observable, the ionospheric delays from Eq. (2.13) are substituted into Eq. (4.9):

$$\widetilde{P}_4 = STEC\frac{40.3(f_2^2 - f_1^2)}{(f_1^2 f_2^2)} + br + bs + \langle \varepsilon_P \rangle_{arc} - \varepsilon_L . \tag{4.10}$$

Finally, STEC can be obtained in TECU (1 TECU = 1.10^6 el./m^2) by:

$$STEC = (\widetilde{P}_4 - br - bs - \langle \varepsilon_P \rangle_{arc} + \varepsilon_L)\frac{(f_1^2 f_2^2)}{40.3(f_2^2 - f_1^2)} . \tag{4.11}$$

Note that the inter-frequency biases for the pseudorange measurements *br* and *bs* are frequently called in the literature as differential code biases (DCB). This terminology will also be followed in the remaining parts of this study to avoid confusion with the biases for the carrier phase measurements (*Br* and *Bs*).

4.2.3 Differential Code Biases

Dual-frequency GPS receivers commonly provide C/A code measurements (C1) besides the phase measurements Φ1 and Φ2. In addition, depending on the type of receiver, they can provide a subset of following code observations:

- P1

- P2

- X2

X2 observation, which is provided by the so-called cross-correlation receivers, is equivalent to C1 + (P2 − P1). Accordingly, GPS receivers can be categorized into three classes depending on their code observables:

- P1/P2 – receivers providing C1, P1 and P2 observables.

- C1/P2 – receivers providing C1 and P2 observations.

- C1/X2 – receivers providing C1 and X2 (=C1 + (P2 – P1)).

Note that in general C1 observations from P1/P2 receivers are disregarded since their precision is lower as compared to P1 observations (Dach et al., 2007).

As stated before, frequency dependent biases due to the hardware of the receivers and the satellites are present for the GPS observables. Although they cannot be obtained in absolute manner, their differential forms, which are present as DCB (or IFB) values in geometry-free linear combination of pseudorange observations, are of vital importance for ionosphere modeling. Essentially, these biases are time dependent. However, they are rather stable over time for periods of days to months so they can be treated as constants for ionosphere modeling (Gao et al.; 1994, Sardon and Zarraoa, 1997; Schaer, 1999)

Geometry-free linear combinations of P1 and P2 (for P1/P2 receiver class), or P1 and X2 (for P1/X2 receiver class) contain DCB values between P1 and P2 (DCB_{P1P2}). However, combination of observables for C1/P2 receivers should consider another differential bias term between P1 and C1 (DCB_{P1C1}). Thus, for STEC calculations of this receiver class, DCB terms for both the receivers and the satellites are corrected with DCB_{P1C1}:

$$br = DCB_{P1P2}^{R} - DCB_{C1P2}^{R}, \qquad (4.12)$$

$$bs = DCB_{P1P2}^{S} - DCB_{C1P2}^{S}, \qquad (4.13)$$

where superscripts R and S denotes biases due to receivers and satellites, respectively. For GPS satellites, the order of DCB_{P1C1} magnitudes is approximately 3 times smaller compared with DCB_{P1P2} values (Dach et al., 2007).

DCB values for the satellites are freely available by IGS analysis centers, e.g. by CODE, through the internet with high accuracy. However, receiver DCBs are generally unknown and should be estimated within ionosphere modeling process.

4.2.4 Cycle Slip Detection:

When a GPS receiver is locked to a satellite (i.e. starts to acquire satellite's signal), an integer counter for the number of cycles of each carrier wave between the satellite and receiver is initialized and fractional part of the signal is recorded as carrier phase observable. The initial integer number, which was described as ambiguity term before, is unknown and remains constant as long as the signal lock continues. If the receiver losses phase lock of the signal, the integer counter is reinitialized causing a jump in carrier phase measurement, which is called clip slip. Cycle slips can occur due to the failures in the receivers, as well as obstructions of the signal, high signal noise or low signal strength. The magnitude of a cycle slip may range from a few cycles to millions of cycles (Seeber, 2003).

As the leveling process described in part 4.2.2 is defined for continuous arcs of carrier-phase observations for which the ambiguity terms are constant, the cycle slips in the phase observations should be determined.

In order to detect the cycle slips, several testing quantities which are based on various combinations of GPS observations have been proposed. A review of them can be seen in Seeber (2003) or Hofmann-Wellenhof et al. (2008). Some of these methods depend on the single, double or triple-differences of observations, for which observations of two receivers are required. Since the software generated

through this work, i.e. TECmapper, processes observation files individually, a single receiver test, which uses the combination of a phase and a code range, is applied for cycle slip detection.

Forming the difference between the carrier-phase and the pseudorange observations ($\Phi1 - P1$) and ($\Phi2 - P2$), the testing quantities for cycle slips for L1 and L2 are obtained, respectively:

$$\Phi1 - P1 = \lambda_1 N_1 - 2I_1 + c(T_1^S + T_1^R - \tau_{P1}^S - \tau_{P1}^R) + \varepsilon_{P1}, \qquad (4.14)$$

$$\Phi2 - P2 = \lambda_2 N_2 - 2I_2 + c(T_2^S + T_2^R - \tau_{P2}^S - \tau_{P2}^R) + \varepsilon_{P2}. \qquad (4.15)$$

In Eqs. (4.14) and (4.15) noise and multipath terms for carrier-phase observations (ε_{L1} and ε_{L2}) has been neglected, as they are much lower than those for the pseudorange observations (ε_{P1} and ε_{P2}). Here, the ambiguity terms N_1 and N_2 are constant, hardware biases τ^S, τ^R, T^S and T^R are stable for periods of days to months and the change of the ionospheric delays are fairly small between closely spaced epochs. Thus, if there are no cycle slips, the temporal variation of testing quantities (4.14) and (4.15) will be small. The sudden jumps in successive values of testing quantities are indicators of cycle slips where new ambiguity terms, thus starting points for new continuous arcs are defined. The main shortcomings for these testing quantities are the noise terms, mainly due to the noise level of pseudorange observations, so that small cycle slips cannot be identified. However, the measurement resolution of geodetic receivers is improved continuously, which makes the combination of phase and code range observations an ideal testing quantity for cycle slip detection (Hofmann-Wellenhof et al., 2008).

4.2.5 Single Layer Model

For 2D ionosphere models, STEC values, e.g. which are obtained by Eq. (4.11), are usually converted to the height independent Vertical Total Electron Content (VTEC) values by the so-called single layer model and corresponding mapping function. In the single layer model, all electrons in the ionosphere are assumed to be contained in a shell of infinitesimal thickness. The height of this idealized layer approximately corresponds to the altitude of the maximum electron density and it is usually set to values between 350 and 450 kilometers (Schaer, 1999). Fig. 4.5 represents the single layer model approach.
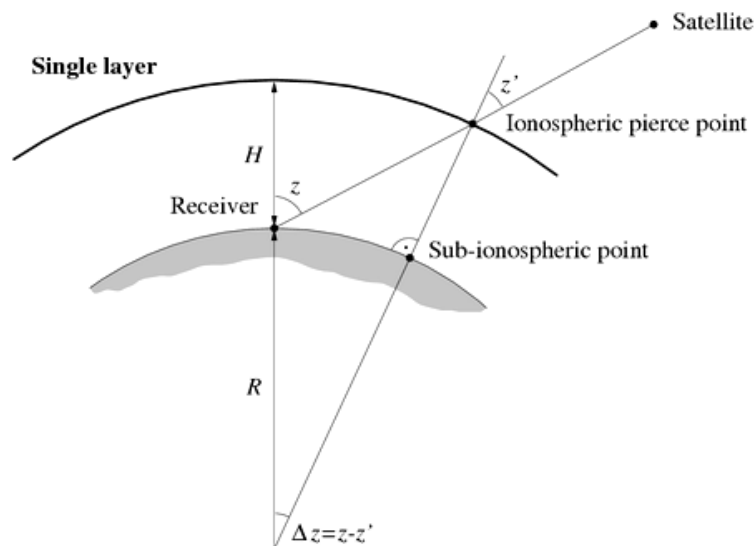
Figure 4.5: Single layer model for the ionosphere (after Schaer, 1999)

In Fig. 4.5, the ionospheric pierce point (IPP) is the intersection point of receiver-to-satellite line of sight with single layer, R is the mean earth radius, H is the single layer height, z and z' are zenith angles of the satellite at the receiver and the IPP respectively.

There are a few mapping functions which relate STEC and VTEC. The one that is used in this study is one of the most commonly used mapping functions, which is described, e.g., by Schaer (1999) or Dach et al. (2007):

$$F(z) = \frac{STEC}{VTEC} = \frac{1}{\cos z'} ,$$

(4.16)

with

$$\sin z' = \frac{R}{R+H} \sin z .$$

(4.17)

Note that VTEC is defined for the point IPP and have the same unit with STEC as TECU. Remember that, STEC is a measure of the integrated electron content between the satellite and the receiver. If STEC in Eq. (4.10) is replaced by Eq. (4.16):

$$\widetilde{P}_4 = VTEC \frac{F(z)}{\gamma} + br + bs + \varepsilon ,$$

(4.18)

where $\gamma = \dfrac{(f_1^2 f_2^2)}{40.3(f_2^2 - f_1^2)}$ and ε is the combined measurement noise on the carrier phase smoothed pseudorange ionospheric observable.

In order to compute IPP coordinates, thus the coordinates of the VTEC observation, following relations can be written by using the law of sines and cosines (Todhunter, 1863) for the spherical triangle formed by the North Pole, receiver and IPP (see Fig. 4.6):

$$\cos(90 - \varphi_{IPP}) = \cos(90 - \varphi_R).\cos(\Delta z) + \sin(90 - \varphi_R).\sin(\Delta z).\cos(A) , \quad (4.19)$$

$$\frac{\sin(A)}{\sin(90 - \varphi_{IPP})} = \frac{\sin(\lambda_{IPP} - \lambda_R)}{\sin(\Delta z)}, \qquad (4.20)$$

where A is the azimuth angle of the satellite as observed at the receiver location, λ_R and λ_{IPP} are geographic longitudes of the receiver location and IPP respectively, φ_R and φ_{IPP} are geographic latitudes of the receiver location and IPP respectively.
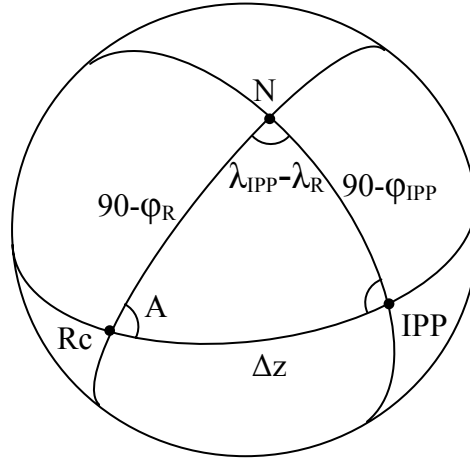
Figure 4.6: Spherical triangle formed by the North Pole (N), receiver (Rc) and ionospheric pierce point (IPP)

Geographic latitude and longitude for IPP can be computed from Eqs. (4.19) and (4.20) by:

$$\varphi_{IPP} = \sin^{-1}(\sin(\varphi_R).\cos(\Delta z) + \cos(\varphi_R).\sin(\Delta z).\cos(A)), \qquad (4.21)$$

$$\lambda_{IPP} = \lambda_R + \sin^{-1}(\frac{\sin(A).\sin(\Delta z)}{\cos(\varphi_{IPP})}). \qquad (4.22)$$

4.3 Ionosphere Modeling

The quantity to be modeled in this study is the VTEC of the ionosphere by using the ground-based GPS observations. If the smoothed pseudorange ionospheric observables are available with the methodology described in the previous parts of this chapter, and assuming that the DCB values for the GPS satellites are available from an external source, e.g. the IGS analysis centers, the fundamental observation equation can be obtained by Eq. (4.18):

$$\left(\widetilde{P}_4 - bs\right)\frac{\gamma}{F(z)} = VTEC + br\frac{\gamma}{F(z)} + \varepsilon \,, \tag{4.23}$$

where the left-hand side of the equation contains the calculated or known quantities, while the unknowns, i.e. VTEC and DCB values for the receivers, are placed on the right-hand side.

VTEC can be modeled in an Earth-fixed or a Sun-fixed reference frame. Ionosphere is highly variable in an Earth-fixed reference frame due to the diurnal motion of the Earth. Thus, the models in an Earth-fixed frame should either consider the time dependency or be used instantaneously, i.e. epoch-specific. However, ionosphere is much more stable in a Sun-fixed reference frame as the Sun is the main source for its ionization. Therefore, it can be assumed as static for a certain modeling period in a Sun-fixed reference frame (Schaer et al., 1995; Wielgosz et al. 2003).

In this study, the VTEC is modeled with three approaches:

1. 2D B-spline modeling depending on geodetic latitude and Sun-fixed longitude (geographic Sun-fixed frame),

2. 3D B-spline modeling depending on geodetic latitude, geodetic longitude and time (Earth-fixed frame),

3. 2D spherical harmonic modeling depending on geodetic latitude and Sun-fixed longitude (geographic Sun-fixed frame).

For all approaches, VTEC is split into two parts as suggested by Schmidt (2007):

$$VTEC = \overline{VTEC} + \Delta VTEC \,, \tag{4.24}$$

where $\overline{VTEC}$ is an approximate value or the reference and $\Delta VTEC$ is the correction term. $\overline{VTEC}$ can be computed from a given reference model like IRI, as proposed by Schmidt (2007). However, in this study it is computed from the low level solutions of the relevant methods. This approach has two apparent advantages:

- Dependency on the results of another model is prevented,

- The reference part will probably be closer to the final solution due to the low accuracy levels of the approximate models like IRI.

Using a reference that is not far from the final solution has two major benefits for a model. Firstly, for the regions with data gaps, reference part provides information. Secondly, in case of problems for the solution of correction term, e.g. due to numerical problems in parameter estimation stage, reference part may offer a firm base.

The fundamentals of B-spline modeling of the ionosphere, for both the electron density and VTEC modeling in an Earth-fixed reference frame, are presented by Schmidt (2007). Besides the modification proposed for the reference part calculation, adaptation of the B-spline approach for a Sun-fixed reference frame is

accomplished for the first time in this study. Note that the implementations of the 2D and 3D B-spline models are only appropriate for local and regional applications, since they are based on Euclidean theory.

Spherical harmonics are widely-used in ionosphere modeling in both global and regional scales with some small variations. In this study, the method that is described by Schaer et al. (1995) or Schaer (1999) is applied with the major modification that the VTEC is split into two parts as described above.

Before describing the modeling methodologies, assume that the Earth-fixed boundary values for the rectangular area under consideration, i.e. for the region to be modeled, is given by $[\lambda_{min}, \lambda_{max}] \times [\varphi_{min}, \varphi_{max}]$ in terms of geodetic longitudes and geodetic latitudes, respectively. Further it is assumed that the modeling will be performed for the time interval $[t_{min}, t_{max}]$, which will be valid for all models.

4.3.1 B-Spline Modeling

For VTEC modeling in this part, B-splines are used as basis functions. B-splines have some desired properties to be used as basis functions such as compact support, continuity, smoothness and computational efficiency (Fok and Ramsay, 2006). The normalized quadratic B-spline $N_{j,k}^m$ is calculated recursively by:

$$N_{j,k}^m(x) = \frac{x - t_k^j}{t_{k+m}^j - t_k^j} N_{j,k}^{m-1}(x) + \frac{t_{k+m+1}^j - x}{t_{k+m+1}^j - t_{k+1}^j} N_{j,k+1}^{m-1}(x). \qquad (4.25)$$

Note that, when their denominators are zero, the fractions should be set to zero in Eq. (4.25) (Stollnitz et al., 1995). The recursion starts with the initial values

$$N_{j,k}^0(x) = \begin{cases} 1 & \text{if} \quad t_k^j \le x < t_{k+1}^j \\ 0 & \text{otherwise} \end{cases}, \qquad (4.26)$$

46

where j is the level, $t_0^j, t_1^j, ..., t_{mj+2}^j$ is a sequence of non-decreasing values called knots and $mj=2^j+2$ (Schmidt, 2007).

For regional modeling, endpoint-interpolation on unit interval [0, 1] is applied for B-spline calculations to avoid edge effect at the boundaries, i.e. the first three knots are set to zero and the last three knots are set to one while the remaining knots are set to be equally spaced (Lyche and Schumacher, 2000; Stollnitz et al., 1995). Fig. 4.7 shows 1D B-spline functions for levels $J = 0$, $J = 1$ and $J = 2$. As the figure indicates, a B-spline is compactly supported, i.e. its value is zero out of a finite range. As the level is increased the B-spline functions becomes narrower so that finer details can be represented.
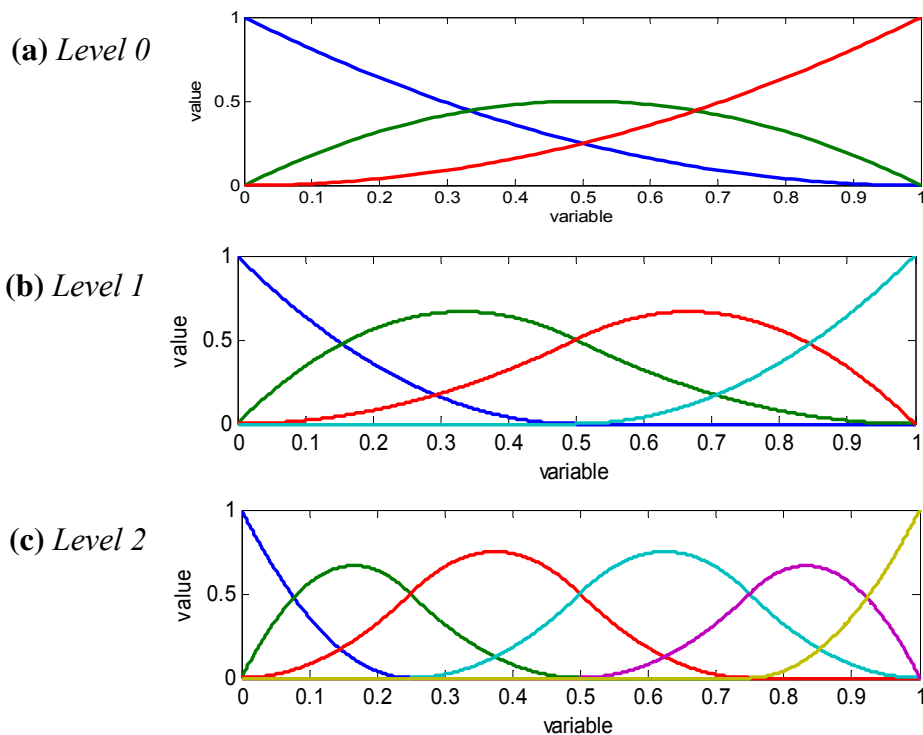
Figure 4.7: 1D B-spline scaling functions for level 0 (panel a), level 1 (panel b) and level 2 (panel c)

47

4.3.1.1 2D B-Spline Modeling

In 2D modeling, the ionosphere is represented as static in a Sun-fixed reference frame for the specified time interval $[t_{min}, t_{max}]$. At this stage, leaving the related explanation for later, it is assumed that the reference $\overline{VTEC}$ is computed beforehand. Thus, we have $VTEC - \overline{VTEC} = \Delta VTEC$ from Eq. (4.24). The correction term $\Delta VTEC$ is modeled by:

$$\Delta VTEC(s,\varphi) = \sum_{k1=0}^{mJ_1-1} \sum_{k2=0}^{mJ_2-1} d_{J_1 J_2, k_1 k_2} \phi_{J_1 J_2, k_1 k_2}(s,\varphi).$$

(4.27)

Here $\phi_{J_1 J_2, k_1 k_2}(s,\varphi)$ are two-dimensional scaling functions of the levels J_1 and J_2 with respect to the Sun-fixed longitude (s) and geodetic latitude (φ), $mJ_i = 2^{Ji} + 2$ and $d_{J_1 J_2, k_1 k_2}$ are unknown scaling coefficients (Schmidt, 2007).

The 2D scaling functions can be computed by applying the tensor product approach, i.e. separating the higher dimension scaling functions into the 1D scaling functions:

$$\phi_{J_1 J_2, k_1 k_2}(s,\varphi) = \phi_{J_1, k_1}(s)\phi_{J_2, k_2}(\varphi).$$

(4.28)

Herein $\phi_{J,k}(x)$ is a 1D scaling function of level J, shift k and variable x (Schmidt, 2007). In this study, the normalized quadratic B-spline $N^2(x)$ which is defined with Eqs. (4.25) and (4.26) is applied as the 1D scaling function, i.e. $\phi_{j,k}(x) = N_{j,k}^2(x)$. Sample 2D B-spline functions with different levels and shifts are shown in Fig. 4.8. As it was stated before in order to represent the finer details in VTEC the level can be increased. However, the number of scaling coefficients (unknowns) is also increased with increased number of scaling functions.

(a) $\phi_{2\,2,2\,3}(x,y)$ (b) $\phi_{3\,3,3\,4}(x,y)$
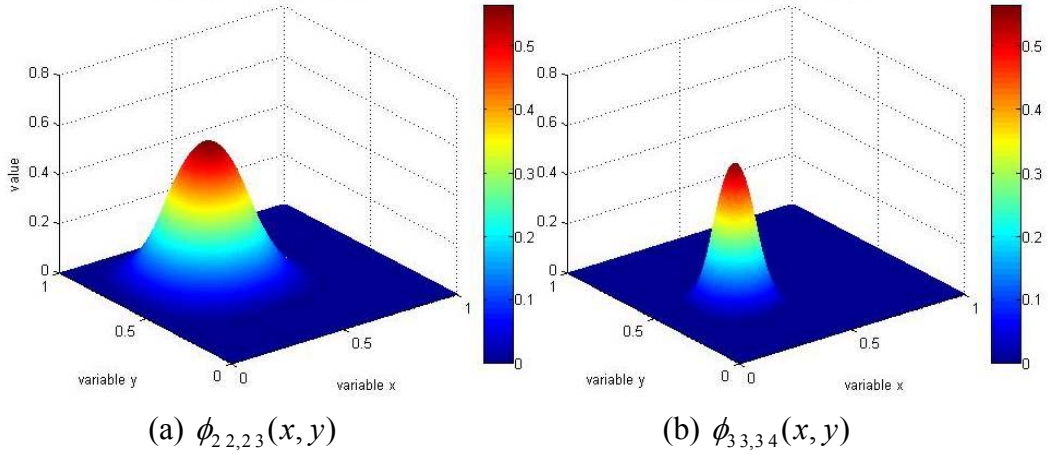
Figure 4.8: 2D B-spline scaling functions for
(a) $J_x = 2$, $J_y = 2$, $k_x = 2$, $k_y = 3$,
(b) $J_x = 3$, $J_y = 3$, $k_x = 3$, $k_y = 4$.

As stated before, the variable x for the scaling function $\phi_{j,k}(x)$ takes values between 0 and 1. Hence, the coordinates s and φ have to be transformed into the coordinates x and y via

$$x = \frac{s - s_{\min}}{s_{\max} - s_{\min}}, \quad y = \frac{\varphi - \varphi_{\min}}{\varphi_{\max} - \varphi_{\min}}, \qquad (4.29)$$

where the quantities $s_{\min}$, $s_{\max}$, $\varphi_{\min}$ and $\varphi_{\max}$ represents the boundary coordinates of the part of the ionosphere to be modeled in the Sun-fixed system. Note that, $s_{\min}$ and $s_{\max}$ are obtained by applying the conversion in Eq. (4.1) to $\lambda_{\min}$ at $t_{\min}$ and $\lambda_{\max}$ at $t_{\max}$, respectively.

After applying the tensor product approach (Eq. (4.28)) and the coordinate transformations (Eq. (4.29)), Eq. (4.27) becomes:

$$\Delta VTEC(x,y) = \sum_{k1=0}^{mJ_1-1} \sum_{k2=0}^{mJ_2-1} d_{J_1 J_2, k_1 k_2} \phi_{J_1, k_1}(x) \phi_{J_2, k_2}(y) \qquad (4.30)$$

The reference $\overline{VTEC}$ in Eq. (4.24) is computed with the same methodology for the correction term $\Delta VTEC$ computation as explained above (Eqs. (4.27) to (4.30)), but only taking the B-spline scaling function levels as 0 ($J_1 = J_2 = 0$) and dropping the correction term, i.e. $VTEC = \overline{VTEC}$.

4.3.1.2 3D B-Spline Modeling

For 3D modeling, ionosphere is represented in an Earth-fixed reference frame depending on geodetic latitude and geodetic longitude; besides a time variable is included in the model as a third dimension for temporal representation. Eq. (4.24) is expanded to 3D as follows:

$$\Delta VTEC(\lambda,\varphi,t) = \sum_{k1=0}^{mJ_1-1} \sum_{k2=0}^{mJ_2-1} \sum_{k3=0}^{mJ_3-1} d_{J_1 J_2 J_3, k_1 k_2 k_3} \phi_{J_1 J_2 J_3, k_1 k_2 k_3}(\lambda,\varphi,t),$$ (4.31)

where $\phi_{J_1 J_2 J_3, k_1 k_2 k_3}(\lambda,\varphi,t)$ are 3D B-spline scaling functions of levels J_1, J_2 and J_3 with respect to geodetic longitude (λ), geodetic latitude (φ) and time (t); see Schmidt et al. (2008).

The 3D scaling functions are again computed by the tensor product approach:

$$\phi_{J_1 J_2 J_3, k_1 k_2 k_3}(\lambda,\varphi,t) = \phi_{J_1,k_1}(\lambda)\phi_{J_2,k_2}(\varphi)\phi_{J_3,k_3}(t),$$ (4.32)

where the 1D scaling functions $\phi_{J,k}(x)$ are computed as described in the previous part.

For 3D modeling, the area under consideration is transformed into a cuboid and the coordinate transformations are performed as analogous to Eq. (4.29) including

the third dimension (t) with the variable z and the boundary values $t_{\min}$ and $t_{\max}$, i.e. the starting and ending epochs for the modeling interval. Note, that the boundary values for the longitudes are $\lambda_{\min}$ and $\lambda_{\max}$ for Eq. (4.29) as we now work in an Earth-fixed frame.

Finally, equation for the correction term is written as:

$$\Delta VTEC(x,y,z) = \sum_{k1=0}^{mJ_1-1} \sum_{k2=0}^{mJ_2-1} \sum_{k3=0}^{mJ_3-1} d_{J_1J_2J_3,k_1k_2k_3}\, \phi_{J_1,k_1}(x)\phi_{J_2,k_2}(y)\phi_{J_3,k_3}(z) \qquad (4.33)$$

For the reference $\overline{VTEC}$ computation the B-spline scaling function levels are set to 0 ($J_1 = J_2 = J_3 = 0$) and the correction term is dropped in Eq. (4.24) as it is applied in 2D case.

4.3.2 Spherical Harmonic Modeling

As analogous to the B-spline modeling, at first the expansion for the correction term into a series of spherical harmonic functions is derived for the time interval $[t_{\min}, t_{\max}]$:

$$\Delta VTEC(s,\varphi) = \sum_{n=0}^{n\max} \sum_{m=0}^{n} \widetilde{P}_{nm}(\sin\varphi)(a_{nm}\cos ms + b_{nm}\sin ms), \qquad (4.34)$$

where, n and m are the degree and order for the expansion with the maximum values $n_{\max}$ and $m_{\max}$, $\widetilde{P}_{nm} = \Lambda(n,m)P_{nm}$ are the normalized associated Legendre functions of degree n and order m, Λ is the normalization function, P_{nm} is the unnormalized Legendre function, a_{nm} and b_{nm} are the unknown spherical harmonic coefficients (Schaer et al., 1995). Note that m is expanded up to minimum of n or m_{max}.

The normalization function is given as:

$$\Lambda(n,m) = \sqrt{\frac{(n-m)!(2n+1)(2-\delta_{0m})}{(n+m)!}} \,, \tag{4.35}$$

where δ is the Kronecker Delta. The number of unknown coefficients a_{nm} and b_{nm} can be computed by:

$$n_c = (n_{max}+1)^2 - (n_{max}-m_{max})(n_{max}-m_{max}+1) \,, \tag{4.36}$$

The reference $\overline{VTEC}$ is also computed with Eqs. (4.34) and (4.35), taking the maximum degree and order as 1 ($n_{max} = m_{max} = 1$).

4.4 Parameter Estimation

The fundamental observation equation (4.23), for both the reference and correction computations of all models, constitutes a linear system of equations (Koch, 1999):

$$\boldsymbol{y} + \boldsymbol{e} = \boldsymbol{X}_1\boldsymbol{\beta}_1 + \boldsymbol{X}_2\boldsymbol{\beta}_2 \qquad \text{with} \quad D(\boldsymbol{y}) = \sigma^2(\boldsymbol{P}^{-1}) \tag{4.37}$$

where $\boldsymbol{y}$ is the vector of observations, $\boldsymbol{e}$ is the vector of observation errors, $\boldsymbol{X_1}$ is the coefficient matrix comprising the function values of the related model, $\boldsymbol{\beta_1}$ is the parameter vector in terms of unknown model coefficients, $\boldsymbol{X_2}$ is the coefficient matrix for DCB values of the receivers, $\boldsymbol{\beta_2}$ is the parameter vector of either the unknown DCB values of the receivers (for reference term computations) or the corrections for the DCBs (for correction term computations), $D(\boldsymbol{y})$ is the variance-covariance matrix of observations, σ^2 is an unknown variance factor and $\boldsymbol{P}$ is the weight matrix of the observations. Note that for reference ($\overline{VTEC}$) computations, the observation vector $\boldsymbol{y}$ is equal to the VTEC observations, i.e. $y_i = VTEC_i$, and it

is equal to the difference between the VTEC observations and the reference ($y_i = VTEC_i - \overline{VTEC_i}$) for the calculation of correction terms ($\Delta VTEC$) for all models. Also note that the parameter vector for the DCB values ($\boldsymbol{\beta_2}$) includes code biases between C1 and P2 (DCB_{C1P2}) for C1/P2 receiver models since the ionospheric observables for this receiver class are constituted by the combination of C1 and P2 pseudorange observables. For the other receiver classes (P1/P2 and P1/X2) the unknown differential biases are DCB values between P1 and P2 (DCB_{P1P2}).

The coefficient matrices and parameter vectors can be combined:

$$\boldsymbol{y} + \boldsymbol{e} = \overline{\boldsymbol{X}}\,\overline{\boldsymbol{\beta}} \qquad \text{with} \qquad D(\boldsymbol{y}) = \sigma^2(\boldsymbol{P}^{-1}), \qquad (4.38)$$

where $\overline{\boldsymbol{X}} = |\boldsymbol{X_1} \vdots \boldsymbol{X_2}|$ and $\overline{\boldsymbol{\beta}} = \begin{vmatrix} \boldsymbol{\beta_1} \\ \cdots \\ \boldsymbol{\beta_2} \end{vmatrix}$. This system can further be simplified to a one

where the observations are uncorrelated and have equal weights as described by Koch (1999):

$$\boldsymbol{y_w} + \boldsymbol{e_w} = \overline{\boldsymbol{X}}_w \overline{\boldsymbol{\beta}} \qquad \text{with} \qquad D(\boldsymbol{y}) = \sigma^2(\boldsymbol{I}^{-1}), \qquad (4.39)$$

where $\boldsymbol{y_w} = \boldsymbol{G}^T \boldsymbol{y}$, $\boldsymbol{e_w} = \boldsymbol{G}^T \boldsymbol{e}$, $\overline{\boldsymbol{X}}_w = \boldsymbol{G}^T \overline{\boldsymbol{X}}$, $\boldsymbol{I}$ is the identity matrix and $\boldsymbol{G}$ denotes a regular lower triangular matrix as a product of Cholesky factorization of the weight matrix $\boldsymbol{P}$, i.e. $\boldsymbol{P} = \boldsymbol{G}\boldsymbol{G}^T$.

The linear system (4.36) should be solved for unknown parameters with appropriate parameter estimation methods.

4.4.1 Least Square Estimation

Probably the most widely-used parameter estimation method is the method of least squares where the unknown parameters are solved by minimizing the sum of the squares of the deviations of the observations from the estimators of their expected values. In other words, method of least squares minimizes the 2-norm of the residual vector to estimate the unknown parameters, where the residual vector is given by:

$$\hat{e} = X\hat{\beta} - y, \tag{4.40}$$

in which $\hat{\beta}$ denotes the estimator vector for the parameters that is computed by the method of least squares for a system with uncorrelated and equally weighted observations as (Koch, 1999):

$$\hat{\beta} = (X^T X)^{-1} X^T y. \tag{4.41}$$

The estimator of the covariance matrix of estimated parameters is given by:

$$\hat{D}(\hat{\beta}) = \hat{\sigma}^2 (X^T X)^{-1}. \tag{4.42}$$

In Eq. (4.42), $\hat{\sigma}^2$ is the unbiased estimated variance of unit weight which is computed by:

$$\hat{\sigma}^2 = \frac{\hat{e}^T \hat{e}}{n-u}, \tag{4.43}$$

where n is the number of observations and u is the number of unknowns (parameters).

4.4.2 Robust Regression

Least squares estimation is extensively used for the solution of linear system of equations. However, this method is sensitive to outliers, which if included in the observation data may distort the estimation of the parameters. One remedy is to detect and remove these data from the least squares estimation. Alternatively, a robust parameter estimation, which is insensitive to outliers, can be employed (Koch, 1999).

In this study, as an alternative to the method of least squares, a robust regression algorithm, namely Iteratively Re-weighted Least Squares (IRLS) with a bi-square weighting function is employed for parameter estimation in order to reduce the effects of outliers. As its name implies, IRLS is an iterative method where at each iteration level the observations are re-weighted depending on the residuals from the previous iteration. This algorithm gives lower weights to the observations that do not fit to the model well.

In this study, a bi-square weighting function is used for IRLS, which is given as:

$$p_B(\hat{e}_i) = \begin{cases} \left[1 - \left(\dfrac{\hat{e}_i}{k\hat{\sigma}} \right)^2 \right]^2 & \text{for} \quad |\hat{e}_i| < k\hat{\sigma} \\ 0 & \text{otherwise} \end{cases} \qquad (4.44)$$

where $\hat{e}_i$ is the residual for observation i, k is the tuning constant which is equal to 4.685 and $\hat{\sigma}$ is an estimate for the standard deviation of the residuals which is commonly taken as $\hat{\sigma} = \text{MAD}/0.6745$, where MAD is the median absolute deviation of the residuals (Cummins and Andrews, 1995).

The robust regression algorithm starts with the computation of parameters and residuals for Eq. (4.39) by applying least squares estimation. At each iteration

level, standardized residuals are calculated as suggested by DuMouchel and O'Brien (1989):

$$\hat{e}_{adj} = \frac{\hat{e}_i}{\sqrt{1 - h_i}} \,, \tag{4.45}$$

where h_i are *leverages* which can be computed as the diagonal elements of the hat matrix $\boldsymbol{H}$ (Koch, 1999):

$$\boldsymbol{H} = \boldsymbol{X}(\boldsymbol{X}^T\boldsymbol{X})^{-1}\boldsymbol{X}^T, \qquad h_i = \boldsymbol{H}_{ii}\,. \tag{4.46}$$

At this point, new weights for each observation are computed with the weighting function given in Eq. (4.44) by replacing the residuals with standardized residuals. Thus, for each iteration a new weighted linear system of equations, i.e. Eq. (4.38), is obtained. This system is transformed into its simplified form (4.39) as described before. The iteration steps for IRLS are repeated until the estimated parameters converge.

4.4.3 Regularization

The linear system that is given in Eq. (4.39) may become ill-conditioned as a consequence of non-uniform data distribution. In other words, observations may be sparse to compute some of the model coefficients in a reliable way. For such a system the least squares solution is potentially sensitive to the perturbations in the observations. For the VTEC models that are used in the study, the linear systems for the computation of reference terms, i.e. the low-level solutions, are stable as the model functions covers wide regions. Therefore, parameter estimation process for reference terms does not comprise regularization algorithms and related solution is obtained with only the least square estimation or robust regression algorithm IRLS without regularization. However, as the level of the model

functions are increased for the computation of correction terms for the same set, the tendency of the system to be ill-conditioned is also increased. Thus, regularization methods should be incorporated to stabilize the solutions for the correction terms.

An important point should be mentioned here for the joint use of robust regression and regularization algorithms. As it will be described in the following sections regularization process introduces new side constraints for the system. Since IRLS introduces new weights for the observations for each iteration of the algorithm, the linear system for regularization process alters at each iteration level. Due to this fact, the convergence for IRLS may be so slow or even may not be possible when it is applied together with regularization algorithms. For this reason, the iterative structure of the robust regression algorithm is only applied for the computation of reference terms. Regularization algorithms are not applied for reference term computations as it was stated before. On the other hand, for the robust solution of correction terms, the weights that were obtained from the last iteration of reference term computations are applied for the observations.

4.4.3.1 Tikhonov Regularization

One of the most common methods for regularization is Tikhonov regularization where the minimizer for the least squares, i.e. the 2-norm of the residual vector, is replaced by $\left(\left\| \hat{e} \right\|_2 + \lambda_r^2 \left\| \hat{\beta} \right\|_2 \right)$. Here, λ_r is the regularization parameter which controls the weight given to the minimization of the side constraint, i.e. the solution norm, relative to the minimization of the residual norm (Hansen, 1994). The corresponding solution for the parameters is:

$$\hat{\boldsymbol{\beta}}_\lambda = (\boldsymbol{X}^T \boldsymbol{X} + \lambda_r^2 \boldsymbol{I})^{-1} \boldsymbol{X}^T \boldsymbol{y}, \tag{4.47}$$

where $\hat{\boldsymbol{\beta}}_\lambda$ denotes the regularized solution.

4.4.3.2 LSQR

Direct regularization methods, e.g. Tikhonov's method, are extensively used in order to stabilize the solution of ill-conditioned systems. However, these methods may become impractical due to storage problems if the system is very large, as they may require great deal of computer memory (Aster et al., 2005).

In case there exist memory problems due to the number of observations and/or number of model coefficients, an alternative iterative method, namely LSQR, is also used in the study. LSQR is a variant of the well-known Conjugate Gradient (CG) method to be applied to the normal equations. LSQR stores only a few vectors, besides the coefficient matrix and the observation vector, and updates these vectors at each iteration level. This structure of LSQR allows solving extremely large problems without matrix decomposition. Interested readers can see the algorithm for LSQR in Paige and Saunders (1982). In addition, LSQR performs a regularization effect on ill-conditioned problems where the iteration number designates the amount of regularization (Hansen, 1994). As the number of iterations is increased, the amount of regularization decreases, which indicates that the maximum regularization is achieved at the first iteration. Unfortunately, like the other iterative inverse problem solvers, LSQR does not provide the variance-covariance matrix of model parameters. However, an approximate solution for the variance-covariance matrix is available by modifying the LSQR algorithm as described, e.g., by Yao et al. (1999).

4.4.3.3 Regularization Parameter Selection

Selection of the appropriate regularization parameter is of vital importance for all regularization methods. In this study, two alternate methods are used for this purpose.

A convenient method to select the appropriate value of the regularization parameter for regularization methods is the L-curve, which is an L-shaped plot of the regularized solution norm ($\left\| \boldsymbol{\beta}_{\lambda} \right\|_2$) versus the residual norm ($\left\| \boldsymbol{X}\boldsymbol{\beta}_{\lambda} - \boldsymbol{y} \right\|_2$) in log-log scale. The corner of the L-curve can be located as an approximation to the optimal regularization parameter (Hansen, 1994). The generic form of the L-curve is provided in Fig. 4.9.
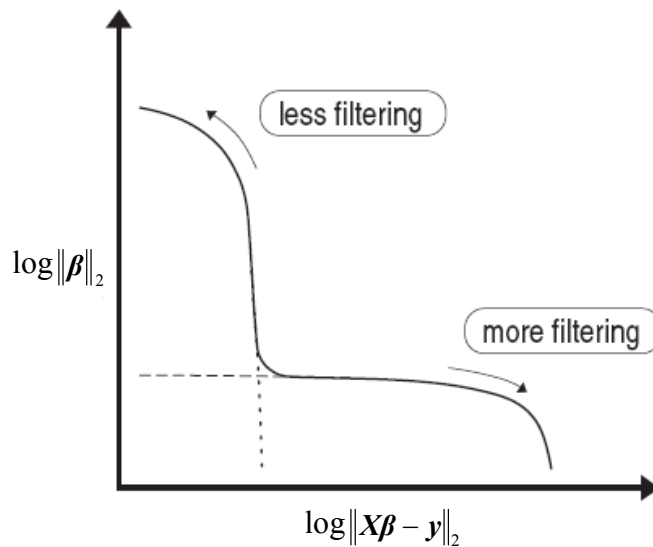
Figure 4.9: The generic form of the L-curve (after Hansen, 1994)

The second method that is used for choosing the regularization parameter in the study is the generalized cross-validation (GCV). With this method the

regularization parameter which minimizes the GCV function is selected as the optimum regularization parameter. The GCV function $G(\lambda_r)$ is defined as:

$$G(\lambda_r) = \frac{\|X\boldsymbol{\beta}_\lambda - \boldsymbol{y}\|_2}{\text{Trace}(\boldsymbol{I} - \boldsymbol{XX}^I)} \qquad (4.48)$$

where $\boldsymbol{X}^I$ is a matrix that produces the regularized solution ($\boldsymbol{\beta}_\lambda$) when multiplied with the observation vector ($\boldsymbol{y}$).

There are some other methods for the selection of the regularization parameter, such as the discrepancy principle, which, in general, require a good estimate for the magnitude of the error in the system. These methods have not been used within the study, since such an estimate is not apparent due to the data sources of different types of GPS receivers.

CHAPTER 5

TECmapper: AN IONOSPHERE MODELING TOOL

5.1 Programming Environment

TECmapper was developed in MATLAB® environment. "MATLAB is a high-performance language for technical computing. It integrates computation, visualization, and programming in an easy-to-use environment where problems and solutions are expressed in familiar mathematical notation. Typical uses include:

- Math and computation,

- Algorithm development,

- Data acquisition,

- Modeling, simulation, and prototyping,

- Data analysis, exploration, and visualization,

- Scientific and engineering graphics,

- Application development, including graphical user interface building.

MATLAB is an interactive system whose basic data element is an array that does not require dimensioning. This allows solving many technical computing problems, especially those with matrix and vector formulations, in a fraction of the

time it would take to write a program in a scalar noninteractive language such as C or Fortran" (The MathWorks Inc., 2004).

5.2 TECmapper

In order to run TECmapper, MATLAB should be installed in the related computer. Installation of MATLAB core files is sufficient as TECmapper does not use MATLAB toolboxes. TECmapper is compatible with MATLAB versions 7.x and has not been tested for the previous versions.

TECmapper consists of 44 files with the total size of 246 KB. Before running the software, TECmapper files should be extracted into same folder of the operating system. A typical Windows® folder that contains the software files is presented in Fig. 5.1.

TECmapper can be run within MATLAB simply typing "*TECmapper*" in the MATLAB's command window. This opens the main window of TECmapper (Fig. 5.2) with the pushbuttons to reach following functions of the software:

- Import observation file,

- Extract TEC information,

- Ionosphere modeling,

- Create GIM map,

which will be described in the subsequent sections.
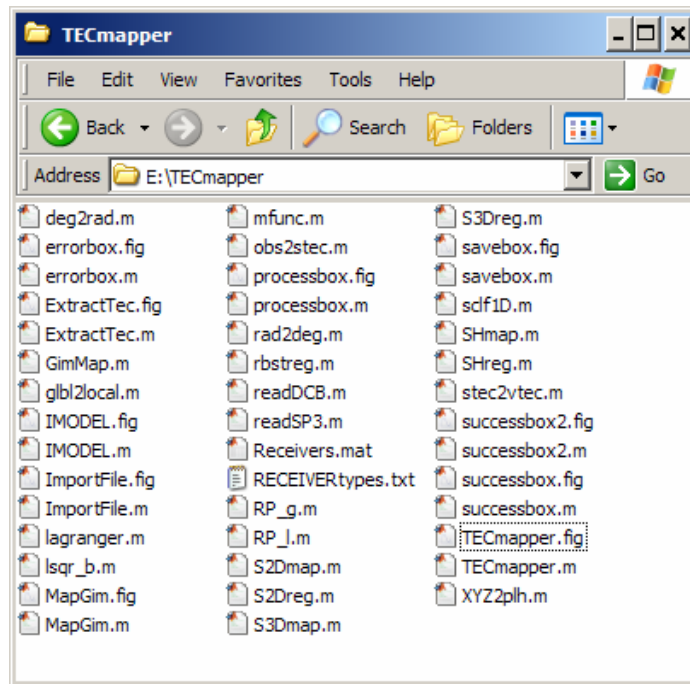
Figure 5.1: A typical Windows folder that contains TECmapper files
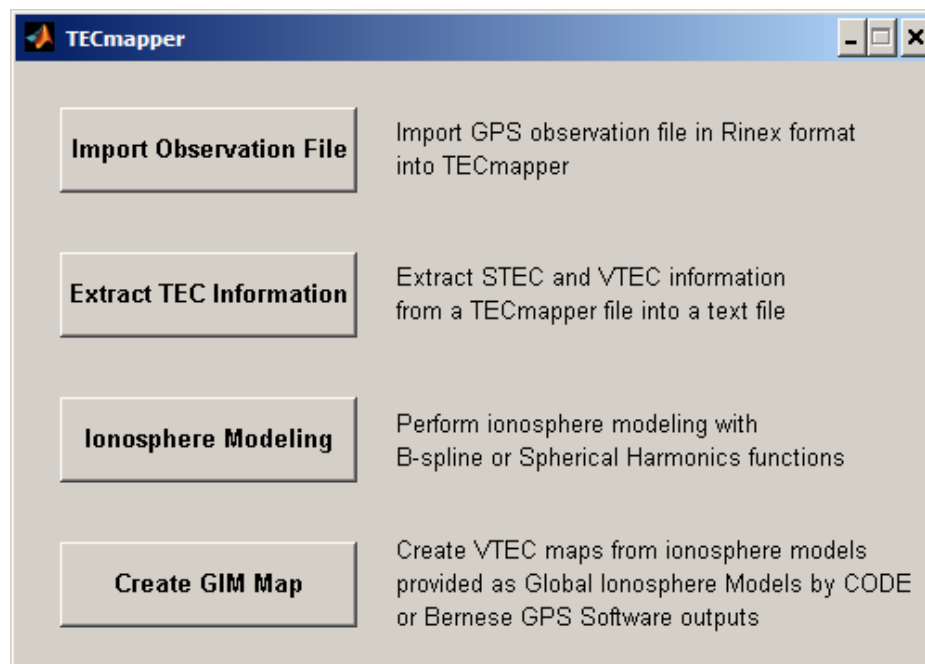
Figure 5.2: Main window of TECmapper

5.2.1 Importing Ground-based GPS Observation Files

With this function GPS observation files in RINEX 2.x format are imported into the TECmapper format. The graphical user interface for "Import File" function is given in Fig. 5.3.
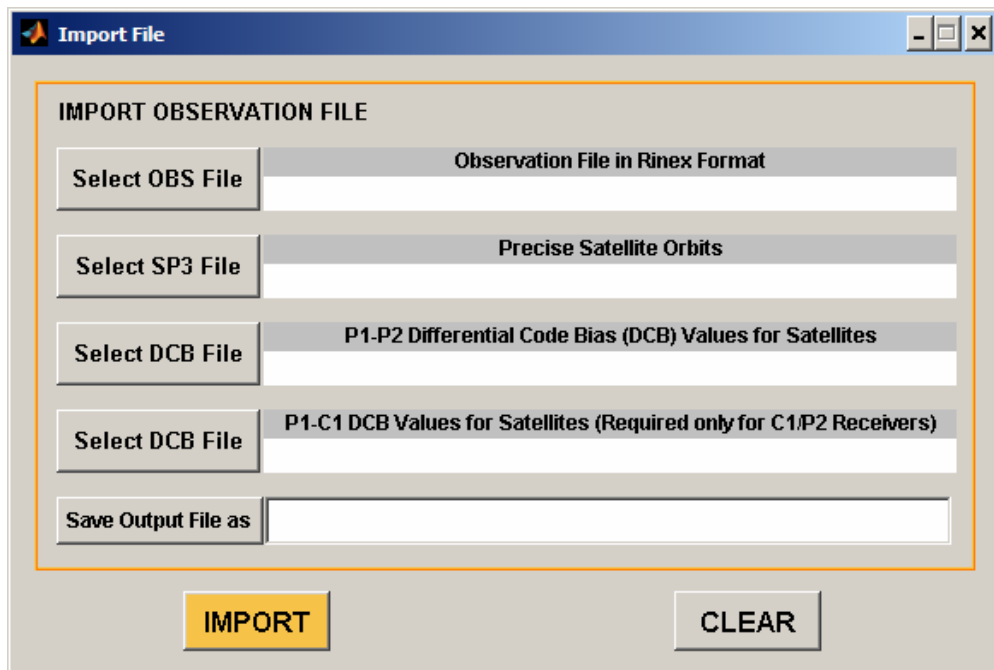
Figure 5.3: The graphical user interface for "Import File" function

The GPS observation file to be imported, precise orbit file for the GPS satellites in SP3 format for the related date, the text file including P1-P2 DCB values for the satellites and output file should be defined within this window. Precise orbit and DCB files are freely available by the IGS through internet as stated in previous chapters. Clicking the "import" pushbutton starts the process to produce a binary output file in the internal format of TECmapper with the file extension "tec". Note that the file for P1-C1 DCB values for the satellites is optional and required only for the receiver classes of C1/P2. The receiver classes for 70 GPS receiver types

have been defined within the software. Having determined the type of the receiver under consideration from the header record of its observation file, the software checks the class of the receiver and the user is warned to define P1-C1 DCB file for C1/P2 receivers (Fig 5.4), if it is not introduced before the import process. The list for the defined receiver classes, which is obtained from the source code of the Bernese GPS Software v5.0, is provided in Appendix A.
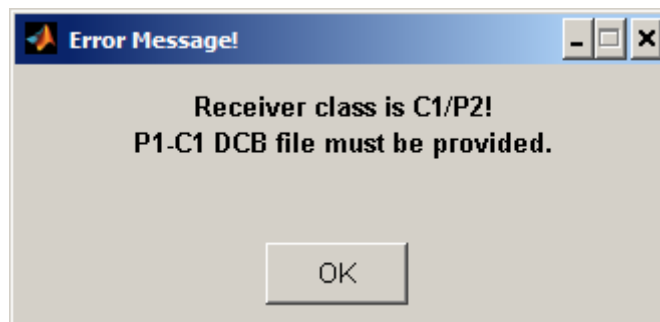
Figure 5.4: Error message if P1-C1 DCB file is not defined within
"Import File" function for C1/P2 receivers

Besides the receiver type, the data for the approximate position of the receiver, types of available observables and time for the first observation are read and saved from the header of the observation file. After the header record, all valid pseudorange and carrier phase observations until the end of the file and their epochs are read and grouped for their satellite number. Note that the RINEX file should contain the observations of the same day. Each observation epoch is compared with the time for the first observation record and the import processes is interrupted with an error message (Fig. 5.4) in case of an inconsistency.

The satellite coordinates for each valid observation epoch are interpolated from the precise orbit file using Lagrange's formula for polynomial interpolation. These coordinates with the coordinates of the receiver are used to determine azimuth and zenith angles of the satellites.
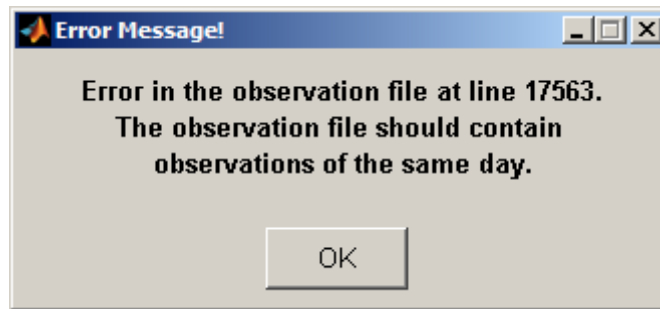
Figure 5.5: Sample error message for an observation file containing observations from different days

After successfully reading the file until the end, observations of each satellite are checked for possible cycle slips and continuous observation arcs are defined. Then, for each continuous arc geometry-free linear combination of observables are calculated. Pseudorange ionospheric observables are smoothed with the carrier to code leveling process. Smoothed ionospheric observables are then corrected with satellite DCBs and they are saved with other information such as the date for the observation file, azimuth and zenith angles and epoch info for each observation and receiver position in the output file. The user is informed with a dialog box after a successful run (Fig. 5.6).
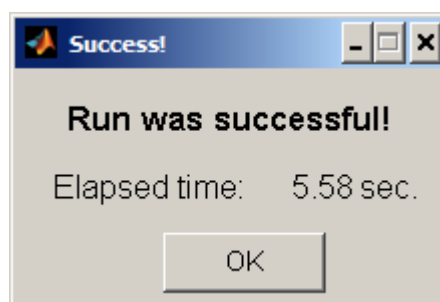
Figure 5.6: Dialog box after a successful run of "Import File" function

5.2.2 Extracting STEC and VTEC Information into a Text File

The user can convert an imported observation file into a text file containing STEC and VTEC information for each observation with this function. The window for "Extract TEC Information" function is provided in Fig. 5.7.
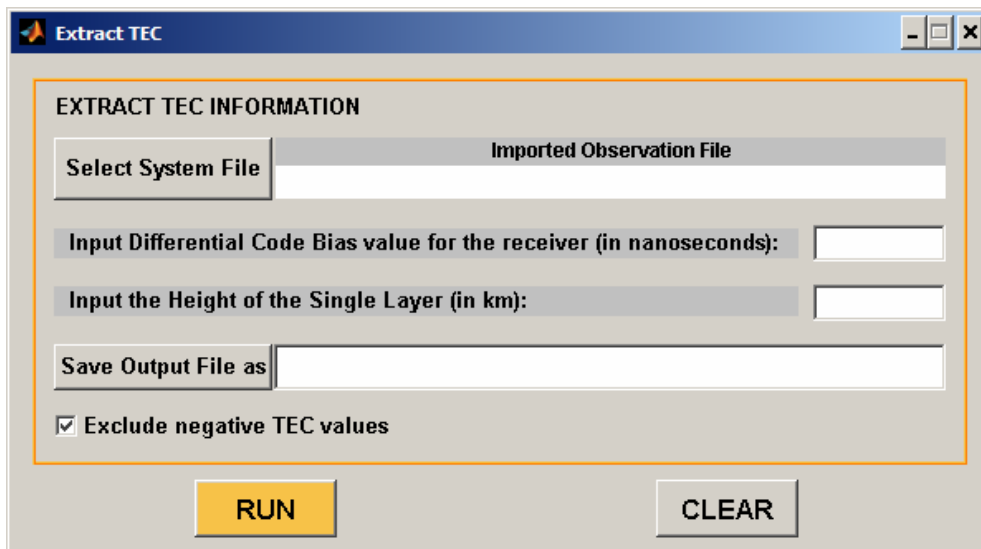
Figure 5.7: The graphical user interface for "Extract TEC Information" function

Remember from the previous chapter that in order to derive STEC from an ionospheric observable, DCB values for the satellite and the receiver are needed. The ionospheric observables in the TECmapper system file are corrected for satellite DCBs during the import process but they are still biased with receiver DCBs. The user should provide DCB value of the related receiver which can be obtained from an external source (e.g. for IGS stations) or can be calculated within the ionosphere modeling stage by TECmapper. The only necessary information to convert STEC to VTEC by means of the mapping function is the height of the single layer, which should be defined by the user. Theoretically, neither the STEC nor the VTEC values can be negative. If exist, negative values are probably due to

measurement noises and they can be excluded from the output file by simply checking the related box in the function window.

The resulting output file comprises STEC value with its azimuth and zenith angles, VTEC value with its geodetic latitude and longitude (i.e. the geodetic coordinates of the IPP) and observed satellite number for each observation, besides the position of the receiver and date information for the observation file. First page of a sample output file from "Extract TEC Information" function is provided in Appendix B.

5.2.3 Ionosphere Modeling

The main task of the software is accomplished by this unit. The user can select one of the three VTEC modeling methods: 2D B-splines, 3D B-splines and spherical harmonics. For any of the methods, following information should be defined within the window of the ionosphere modeling unit:

- Level values for B-spline models or maximum degree and order for spherical harmonic model,

- Modeling date,

- Height of the single layer,

- Cut-off angle for the observations,

- List of the system files, i.e. the imported observation files, that will be used for the model,

- Boundary values for the modeling area and modeling interval in terms of minimum and maximum values of the latitude, longitude and time,

- Epoch(s) for which VTEC maps will be generated,

- Grid interval in latitude and longitude directions for reference points that will be used to generate VTEC maps.

Optionally, limits for color scale of VTEC maps can also be specified. Initial state of the ionosphere modeling window is presented in Fig. 5.8.
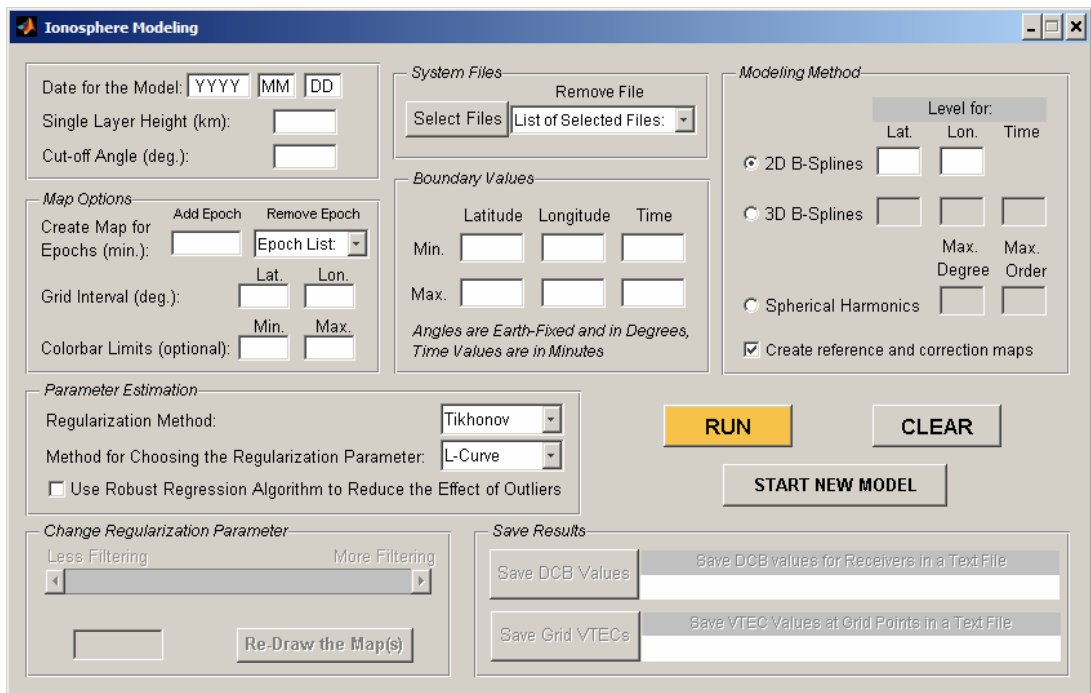
Figure 5.8: The graphical user interface for "Ionosphere Modeling" function

Immediately after the click of run button, the software performs several checks on the provided information, and if any, the user is warned for inappropriate data. Some of the error windows that orientate the user for proper data input are given in Appendix C.

The user can manipulate the parameter estimation stage of the ionosphere modeling process by the option to use the robust regression algorithm (IRLS) instead of least squares adjustment. Besides, Tikhonov or LSQR for regularization

69

method and L-curve or GCV methods for selection of the regularization parameter can be optionally specified by the user. A sample VTEC map window as a product of the ionosphere modeling process is given in Fig. 5.9. The map windows include the root mean square error (RMSE) values for the related solutions which are computed as the square root of the average of the residual squares. RMSE, or root mean square deviation (RMSD), is a frequently-used measure of the differences between the values predicted by a model and the observations where the residuals are the differences between the observed data and fitted model. The user has the possibility to exclude reference and correction maps from the map window. Note that although the modeling tasks for 2D B-spline and spherical harmonic models are performed in the geographic Sun-fixed reference frame, the resulting maps are provided in the Earth-fixed reference frame by TECmapper.
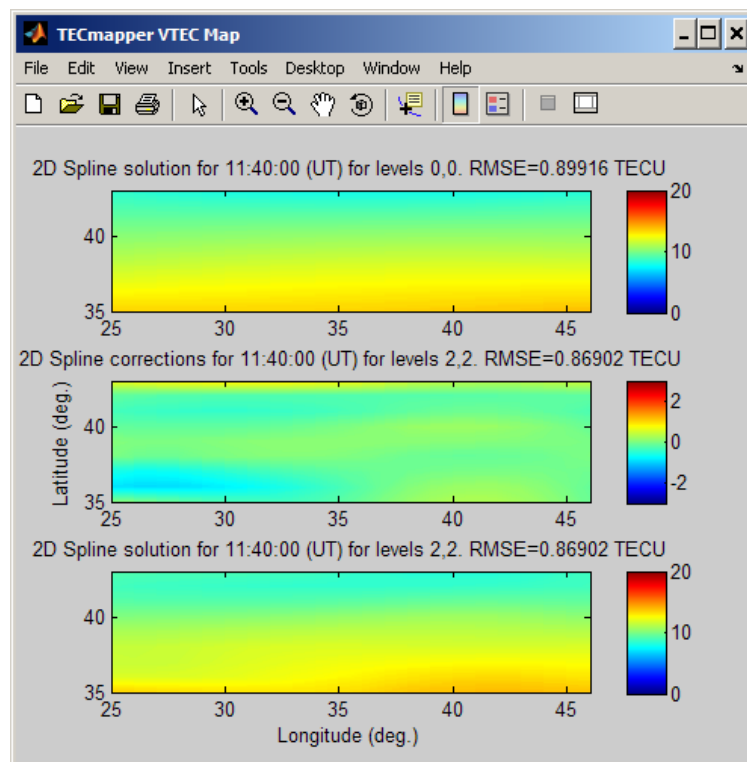
Figure 5.9: A sample VTEC map window generated by "Ionosphere Modeling" function

The methods for the selection of the regularization parameter, i.e. L-curve and GCV, may frequently produce unsatisfactory results. As a consequence of inappropriate regularization parameter, VTEC maps may represent sharp variations. In such a case, the regularization parameter can be altered via interactively operating slider bar or text box in order to change the amount of filtering on the map. Remember that the amount of filtering is enhanced by increasing the regularization parameter for Tikhonov regularization while the maximum amount of regularization for LSQR is achieved at its first iteration.

After a successful run, the software allows the user to save calculated DCB values for the receivers and VTEC values at the specified grid points in separate text files. Sample DCB and grid files are given in appendices D and E, respectively.

5.2.4 Generating VTEC Maps from Global Ionosphere Models

The Bernese GPS Software uses spherical harmonic functions to represent VTEC globally or regionally. VTEC can be modeled in static or dynamic modes in a geographic Sun-fixed or a geomagnetic reference frame within the Bernese Software. The dynamic mode refers to the time-dependent representation of VTEC with piecewise-linear spherical harmonic coefficients while in the static mode VTEC is modeled with constant parameters. Details can be seen in Dach et al. (2007). The Bernese Software can present VTEC model results by means of files in the IONEX (IONosphere map Exchange) format and the ionosphere model files with "ion" extension. The latter contains the related information for the settings of the modeling task besides the calculated spherical harmonic coefficients of the VTEC representation.

Being one of the IGS analysis centers, CODE (Center for Orbit Determination in Europe) performs its global VTEC modeling tasks with the Bernese GPS Software. Besides the Global Ionosphere Maps in IONEX format with a resolution

of 2 hr, 5º and 2.5º in time, longitude and latitude respectively, the CODE analysis center provides daily Global Ionosphere Model files with "ion" extension which are outputs of the Bernese Software. Currently, the Global Ionosphere Models of CODE are produced in dynamic mode with spherical harmonic coefficients up to maximum degree and order of 15 (for both) depending on the geomagnetic reference frame. It may be useful to emphasize that the Global Ionosphere Maps and the Global Ionosphere Models differ in content and format. While the former include VTEC values and their accuracies at specified grid points, the latter contain the calculated coefficients for spherical harmonic representation.

In general, the resolution of the IONEX formatted Global Ionosphere Maps is not satisfactory to represent the highly variable (both spatially and temporarily) structure of the ionosphere as discussed before. On the other hand, the spherical harmonic coefficients provided via the Global Ionosphere Models, or the ionosphere models of the Bernese Software in general, are not so meaningful without related software to extract VTEC information from these coefficients.

TECmapper was included a function to generate VTEC maps for desired epochs and to save VTEC values at user specified grid points from the ionosphere models of the Bernese GPS Software and thus from the CODE's Global Ionosphere Models. This unit can utilize static or dynamic ionosphere models produced in the geographic Sun-fixed or the geomagnetic reference frames by the Bernese Software. All model related information is obtained from the ionosphere model file. The user should only provide the mapping options such as the boundary values, grid interval and epoch(s) for the VTEC map(s) to be generated via the graphical user interface which is given in Fig. 5.10.

The VTEC maps generated by this function are presented in the Earth-fixed reference frame. A sample VTEC map is given in Fig. 5.11. VTEC values within the map boundaries at the user-defined grid intervals can be saved in a text file. This file is very similar in format to the one which is presented in Appendix E.
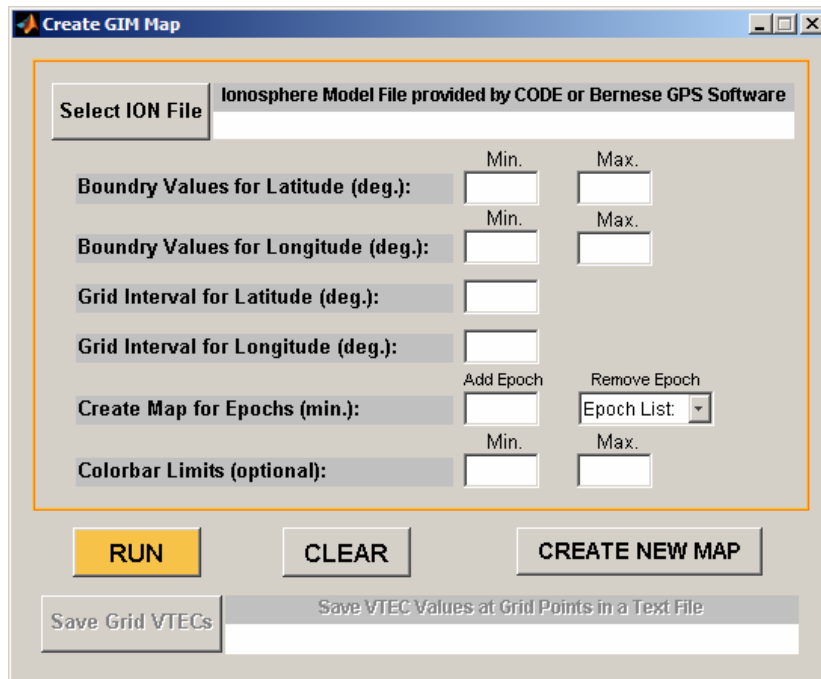
Figure 5.10: The graphical user interface for "Create GIM Map" function
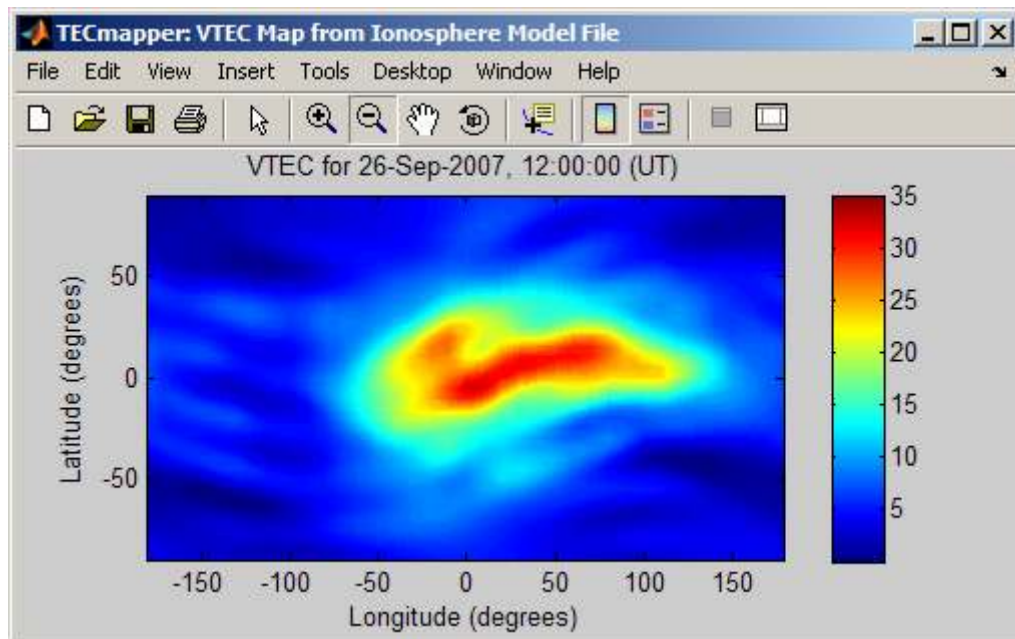
Figure 5.11: A sample VTEC map window generated by
"Create GIM Map" function

CHAPTER 6

APPLICATION

6.1 Application Data

In order to evaluate the performance of TECmapper and the models it uses with real data, observations of 27 ground-based dual-frequency GPS receivers located over Turkey were used. The data belong to date 26.09.2007 and have a 30 sec. sampling interval. Fig. 6.1 demonstrates the distribution of the GPS sites that were used in the study. The data for all stations regarding the receiver types, receiver classes and ellipsoidal geographic coordinates that are computed from the header record of the observation files are provided in Appendix F.
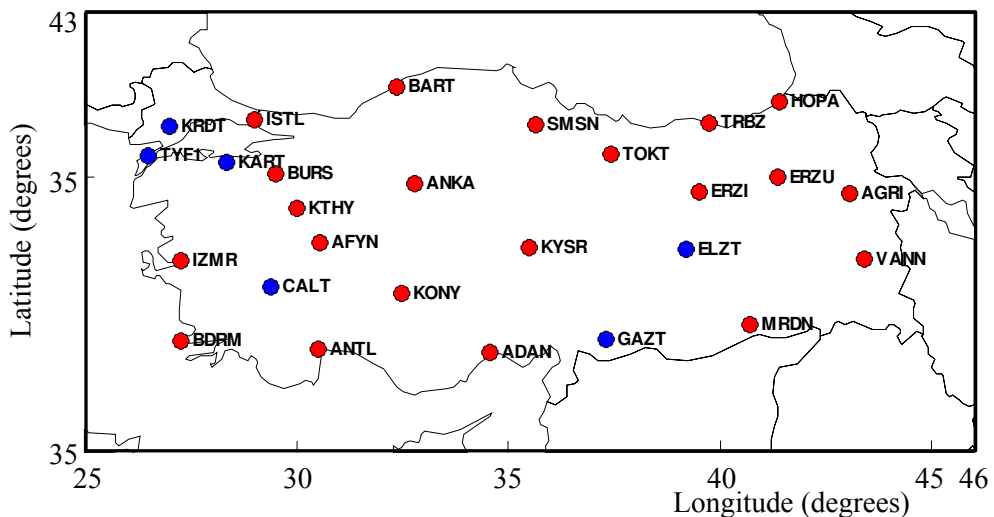
Figure 6.1: Geometry of 27 GPS stations that were used in the study

Observations for the stations that are marked as red were obtained within the content of a project that was supported by the Scientific and Technological Research Council of Turkey (TÜBİTAK). Observations for the other stations (marked as blue) were provided by TÜBİTAK-MAM (Marmara Research Center) from their permanent networks.

The DCB values for the satellites which are introduced to Eq. (4.23) as known quantities and the precise orbit files comprising the daily Cartesian coordinates of the GPS satellites at each 15 minutes were obtained from the CODE analysis center through the internet. The rectangular region between $25° – 46°$ in geodetic longitudes and $35° – 43°$ in geodetic latitudes was chosen as the modeling area by considering the distribution of the GPS sites.

6.2 VTEC Modeling for Varying Model Levels

For the first part of the application, the data corresponding to 12:00:00 – 13:00:00 (UT) time slice was selected as test case since it was one of the most active periods of the ionosphere over Turkey during the selected day. A single layer height of 400 km and an elevation cut-off angle of $15°$ were employed for the calculations. VTEC was modeled for the mentioned period with TECmapper using the methods 2D B-splines, 3D B-splines and spherical harmonics for varying model levels.

The 2D B-spline solution for the levels $J_1 = 0$ and $J_2 = 0$ (B-spline levels for the Sun-fixed longitude and geodetic latitude, respectively) has 9 coefficients (= $(2^0+2)^2$) and this solution is also the reference ($\overline{VTEC}$) for the higher level solutions. As stated before, TECmapper provides root-mean-square error (RMSE) values as a measure of regression accuracy, which are computed as the square root of the average of the residual squares. For the reference solution the RMSE value is 1.1696. The RMSE values for the correction terms ($\Delta VTEC$) for three sets of

solution levels of (1) $J_1 = 1$, $J_2 = 1$, (2) $J_1 = 3$, $J_2 = 3$ and (3) $J_1 = 5$, $J_2 = 4$ are 1.1458, 1.1056 and 1.0580 TECU with 16, 100 and 612 coefficients, respectively. VTEC maps of 2D B-spline analysis for the mid-point of the modeling period (12:30:00 UT) are given in Fig. 6.2. The figure includes the correction maps and the final VTEC maps of each solution level where the final maps are obtained by adding the corresponding corrections to the reference solution.

An important point to be mentioned about the figures provided in this chapter is that TECmapper neither applies a projection for the figures, nor provides the boundaries for the continents or states, at least for the time being. The boundaries were added to the maps generated by TECmapper subsequently to provide a better understanding about them.

In Fig. 6.2, while the reference solution is fairly smooth, as expected, the degree of details increases, as the solution levels are increased. An important point about Fig. 6.2 to be mentioned here is that, although the region under consideration extends between 25° - 46° in geodetic longitudes, the 2D solution considers a wider area in the Sun-fixed frame due to the diurnal motion of the Earth. For example, for the test case in this section, the Sun-fixed boundary values for longitude are 25° - 61°, which were computed by applying the conversion in Eq. (4.1) to 25° (λ_{min}) at 12:00:00 (t_{min}) and 46° (λ_{max}) at 13:00:00 (t_{max}), respectively.

For the 3D B-spline analysis, the number of coefficients for the reference level solution at levels $J_1 = 0$, $J_2 = 0$, $J_3 = 0$ (B-spline levels for the geodetic longitude, geodetic latitude and time, respectively) is 27 (= $(2^0+2)^3$) and its RMSE value is 0.9608 TECU. The RMSE values for the correction terms for three sets of solution levels of (1) $J_1 = 1$, $J_2 = 1$, $J_3 = 1$, (2) $J_1 = 2$, $J_2 = 2$, $J_3 = 2$ and (3) $J_1 = 3$, $J_2 = 3$, $J_3 = 3$ are 0.9177, 0.8565 and 0.6866 TECU with 64, 216 and 1000 coefficients, respectively. VTEC maps of the 3D analysis for the mid-point of the modeling period (12:30:00 UT) are shown in Fig. 6.3.

Figure 6.2: 2D B-spline model results for 26.09.2007, 12:30 (UT). Modeling period is 12:00:00 – 13:00:00 (UT)

(a) $\overline{VTEC}$ for $J_1 = J_2 = 0$ with 9 coefficients. RMSE= 1.1696 TECU
(b) $\Delta VTEC$ for $J_1 = J_2 = 1$ with 16 coefficients. RMSE= 1.1458 TECU
(c) $VTEC$ solution for $J_1 = J_2 = 1$ by adding levels 1, 1 corrections (panel b) to reference (panel a)
(d) $\Delta VTEC$ for $J_1 = J_2 = 3$ with 100 coefficients. RMSE= 1.1056 TECU
(e) $VTEC$ solution for $J_1 = J_2 = 3$ by adding levels 3, 3 corrections (panel d) to reference (panel a)
(f) $\Delta VTEC$ for $J_1 = 5$, $J_2 = 4$ with 612 coefficients. RMSE = 1.0580 TECU
(g) $VTEC$ solution for $J_1 = 5$, $J_2 = 4$ by adding levels 5, 4 corrections (panel f) to reference (panel a)
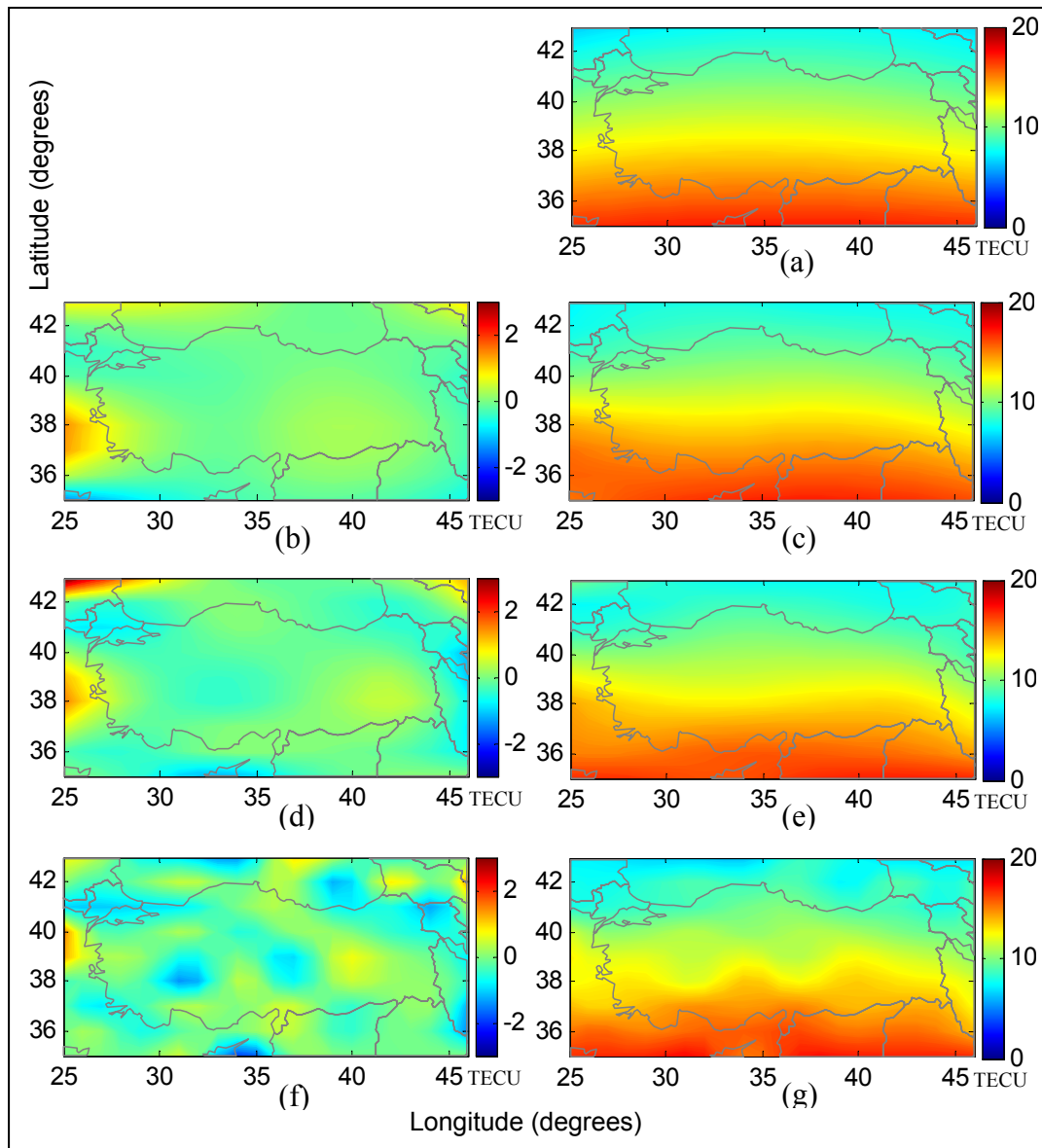
Figure 6.3: 3D B-spline model results for 26.09.2007, 12:30 (UT).
Modeling period is 12:00:00 – 13:00:00 (UT)

(a) $\overline{VTEC}$ for $J_1= J_2= J_3= 0$ with 27 coefficients. RMSE= 0.9608 TECU

(b) $\Delta VTEC$ for $J_1= J_2= J_3= 1$ with 64 coefficients. RMSE= 0.9177 TECU

(c) *VTEC* solution for $J_1= J_2= J_3= 1$ by adding levels 1, 1, 1 corrections (panel b)
to reference (panel a)

(d) $\Delta VTEC$ for $J_1= J_2= J_3= 2$ with 216 coefficients. RMSE= 0.8565 TECU

(e) *VTEC* solution for $J_1= J_2= J_3= 2$ by adding levels 2, 2, 2 corrections (panel d)
to reference (panel a)

(f) $\Delta VTEC$ for $J_1= J_2= J_3= 3$ with 1000 coefficients. RMSE= 0.6866 TECU

(g) *VTEC* solution for $J_1= J_2= J_3= 3$ by adding levels 3, 3, 3 corrections (panel f) to
reference (panel a)

The RMSE values provided above indicate that the 3D B-spline solutions fit the data better than the 2D B-spline solutions. This result is not surprising since the 3D solutions use the time as an extra variable to represent the temporal change in the ionosphere. On the other hand, the 2D solutions are numerically more stable and require lower computer memory as they include far less coefficients as compared to the 3D solutions. As in the 2D case, higher level solutions for the 3D modeling provide more details with smaller RMSE values.

Spherical harmonic solutions with TECmapper were performed for three sets of maximum degree (n_{max}) and maximum order (m_{max}), as $n_{max} = 4$, $m_{max} = 3$ with 23 coefficients; $n_{max} = 9$, $m_{max} = 9$ with 100 coefficients; and $n_{max} = 15$, $m_{max} = 15$ with 256 coefficients. In TECmapper, the maximum degree and order for the reference solution is fixed and equal to 1 (for both), which requires the computation of 4 coefficients. The corresponding RMSE value for the reference solution is 1.2224 TECU while those for higher levels are 1.1756, 1.1665 and 1.1474 TECU, respective to the above order. The VTEC maps for the spherical harmonic solutions are given in Fig. 6.4.

If we consider the RMSE values and the VTEC plots given in Fig. 6.2 and Fig. 6.4, it can be concluded that the VTEC solutions of the spherical harmonics are comparable with the reference solution of the 2D B-spline solution (panel a in Fig. 6.2). However, on the contrary to the B-Spline solutions, increasing the maximum degree and order of spherical harmonics does not improve the detail level in VTEC maps significantly, which is probably due to the global nature of the spherical harmonic functions.

The B-spline algorithms that are used in TECmapper have a further advantage over the one for spherical harmonics in that they require shorter computation time. As a specific example, the computation time for the 2D B-spline levels $J_1 = J_2 = 3$ was about 7 seconds, whereas the one for the spherical harmonic solution for $n_{max} = m_{max} = 9$ was about 37 seconds, with 100 estimated coefficients for both method.
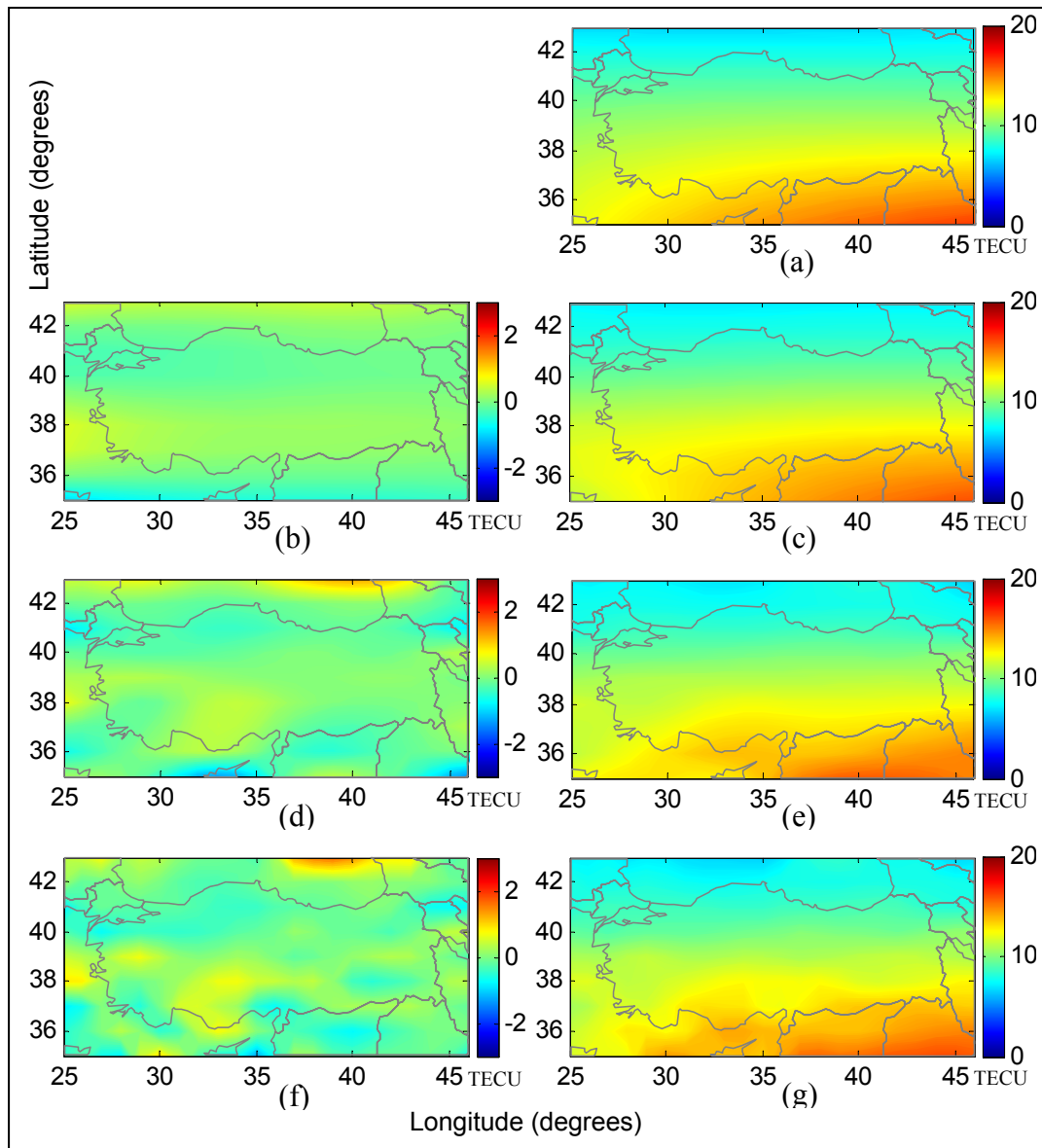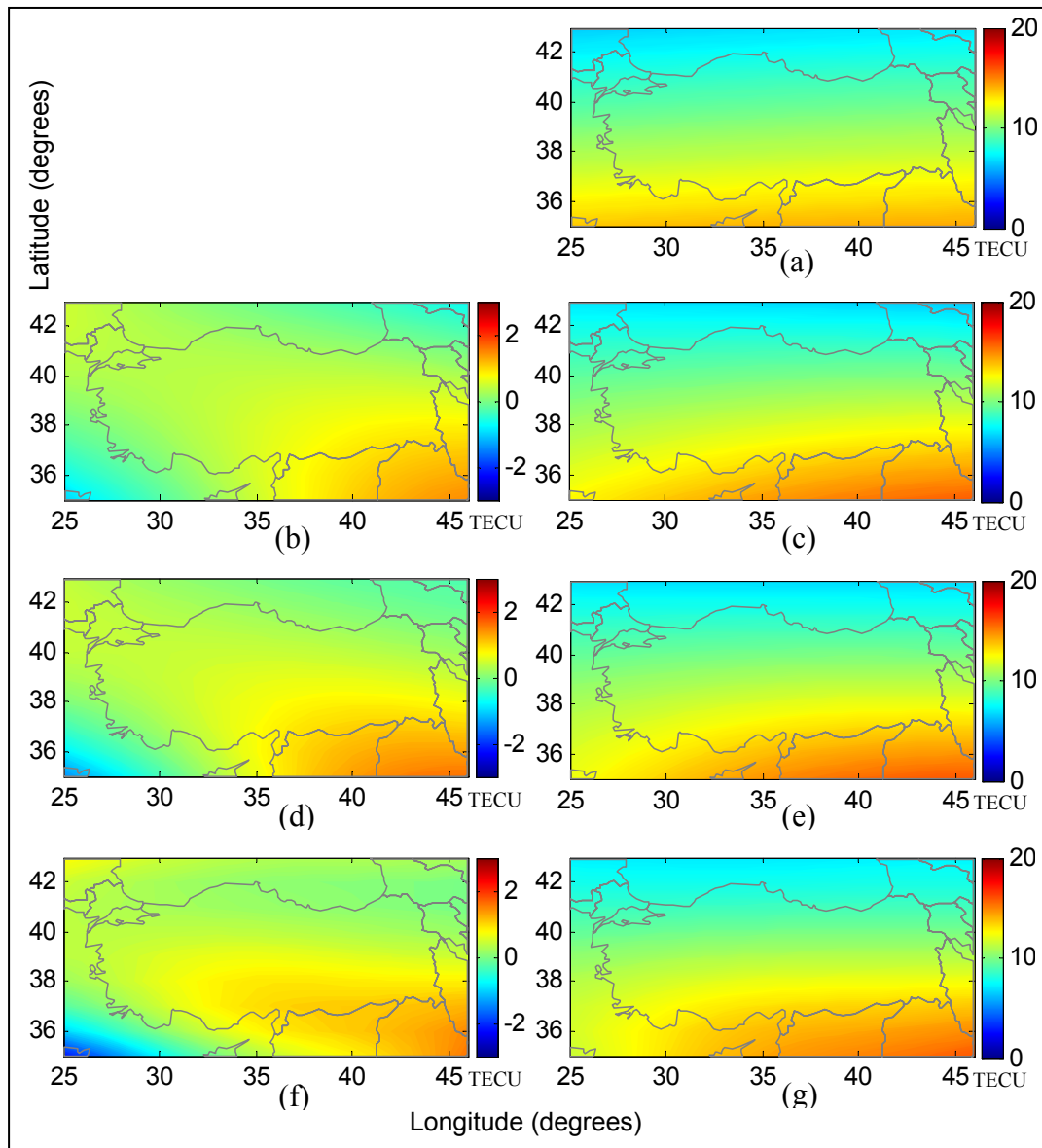
Figure 6.4: Spherical harmonic model results for 26.09.2007, 12:30 (UT).
Modeling period is 12:00:00 – 13:00:00 (UT)

(a) $\overline{VTEC}$ for $n_{max}= 1$, $m_{max}= 1$, with 4 coefficients. RMSE= 1.2224 TECU
(b) $\Delta VTEC$ for $n_{max}= 4$, $m_{max}= 3$ with 23 coefficients. RMSE= 1.1756 TECU
(c) $VTEC$ solution for $n_{max}= 4$, $m_{max}= 3$ by adding n_{max}, $m_{max}= 4$, 3 corrections
(panel b) to reference (panel a)
(d) $\Delta VTEC$ for $n_{max}= 9$, $m_{max}= 9$ with 100 coefficients. RMSE= 1.1665 TECU
(e) $VTEC$ solution for $n_{max}= 9$, $m_{max}= 9$ by adding n_{max}, $m_{max}= 9$, 9 corrections
(panel d) to reference (panel a)
(f) $\Delta VTEC$ for $n_{max}= 15$, $m_{max}= 15$ with 256 coefficients. RMSE= 1.1474 TECU
(g) $VTEC$ solution for $n_{max}= 15$, $m_{max}= 15$ by adding n_{max}, $m_{max}= 15$, 15 corrections
(panel f) to reference (panel a)

80

Accurate computation of the receiver DCB values is of vital importance for ionosphere modeling. Accuracy and consistency of these values are also indicators for the success of the modeling process. Receiver DCB values for all level solutions performed within Section 6.1 are tabulated in Table 6.1.

Table 6.1: DCB values for the receivers that were used in the study as solutions of TECmapper models with varying levels.
Modeling period is 12:00:00 – 13:00:00 (UT) of 26.09.2007.

| | Differential Code Biase Values (ns) for | | | | | | | | |
| | 2D B-Splines Levels | | | 3D B-Splines Levels | | | Spherical Harmonics Degree and Order | | |
Station	1, 1	3, 3	5, 4	1, 1, 1	2, 2, 2	3, 3, 3	4, 3	9, 9	15, 15
ADAN	20.993	21.029	20.986	21.606	21.561	21.633	20.870	20.928	20.948
AFYN	26.105	26.110	26.066	26.562	26.505	26.588	26.036	26.083	26.092
AGRI	-6.201	-6.211	-6.263	-5.915	-5.972	-5.983	-6.264	-6.251	-6.239
ANKA	4.534	4.509	4.498	4.864	4.737	4.603	4.477	4.508	4.508
ANTL	20.569	20.558	20.488	21.295	21.288	21.116	20.417	20.473	20.508
BART	-11.602	-11.600	-11.625	-11.335	-11.313	-11.387	-11.696	-11.674	-11.632
BDRM	-3.422	-3.390	-3.427	-2.685	-2.683	-2.514	-3.586	-3.536	-3.489
BURS	-0.434	-0.478	-0.507	-0.133	-0.261	-0.323	-0.493	-0.461	-0.460
CALT	19.654	19.675	19.608	20.213	20.193	20.182	19.552	19.606	19.631
ELZT	18.911	18.917	18.900	19.269	19.233	19.217	18.849	18.881	18.880
ERZI	4.287	4.222	4.217	4.609	4.561	4.488	4.228	4.248	4.250
GAZT	19.207	19.218	19.210	19.719	19.722	19.721	19.122	19.180	19.178
HOPA	4.572	4.633	4.579	4.736	4.742	4.787	4.470	4.510	4.548
ISTC	15.907	15.908	15.856	16.124	16.081	16.202	15.824	15.840	15.864
IZMR	-4.478	-4.449	-4.498	-3.967	-4.004	-4.143	-4.572	-4.520	-4.496
KART	-2.280	-2.319	-2.340	-1.911	-2.013	-2.036	-2.339	-2.310	-2.308
KONY	-2.845	-2.831	-2.848	-2.334	-2.341	-2.216	-2.922	-2.870	-2.859
KRDT	-14.210	-14.209	-14.268	-14.017	-14.039	-13.985	-14.284	-14.265	-14.247
KTHY	-5.319	-5.337	-5.339	-4.880	-4.982	-4.982	-5.379	-5.339	-5.337
KYSR	-3.352	-3.376	-3.390	-2.923	-2.956	-3.000	-3.405	-3.366	-3.368
MRDN	1.069	1.046	1.047	1.415	1.385	1.355	0.995	1.026	1.036
SMSN	-1.074	-1.055	-1.106	-0.724	-0.738	-0.719	-1.168	-1.145	-1.108
TOKT	-17.718	-17.726	-17.754	-17.374	-17.409	-17.384	-17.796	-17.771	-17.753
TRBZ	10.107	10.121	10.118	10.344	10.324	10.282	10.006	10.037	10.076
TYF1	-8.996	-9.029	-9.055	-8.406	-8.449	-8.419	-9.056	-9.028	-9.024
VANN	3.740	3.713	3.731	3.891	3.859	3.776	3.699	3.706	3.709

Note about Table 6.1 that DCB values for the receivers located at CALT, ELZT and GAZT stands for the differential biases between C1 and P2 (DCB_{C1P2}) since these receivers are of C1/P2 class. Remaining stations host P1/P2 or P1/X2 class receivers, thus for these stations the given values are for DCB values between P1 and P2 (DCB_{P1P2}). Also note that DCB values for the receiver located at ERZU station are not given in the table, as it does not have observations for the modeling period 12:00:00 – 13:00:00.

Table 6.1 designates that TECmapper produce quite similar DCB values for different modeling methods. Moreover, there exists high consistency for code bias values within each method for varying model levels which indicates that DCB calculations are poorly affected from the selection of model level.

6.3 2D VTEC Modeling for Varying Modeling Intervals

The 2D analysis in TECmapper, i.e. 2D B-spline and spherical harmonic modeling tasks, are performed with the assumption that the ionosphere is static (or frozen) for the modeling period by neglecting the relatively small temporal variations in the ionosphere in the Sun-fixed reference frame. Therefore, the 2D modeling results reflect the average state of the ionosphere within the related period.

In order to assess the effect of the length of the modeling period on the results of 2D B-spline and spherical harmonic methods, 2D analysis were performed for varying modeling periods with fixed model levels. Periods of 15, 30, 60 and 120 minutes were selected to have the same mid-point with the previous analysis, i.e. 12:30:00, so the related periods are 12:22:30 - 12:37:30, 12:15:00 - 12:45:00, 12:00:00 - 13:00:00 and 11:30:00 - 13:30:00 in UT.

2D B-spline solutions were performed for the levels $J_1 = 2$ and $J_2 = 2$. The RMSE values for the periods of 15, 30, 60 and 120 minutes are 0.8320, 0.9888, 1.1232

and 1.2193 TECU, respectively. For a clear demonstration of the results, only the final VTEC maps for the levels $J_1 = 2$ and $J_2 = 2$ are given in Fig. 6.5, excluding the plots for references and corrections.
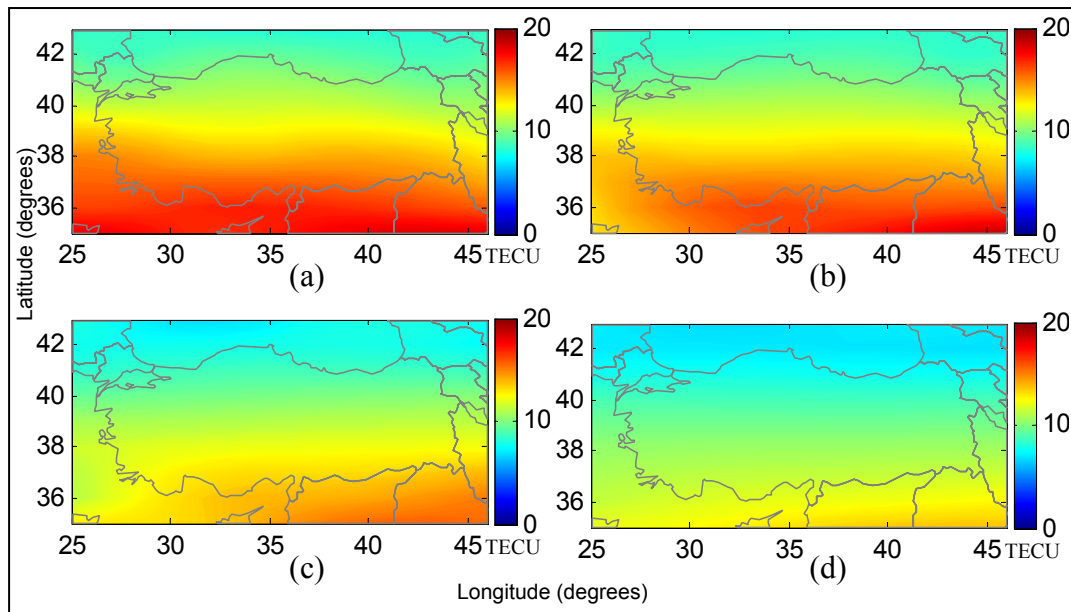
Figure 6.5: 2D B-spline model results for 26.09.2007, 12:30:00 (UT). VTEC maps are obtained for levels of $J_1 = 2$ and $J_2 = 2$ for the modeling periods (UT) of:

(a) 12:22:30 – 12:37:30 (15 min.) with RMSE= 0.8320 TECU
(b) 12:15:00 – 12:45:00 (30 min.) with RMSE= 0.9888 TECU
(c) 12:00:00 – 13:00:00 (60 min.) with RMSE= 1.1232 TECU
(d) 11:30:00 – 13:30:00 (120 min.) with RMSE= 1.2193 TECU

A maximum degree of 8 and a maximum order of 6 were used for the spherical harmonic analysis. The corresponding RMSE values for the periods of 15, 30, 60 and 120 minutes are 0.8664, 1.0366, 1.1234 and 1.2156 TECU, respectively. The resulting VTEC maps are provided in Fig. 6.6. Again for a clear demonstration of the results, the plots for references and corrections are excluded from the related figure.

83
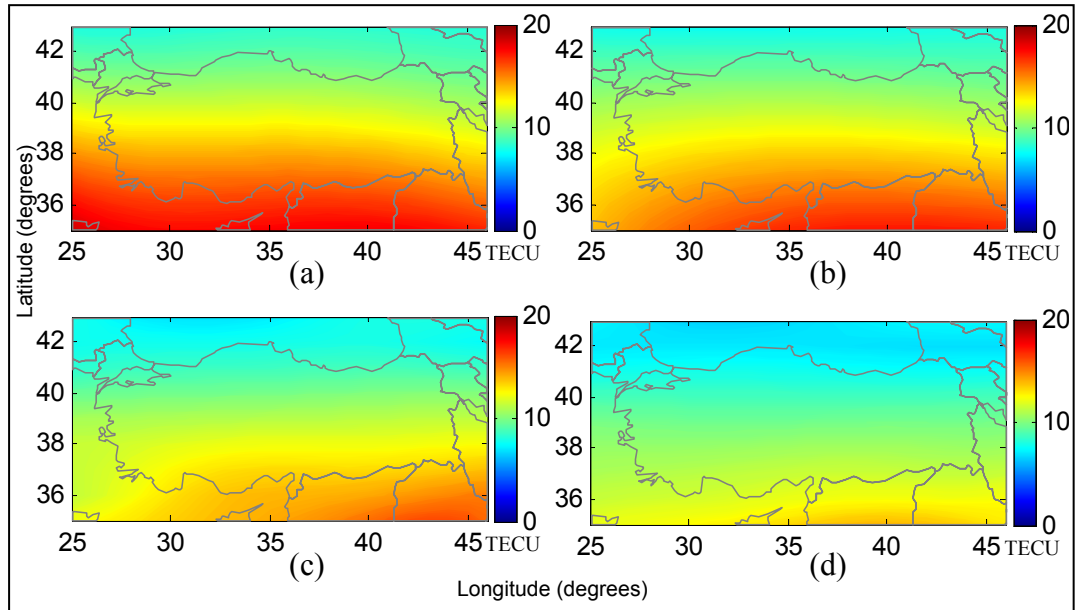
Figure 6.6: Spherical harmonic model results for 26.09.2007, 12:30:00 (UT). VTEC maps are obtained for $n_{max}= 8$, $m_{max}= 6$ for the modeling periods (UT) of:

(a) 12:22:30 − 12:37:30 (15 min.) with RMSE= 0.8664 TECU
(b) 12:15:00 − 12:45:00 (30 min.) with RMSE= 1.0366 TECU
(c) 12:00:00 − 13:00:00 (60 min.) with RMSE= 1.1234 TECU
(d) 11:30:00 − 13:30:00 (120 min.) with RMSE= 1.2156 TECU

The resulting maps and the RMSE values of both methods for each modeling period are very similar. However, note that the spherical harmonic solutions depend on 75 coefficients while only 36 unknowns were calculated for the 2D B-spline solutions. Nevertheless, the aim of this section is not to compare these methods, which was accomplished in the previous section in more detail.

The increase in the RMSE values for longer modeling periods for both the 2D B-spline and spherical harmonic solutions is an expected result as the 2D models of VTEC in a Sun-fixed reference frame demonstrate the average state of the ionosphere for the related period as mentioned before. Thus, as the modeling period gets longer, the deviations from this average state increases resulting in

higher RMSE values. Another interesting fact about the figures is that, as the modeling period gets more narrow, the 2D VTEC plots resemble the 3D VTEC plots more and more (compare Fig. 6.5 and Fig. 6.6 with Fig. 6.3), which indicates that the 3D modeling localizes the temporal variations in the ionosphere more appropriately. On the other hand, narrowing the modeling period reduces the amount of available observations for the model.

As a result of the implementations performed in Section 6.1 and Section 6.2, it can be concluded that the models based on B-spline approach are more successful for local or regional VTEC modeling as compared to spherical harmonic model. In particular, 3D B-spline approach can represent the temporal variations in the ionosphere more successfully taking the advantage of the additional time variable. The price of the higher dimension is the increased number of unknowns to be solved, which can cause difficulties for the solution of large systems with the requirement of higher computer memory. Therefore, for the applications possessing excessive number of observations 2D B-spline method can be preferred over 3D B-spline approach depending on the memory constraints. On the other hand, spherical harmonic model is the only choice for global or wide area applications as the B-spline approach is based on Euclidean theory.

In addition, related applications demonstrated that the modeling interval affects the results of 2D VTEC modeling considerably. Consequently, especially for the periods of high ionospheric activity the length of the modeling interval should be selected cautiously.

The VTEC maps over Turkey generated by using 3D B-spline model for the date 26.09.27 at every 2 hours are available in Appendix G.

CHAPTER 7

CONCLUSION

7.1 Summary and Discussion

The widespread effect of the ionosphere on various disciplines such as satellite systems and sub-systems, communication and surveillance systems and space weather studies made ionosphere modeling a popular subject within the scientific and engineering community. With the development of the GPS, which provides accurate ionospheric information that can be inferred by utilizing the dual frequency structure of the GPS signals, a new period in monitoring of the ionosphere has started. Consequently, numerous GPS-based ionosphere modeling studies have been accomplished. The main deficiency for the ionosphere modeling studies that do not depend on nearby data, such as the IRI and the Bent ionospheric model, is their relatively low accuracy. Therefore the large amount of data provided by the extensive ground-based GPS networks with high accuracy offer a valuable source for modeling of the ionosphere. On the other hand, in general the GPS-based ionosphere models are not supported with related software accessible to scientific and engineering community which restricts the practical use of these models.

Being aware of the limitations for the research community to reach GPS-based ionospheric modeling results, a new MATLAB® based ionosphere modeling

86

software, i.e. TECmapper was developed within the study. Note that TECmapper does not require MATLAB knowledge as it has its own graphical user interface.

TECmapper utilizes appropriate methods to extract ionospheric information from ground-based GPS observations, to model VTEC of the ionosphere and to estimate the unknown model parameters. The ionospheric data can be obtained by the so-called geometry free linear combination of GPS carrier phase or pseudorange observations. The noise level of carrier phase measurements is significantly lower than for pseudorange ones. However, carrier phase measurements are biased with ambiguity terms, while pseudorange observations are unambiguous. In this study, the carrier phase observations were used to smooth the pseudorange measurements with the carrier to code leveling process. For a successful smoothing process, an efficient technique was employed to detect possible cycle slips, which are discontinuities in the carrier signals.

VTEC can be modeled in an Earth-fixed or a Sun-fixed reference frame. Ionosphere is highly variable in an Earth-fixed reference frame due to the diurnal motion of the Earth. Thus, the models in an Earth-fixed frame should either consider the time dependency or be used instantaneously, i.e. epoch-specific. However, ionosphere is much more stable in a Sun-fixed reference frame as the Sun is the main source for its ionization. Therefore, it can be assumed as static for a certain modeling period in a Sun-fixed reference frame.

TECmapper uses three different methods for the modeling of VTEC, namely, 2D B-spline, 3D B-spline and spherical harmonic models. In the software, 2D B-spline and spherical harmonic modeling tasks are performed in a geographic Sun-fixed frame depending on geodetic latitude and Sun-fixed longitude while 3D B-spline model is performed in an Earth-fixed frame depending on geodetic latitude, geodetic longitude and time.

The fundamentals of B-spline modeling of VTEC in an Earth-fixed reference frame are presented by Schmidt (2007). Schmidt proposed to split the VTEC into a reference part, which can be computed from a given model like the IRI, and an unknown correction term to be modeled by B-spline functions in an Earth-fixed reference frame. For spherical harmonic approach on the other hand, the works proposed by Schaer et al. (1995) or Schaer (1999) was followed.

Modifications for the original forms of both modeling approaches were proposed in this study. For both approaches, VTEC was split into two parts as the reference and the correction terms, as suggested by Schmidt. However, the reference terms were computed from the low level solutions of the relevant methods, instead of a given model like the IRI. This approach provided two apparent advantages that; dependency on the results of another model was prevented and probably closer references to the final solution were obtained due to the low accuracy levels of the approximate models like IRI. Note that using a reference that is not far from the final solution has two major benefits for a model. Firstly, for the regions with data gaps, reference part provides information. Secondly, in case of problems for the solution of correction term, e.g. due to numerical problems in parameter estimation stage, reference part may offer a firm base. In addition to these modifications, B-spline model was adapted to be used in a Sun-fixed reference frame for the first time in this study.

For the estimation of unknown model coefficients, IRLS, which is an iterative robust regression algorithm, was employed as an alternative to the method of least squares in order to reduce the effects of possible outliers in the observation data. Both the least square method and IRLS produce numerically stable results for the solution of reference terms since the low level model functions are wide enough to include large amount of observations. However, as the model functions are narrowed for higher levels of the models to represent the finer details of VTEC, the system may become ill-conditioned. Thus, in order to stabilize the correction term computations, LSQR and Tikhonov regularization methods were included in

TECmapper. Tikhonov regularization is the most widely used method to regularize the ill-conditioned problems. However, like any other direct method, it may become impractical due to storage problems if the system is very large. LSQR on the other hand, is an iterative sparse system solver which can provide solutions for extremely large problems without matrix decomposition. The disadvantages of LSQR as compared to Tikhonov's method are that, it can provide regularization effects for discrete number of iterations and only an approximate solution for the variance-covariance matrix of model parameters can be available by modifying the LSQR algorithm, which has not been accomplished in TECmapper algorithm yet.

In order to avoid convergence problems that can arise due to joint use of robust regression and regularization algorithms, the iterative structure of IRLS was only applied for the reference term computations. For the robust solution of correction terms on the other hand, the weights obtained from the last iteration of reference term computations were applied for the observations.

For the selection of appropriate regularization parameter for Tikhonov's method, L-curve and GCV techniques were employed in the software. However, neither of these methods can guarantee the selection of optimum regularization parameter. For that reason, TECmapper allows the user to change the regularization parameter until satisfactory results are obtained.

Local, regional or global modeling of VTEC can be performed within TECmapper with the selection of appropriate model depending on the data and the user needs. Application of the software to a real data set over Turkey demonstrated that B-spline models, in particular 3D B-spline model, give more successful results for local/regional VTEC modeling. 2D B-spline model can be preferred over 3D approach considering the number of available observations and the constraints on the computer memory. Spherical harmonic model should be used for global or wide area applications as the B-spline approach is based on Euclidean theory. The application also showed that, as the modeling period is increased, the accuracy

level for 2D models decreases since they do not possess a time variable to represent the temporal changes in VTEC.

Besides the related functions to model VTEC by means of mentioned methods, the ability to utilize the ionosphere models produced by the Bernese GPS Software was also included in TECmapper. With this function, it is possible to generate VTEC maps and save VTEC values at user specified grid points for desired epochs by using the Global Ionosphere Models of the CODE analysis center.

TECmapper is expected to cover an important gap in ionosphere modeling field. The opportunities that it provides to the user, such as:

- Performing the modeling process for the interval that are specified by the user,

- Generating 2D VTEC maps for specified epochs,

- Converting observation files into text files of STEC and VTEC data,

- Option to save VTEC values as products of modeling process at specified grid points in a text file,

- Interactive environment that provides user to control the parameter estimation stage,

are not offered even by the Bernese GPS Software, which is one of the most successful and sophisticated tools in its area.

TECmapper can be used by the researchers from any disciplines who can provide ground-based GPS observations since it does not require background of GPS processing. Today, excessive amount of GPS data from various local or regional GPS networks all over the world, including the networks of continuously operating reference stations (CORS), are freely available through the internet. In particular

for Turkey, within the content of CORS-TR (TUSAGA-AKTIF) project a network of 146 continuously operating reference stations was established for the infrastructure by the end of 2008 (Eren and Uzel, 2008). Since this date, the data provided by this network is a valuable source for the use TECmapper to continuously monitor the ionosphere over Turkey.

7.2 Future Work

The work about the study that is planned to be completed in the near future can be listed as:

- Adding ability to TECmapper to save the modeling results in IONEX format,

- Presenting the software to the scientific and engineering community through the internet.

Further improvements for the software may include the followings:

- Additional VTEC models,

- Additional regularization methods,

- Application of regularization parameter estimation methods, i.e. L-curve and GCV, for LSQR,

- Ability for projecting VTEC maps,

- Ability for the inclusion of continent and state boundaries in VTEC maps,

- Transportation of the software to a new programming environment, such as C or C++, or development of a stand-alone version within MATLAB in order to provide independency from MATLAB.

REFERENCES

Afraimovich E.L., Kosogorov E.A., and Lesyuta O.S. (2002): Effects of the August 11, 1999 total solar eclipse as deduced from total electron content measurements at the GPS network. Journal of Atmospheric and Solar-Terrestrial Physics, Vol. 64, pp. 1933-1941.

Aster R.C., Borchers B., and Thurber C.H. (2005): Parameter estimation and inverse problems. Elsevier Academic Press, USA.

Bilitza D. (2001): International Reference Ionosphere 2000. Radio Science, Vol. 36, No. 2, pp. 261–275.

Brunini C.A. (1998): Global ionospheric model from GPS measurements. Ph.D. thesis, Facultad de Ciencias Astronomicas y Geofisicas, La Plata, Argentina.

Brunini C., Meza A., Azpilicueta F., Van Zele M.A., Gende M., and Diaz A. (2004): A new ionosphere monitoring technology based on GPS. Astrophysics and Space Science, Kluwer Academic Publishers, Netherlands, Vol. 290, pp. 415-429.

Chambodut A., Panet I., Mandea M., Diament M., Holschneider M., and Jamet O. (2005): Wavelet frames - an alternative to spherical harmonic representation of potential fields. Geophysical Journal International, Vol. 163, pp. 875–899.

Ciraolo L., Azpilicueta F., Brunini C., Meza A., and Radicella S.M. (2007): Calibration errors on experimental Slant Total Electron Content (TEC) determined with GPS. Journal of Geodesy, Vol. 81, No. 2, pp. 111–120.

Cummins D.J. and Andrews C.W. (1995): Iteratively reweighted partial least squares: a performance analysis by Monte Carlo simulation. Journal of Chemometrics, Vol. 9, pp. 489-507.

Dach R., Hugentobler U., Fridez P., Meindl M. (Eds.) (2007): Bernese GPS Software Version 5.0. Astronomical Institute, University of Bern, Switzerland.

Daniell R.E., Brown L.D., Anderson D.N., Fox M.W., Doherty P.H., Decker D.T., Sojka J.J., and Schunk R.W. (1995): Parameterized Ionospheric Model: a global ionospheric parameterization based on first principles models. Radio Science, Vol. 30, No. 5, pp. 1499-1510.

Davies K. (1989): Ionospheric Radio. Peter Peregrinus Ltd., London.

Dettmering D. (2003): The Utilization of the GPS for modeling the ionosphere in three dimensions (in German). Ph.D. Thesis, Technical Reports, Report Nr. 2003.1, Universität Stuttgart, Germany.

Doherty P.H., Decker D.T., Sultan P.J., Rich F.J., Borer W.S., and Daniell Jr. R.E. (1999): Validation of prism: the climatology. In: Proceedings of the Ionospheric Effects Symposium, 1999, Springfield, VA, pp. 330-339.

DuMouchel W.H., and O'Brien F.L. (1989): Integrating a robust option into a multiple regression computing environment. In: Computer Science and Statistics: Proceedings of the 21st Symposium on the Interface, Alexandria, VA, American Statistical Association, 9-12 April 1989, pp. 297-301.

El-Gizawy M.L. (2003): Development of an ionosphere monitoring technique using GPS measurements for high latitude GPS users. M.S. Thesis, University of Calgary, Canada.

Eren K., and Uzel T. (2008): CORS-TR: establishment of national CORS system and datum transformation project (in Turkish). TUSAGA Active Workshop 3, Istanbul Culture University, İstanbul, Turkey, 28-29 November 2008.

Feltens J. (1998): Chapman profile approach for 3-D global TEC representation. In: Proceedings of the IGS Analysis Centers Workshop, ESOC, Darmstadt, Germany, 9–11 February 1998, pp 285–297.

Feltens J., and Schaer S. (1998): IGS Products for the Ionosphere. In: Proceedings of the IGS Analysis Centers Workshop, ESOC, Darmstadt, Germany, 9–11 February 1998, pp. 225–232.

Fok C.C.T., and Ramsay J.O. (2006): Fitting curves with periodic and nonperiodic trends and their interactions with intensive longitudinal data. In: Models for Intensive Longitudinal Data, Walls T.A., and Schafer J.L. (Eds.), Oxford University Press, New York.

Gao, Y., Heroux P., and Kouba J. (1994): Estimation of GPS receiver and satellite L1/L2 signal delay biases using data from CACS. In: Proceedings of KIS-94, Banff, Canada, August 30 - September 2, 1994, pp. 109-117.

Gao Y., Liao X. and Liu Z.Z. (2002): Ionosphere modeling using carrier smoothed ionosphere observations from a regional GPS network. Geomatica, Vol. 56, No. 2, pp. 97-106.

García-Fernández M. (2004): Contributions to the 3D ionospheric sounding with GPS data. Ph.D. Thesis, Technical University of Catalonia, Spain.

García-Fernández M., Hernández-Pajares M., Juan J.M., Sanz J., Orús R., Coisson P., Nava B., and Radicella S.M. (2003): Combining ionosonde with ground GPS data for electron density estimation. Journal of Atmospheric and Solar-Terrestrial Physics, Vol. 65, pp. 683-691.

Gurtner W. (2004): RINEX: The receiver independent exchange format version 2.11. Available via Internet from IGS.

Hansen P.C.: Regularization tools (1994): A Matlab package for analysis and solution of discrete ill-posed problems. Numerical Algorithms, Vol. 6, pp. 1–35.

Hargreaves J.K. (1992): The solar-terrestrial environment. Cambridge Atmospheric and Space Science Series, Cambridge University Press.

Hatch, R. (1982): Synergism of GPS code and carrier measurements. In: Proceedings of the Third International Geodetic Symposium on Satellite Doppler Positioning, New Mexico State University, NM, USA, 8–12 February 1982, Vol. 2, pp. 1213–1231.

Hernández-Pajares M., Juan J.M., Sanz J. (1999): New approaches in global ionospheric determination using ground GPS data. Journal of Atmospheric and Solar-Terrestrial Physics, Vol. 61, pp. 1237–1247.

Hernández-Pajares M., Juan J.M., Sanz J., Orus R., Garcia-Rigo A., Feltens J., Komjathy A., Schaer S.C., and Krankowski A. (2009): The IGS VTEC maps: a reliable source of ionospheric information since 1998. Journal of Geodesy, Vol. 83, 263-275.

Hochegger G., Nava B., Radicella S., and Leitinger R. (2000): A family of ionospheric models for different uses. Physics and Chemistry of the Earth, Vol. 25, No. 4, pp. 307–310.

Hofmann-Wellenhof B., Lichtenegger H., and Wasle E. (2008): GNSS − Global Navigation Satellite Systems − GPS, GLONASS, Galileo & more., Springer-Verlag, Wien.

Kleusberg A. (1998): Atmospheric models from GPS. In: GPS for Geodesy, 2nd Ed., Teunissen P.J.G. and Kleusberg A. (Eds.), Springer, Berlin-Heidelberg.

Klobuchar J.A. (1996): Ionospheric effects on GPS. In: Global Positioning System: theory and applications, Parkinson B.W. and Spilker J.J (Eds.), American Institute of Aeronautics and Astronautics, Washington DC, Vol. I.

Klobuchar J.A., and Kunches J.M. (2000): Eye on the ionosphere: correcting for ionospheric range delay on GPS − temporal decorrelation. GPS Solutions, Vol. 4, No. 2, pp. 78-82.

Koch K.R. (1999): Parameter estimation and hypothesis testing in linear models. 2nd Ed., Springer, Berlin-Heidelberg-New York.

Kunches J.M., and Klobuchar J.A. (2001): Eye on the ionosphere: GPS after SA. GPS Solutions, Vol. 4, No. 3, p. 52.

Komjathy A., and Born G.H. (1999): GPS-based ionospheric corrections for single frequency radar altimetry. Journal of Atmospheric and Solar-Terrestrial Physics, Vol. 61, pp. 1197-1203.

Lachapelle G., Hagglund J., Falkenberg W., Bellemare P., Casey M., and Eaton M. (1986): GPS land kinematic positioning experiments. In: Proceedings of the 4th

International Geodetic Symposium on Satellite Positioning, Austin, TX, USA, 28 April – 2 May 1986, Vol. 2, pp. 1327–1344.

Langrey R.B. (1998): GPS receivers and the observables & Propagation of the GPS signals. In: GPS for Geodesy, 2nd Ed., Teunissen P.J.G. and Kleusberg A. (Eds.), Springer, Berlin-Heidelberg.

Leigh R.P., Robinson T.R., and Lester M. (1988): Ionospheric corrections for radar altimetry. In: Proceedings of IGARSS 88 Symposium: Geoscience and Remote Sensing, Edinburg, Scotland, 13–16 Sep. 1988, pp. 989–992.

Liu Z. and Gao Y. (2004): Ionospheric TEC predictions over a local area GPS reference network. GPS Solutions, Vol. 8, No. 1, pp. 23-29.

Llewellyn S.K. and Bent R. (1973): Documentation and description of Bent ionospheric model. Report AFCRL-TR-73-0657, AD772733, Geophysics Laboratory, Hanscom Air Force Base.

Lyche T., Schumaker L.L. (2000): A multiresolution tensor spline method for fitting functions on the sphere. SIAM Journal of Scientific Computing, Vol. 22, No. 2, pp. 724–746.

Mannucci A.J., Wilson B.D., Yuan D.N., Ho C.H., Lindqwister U.J., and Runge T.F. (1998): A global mapping technique for GPS-derived ionospheric total electron content measurements. Radio Science, Vol. 33, pp. 565–582.

Manucci A.J., Iijima B.A., Lindqwister U.J., Pi X., Sparks L. and Wilson B.D. (1999): GPS and ionosphere. Revised Submission to URSI Reviews of Radio Science, Jet Propulsion Laboratory, Pasadena, CA.

Mautz R., Ping J., Heki K., Schaffrin B., Schum C., and Potts L. (2005): Efficient spatial and temporal representations of global ionosphere maps over Japan using B-spline wavelets. Journal of Geodesy, Vol. 78, pp. 660-667.

McCarthy D. (2000): IERS conventions, 2000. IERS Technical Note, International Earth Rotation Service.

Meza A. (1999): Three dimensional ionospheric models from Earth and space based GPS observations. Ph.D. Thesis, Universidad Nacional de La Plata, Argentine.

Mohinder S.G., Lawrence R.W., and Angus P.A. (2007): Global Positioning Systems, inertial navigation and integration, 2nd Ed., John Wiley & Sons, Inc., Hoboken, New Jersey.

Nohutcu M., Karslioglu M. O., Gucluer B., Schmidt M., Zeilhofer C., Zhang Z., and Ergintav S. (2008): Local modeling of VTEC using GPS observations. In: Proceedings of the TUJK Annual Scientific Meeting 2007, Monitoring and Modeling of the Ionosphere and Troposphere, 14-16 November 2007, Ankara, Turkey, pp. 33-37.

Paige C.C. and Saunders M.A.: LSQR (1982): An algorithm for sparse linear equations and sparse least squares. ACM Transactions on Mathematical Software, Vol. 8, pp. 43-71.

Parkinson B.W. (1994): History and operation of NAVSTAR, the Global Positioning System. IEEE Transactions on Aerospace and Electronic Systems, Vol. 30, No. 4.

Reilly, M.H. (1993): A transionospheric radio propagation model. In: Proceedings of the Seventh International Ionospheric Effects Symposium, Alexandria, VA, pp. 400-408.

Rius A., Ruffini G. and Cucurull L. (1997): Improving the vertical resolution of ionospheric tomography with GPS occultations. Geophysical Research Letters, Vol. 24, No: 18, pp. 2291-2294.

Sardon E., and Zarraoa N. (1997): Estimation of total electron-content using GPS data: how stable are the differential satellite and receiver instrumental biases? Radio Science, Vol. 32, pp. 1899–1910.

Schaer S. (1999): Mapping and predicting the Earth's ionosphere using the Global Positioning System. Ph.D. Thesis, Astronomical Institute, University of Berne, Switzerland.

Schaer S., Beutler G., Mervart L., Rothacher M., and Wild U. (1995): Global and regional ionosphere models using the GPS double difference phase observable. In: Proceedings on Special Topics and New Directions, IGS Workshop, GFZ, Potsdam, Germany, 15–18 May 1995, pp. 77–92.

Schaer S., Beutler G., Rothacher M., and Springer T.A. (1996): Daily global ionosphere maps based on GPS carrier phase data routinely produced by the CODE analysis center. In: Proceedings of the IGS Analysis Center Workshop, Silver Spring, Maryland, USA, 19-21 March 1996, pp. 181-192.

Schmidt M. (2007): Wavelet modeling in support of IRI. Advances in Space Research, Vol. 39, pp. 932-940.

Schmidt M., Fengler M., Mayer-Gurr T., Eicker A., Kusche J., Sanchez L., and Han S.-C. (2007a): Regional gravity modeling in terms of spherical base functions. Journal of Geodesy, Vol. 81, pp.17–38.

Schmidt M., Bilitza D., Shum C.K., and Zeilhofer C. (2007b): Regional 4-D modeling of the ionospheric electron content, Advances in Space Research, Vol. 42, pp. 782-790.

Schmidt, M., Karslioglu M.O., and Zeilhofer C. (2008): Regional multi-dimensional modeling of the ionosphere from satellite data. In: Proceedings of the TUJK Annual Scientific Meeting 2007, Monitoring and Modeling of the Ionosphere and Troposphere, 14-16 November 2007, Ankara, Turkey, pp. 88-92.

Schreiner W.S., Markin R.E., and Born G.H. (1997): Correction of single frequency altimeter measurements for ionosphere delay. IEEE Transactions on Geoscience and Remote Sensing, Vol. 35, No. 2, pp. 271–277.

Seeber G. (2003): Satellite geodesy. 2nd Ed., Walter de Gruyter, Berlin, New York.

SIDC: Sunspot data, http://sidc.oma.be/html/wolfmms.html, last visited on April 2009.

Spilker J.J. (1996): Tropospheric effects on GPS. In: Global Positioning System: Theory and applications, Parkinson B.W. and Spilker J.J (Eds.), American Institute of Aeronautics and Astronautics, Washington DC, Vol. I.

Springer, T.A. (2000): Modeling and validating orbits and clocks using the Global Positioning System: Geodätisch-geophysikalische Arbeiten in der Schweiz, Vol. 60, SchweizerischeGeodätische Kommission, Institut für Geodäsie und Photogrammetrie, Eidg. Technische Hochschule Zurich, Switzerland.

Stolle C., Schlüter S., Jacobi Ch. and Jakowski N. (2003): 3-dimensional ionospheric electron density reconstruction based on GPS measurements. Advances in Space Research, Vol. 31, No. 8, pp. 1965-1970.

Stollnitz E.J., DeRose T.D., and Salesin D.H. (1995): Wavelets for computer graphics: A primer. Part I, IEEE Computer Graphics and Applications, Vol. 15, No. 3, pp. 76–84; Part II, IEEE Computer Graphics and Applications, Vol. 15, No. 4, pp. 75–85.

The MathWorks Inc. (2004): Getting Started with MATLAB. Version 7, The MathWorks, Inc., Natick, MA.

Todhunter I. (1863): Spherical trigonometry. 2nd Ed., Macmillan & Co., Cambridge and London.

Wielgosz P., Brzezinska D.R., and Kashani I. (2003): Regional ionosphere mapping with kriging and Multiquadric methods. Journal of Global Positioning Systems, Vol. 2, No. 1, pp. 48-55.

Wild U. (1994): Ionosphere and geodetic satellite systems: permanent GPS tracking data for modelling and monitoring. Ph.D. thesis, Geodätisch-geophysikalische Arbeiten in der Schweiz, Zurich, Switzerland, Vol. 48.

Wilson B.D., Mannucci A.J., and Edwards C.D. (1995): Subdaily northern hemisphere ionospheric maps using an extensive network of GPS receivers. Radio Science, Vol. 30, pp. 639-648.

Xu Z.W., Wu J., and Wu Z.S. (2004): A survey of ionospheric effects on space-based radar. Waves in Random Media, Vol. 14, pp. S189-S273.

Yao Z.S., Roberts R.G., and Tryggvason A. (1999): Calculating resolution and covariance matrices for seismic tomography with the LSQR method. Geophysical Journal International, Vol. 138, pp. 886-894.

Zeilhofer C. (2008): Multi-dimensional B-spline modeling of spatio-temporal ionospheric signals. German Geodetic Commission, Series A, 123, Munich, Germany.

Zeilhofer C., Schmidt M., Bilitza D., and Shum C.K. (2009): Regional 4-D modeling of the ionospheric electron density from satellite data and IRI. Advances in Space Research, Vol. 43, pp. 1669-1675.

Zeng W., and Zhang X.J. (1999): Predictions of HF communication MUF in the region of the South China Sea. IEEE Antennas and Propagation Magazine, Vol. 41, No. 4, pp. 35–38.

APPENDIX A

LIST OF THE RECEIVER TYPES AND THEIR CLASSES DEFINED WITHIN TECmapper

Table A.1: The receiver types and their classes that are defined within TECmapper (obtained from the source code of Bernese GPS Software v5.0)

RECEIVER TYPE	RECEIVER CLASS $(X2=C1+(P2-P1))$
AOA BENCHMARK ACT	P1/P2
AOA ICS-4000Z	C1/X2
AOA ICS-4000Z ACT	P1/P2
AOA SNR-12 ACT	P1/P2
AOA SNR-8000 ACT	P1/P2
AOA SNR-8100 ACT	P1/P2
ASHTECH GG24C	P1/P2
ASHTECH P-XII3	P1/P2
ASHTECH UZ-12	P1/P2
ASHTECH Z18	P1/P2
ASHTECH Z-X	P1/P2
ASHTECH Z-XII3	P1/P2
ASHTECH Z-XII3T	P1/P2
BLACKJACK	P1/P2
JPS E_GGD	P1/P2
JPS EGGDT	P1/P2
JPS EUROCARD	P1/P2
JPS LEGACY	P1/P2
LEICA CRS1000	C1/P2
LEICA GRX1200	C1/P2
LEICA GRX1200GGPRO	C1/P2
LEICA GRX1200PRO	C1/P2
LEICA GX1230GG	C1/P2
LEICA MC1000	C1/P2
LEICA RS500	C1/P2
LEICA SR399E	C1/P2

LEICA SR520	C1/P2
LEICA SR530	C1/P2
LEICA SR9500	C1/P2
LEICA SR9600	C1/P2
NOV EURO4-1.00-222	C1/P2
NOV MILLEN-RT2	C1/P2
NOV MILLEN-STD	C1/P2
NOV MILLEN-STDW	C1/P2
NOV OEMV3	C1/P2
NOV WAASGII	C1/P2
ROGUE SNR-8	C1/X2
ROGUE SNR-8C	C1/X2
ROGUE SNR-12	C1/X2
ROGUE SNR-12 RM	C1/X2
ROGUE SNR-800	C1/X2
ROGUE SNR-8000	C1/X2
ROGUE SNR-8100	C1/X2
SEPT POLARX2	P1/P2
SEPT POLARX2E	P1/P2
SIMULA	P1/P2
SPP GEOTRACER100	C1/X2
TOPCON GP-DX1	C1/X2
TOPCON GP-R1DY	P1/P2
TOPCON TT4000SSI	C1/X2
TPS E_GGD	P1/P2
TPS EGGDT	P1/P2
TPS EUROCARD	P1/P2
TPS GB-1000	P1/P2
TPS LEGACY	P1/P2
TPS NETG3	P1/P2
TPS ODYSSEY_E	P1/P2
TRIMBLE 4000SSE	C1/X2
TRIMBLE 4000SSI	C1/X2
TRIMBLE 4000SST	C1/X2
TRIMBLE 4700	C1/P2
TRIMBLE 5700	C1/P2
TRIMBLE MS750	C1/P2
TRIMBLE NETR5	C1/P2
TRIMBLE NETRS	C1/P2
TRIMBLE R7	C1/P2
TRIMBLE R8	C1/P2
TRSR	P1/P2
TTS-3	P1/P2
ZY12	P1/P2

APPENDIX B

FIRST PAGE OF A SAMPLE OUTPUT FILE FROM "EXTRACT TEC INFORMATION" FUNCTION

```
TECmapper OUTPUT FILE FOR STEC AND VTEC VALUES FOR THE FILE:
E:\TECmapper\07-269\ADAN2690.tec
                                  12-Aug-2009 14:59:59


DCB VALUE FOR THE RECEIVER (NS):  20.523
HEIGHT OF THE SINGLE LAYER (KM): 400.000

UNIT FOR ANGLES            : DECIMAL DEGREES

RECEIVER POSITION (WGS84)  :
     X (M): 4210749.3800  |  LATITUDE  :   36.8089
     Y (M): 2900149.9400  |  LONGITUDE :   34.5571
     Z (M): 3800531.1200  |  HEIGHT (M):  159.0034

YEAR/MONTH/DAY FOR THE FILE   : 2007/09/26
```

EPOCH INFO:			SLANT TEC INFORMATION:			VERTICAL TEC INFORMATION:			SAT
Hr.	Min	Sec	STEC(TECU)	Azimuth	Zenith	VTEC(TECU)	Latitude	Longitude	PRN
0	0	0	4.8370	41.7976	37.8668	3.9487	38.7175	36.7670	1
0	0	0	5.0237	265.9904	20.2030	4.7511	36.7122	33.0131	11
0	0	0	22.1492	44.5134	71.4989	9.9993	42.4998	42.4809	14
0	0	0	8.6662	313.7956	76.8262	3.4735	43.6104	24.1349	17
0	0	0	16.0939	197.4895	72.9215	7.0340	28.3406	31.5499	19
0	0	0	4.1795	299.7835	47.4738	3.0114	38.5178	30.5948	20
0	0	0	6.0930	229.9823	60.3119	3.5099	33.1746	29.5395	23
0	0	0	7.1178	98.5047	48.4837	5.0513	36.1769	39.0820	31
0	0	0	8.4718	73.4142	61.2472	4.7888	38.2278	41.4773	32
0	0	30	4.8616	41.7742	38.0887	3.9589	38.7329	36.7836	1
0	0	30	5.0317	265.3149	20.1519	4.7600	36.6979	33.0190	11
0	0	30	22.1982	44.5608	71.6928	9.9772	42.5373	42.5552	14
0	0	30	8.6720	313.6093	76.7461	3.4817	43.5611	24.1478	17
0	0	30	16.1097	197.3894	73.1167	7.0098	28.2669	31.5444	19
0	0	30	4.1926	299.9996	47.3157	3.0279	38.5212	30.6237	20
0	0	30	6.0456	230.1355	60.1175	3.4961	33.2105	29.5601	23

APPENDIX C

SAMPLE ERROR WINDOWS GENERATED BY "IONOSPHERE MODELING" FUNCTION

(a)

(b)

(c)
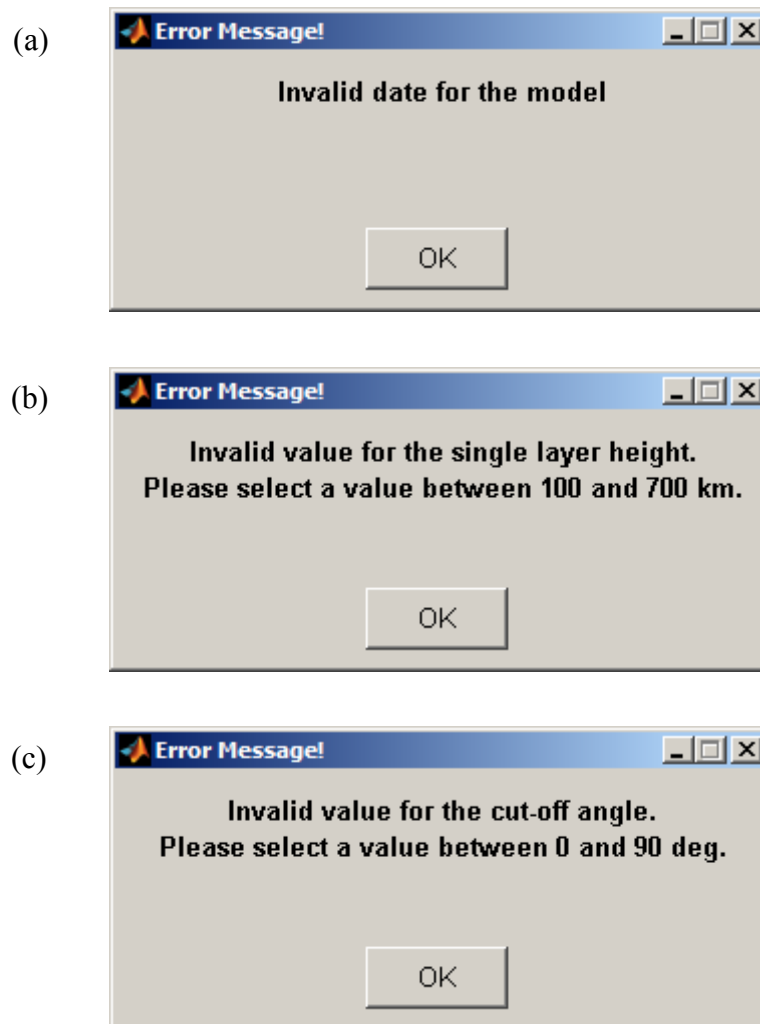
Figure C.1: Error windows generated by "Ionosphere Modeling" function

(d)

Error Message!

Invalid latitude value.
Please select a value between -90 and 90 deg.

OK

(e)

Error Message!

Invalid latitude values.
Max. latitude value should be greater than min.
latitude value.

OK

(f)

Error Message!

Invalid longitude value.
Please select a value between -180 and 180 deg

OK

(g)

Error Message!

Invalid longitude values.
Max. longitude value should be greater than
min. longitude value.

OK

Figure C.1: *Continued*

(h)

Error Message!

**Invalid time values.
Map epochs should be within boundary values
for time.**

OK

(i)

Error Message!

Missing level value for 2D B-Splines

OK

(k)

Error Message!

**Invalid level value for 2D B-Splines.
Level values should be integers greater than
zero.**

OK

(l)

Error Message!

**Maximum order cannot be greater than
maximum degree for Spherical Harmonics**

OK

Figure C.1: *Continued*

APPENDIX D

SAMPLE OUTPUT FILE FOR P1-P2 DCB SOLUTIONS OF "IONOSPHERE MODELING" FUNCTION

```
TECmapper OUTPUT FILE FOR P1-P2 DIFFERENTIAL CODE BIAS SOLUTIONS
                                          02-Aug-2009 03:46:24

DATE FOR THE MODEL: 26/09/2007


RECEIVER                  DCB(ns)      RMS(ns)
----------                --------     --------
ADAN2690                   20.4498      0.0005
AFYN2690                   25.9160      0.0005
AGRI2690                   -7.8138      0.0004
ANKR2690                    0.9395      0.0004
ANTL2690                   20.7004      0.0005
BART2690                  -11.4910      0.0005
BDRM2690                   -3.1950      0.0006
BURS2690                   -0.4362      0.0005
CALT2690                   19.6380      0.0006
ELZT2690                   18.4904      0.0005
ERZI2690                  999.9999    999.9999
ERZU2690                    1.0519      0.0009
GAZT2690                   18.4735      0.0006
HOPA2690                    4.3603      0.0005
ISTC2690                   15.6656      0.0005
IZMR2690                   -4.6063      0.0005
KART2690                   -2.5964      0.0005
KRDT2690                  -13.8676      0.0005
KTHY2690                   -5.4898      0.0005
KYSR2690                   -3.3266      0.0005
MRDN2690                    0.3120      0.0005
SMSN2690                   -1.2377      0.0005
TOKT2690                  -18.1992      0.0004
TRBZ2690                    9.7482      0.0004
TYF12690                   -9.6815      0.0005
VANN2690                    2.8004      0.0004


999.9999: There are no observations for the receiver within
modeling period.DCB value for the receiver could not be computed.
```
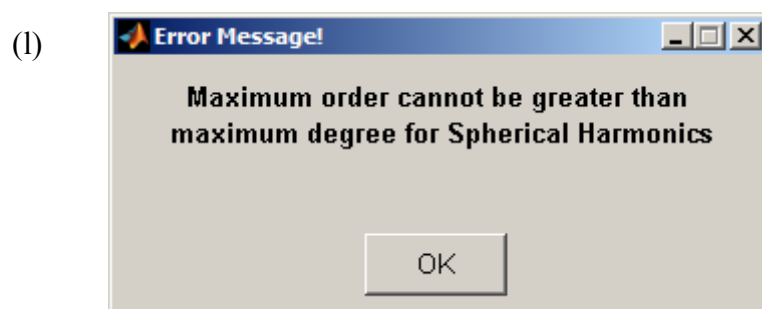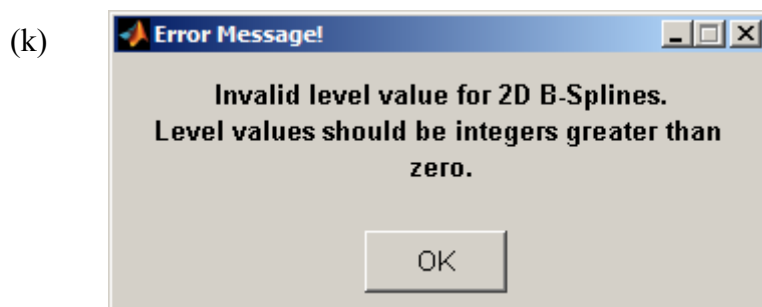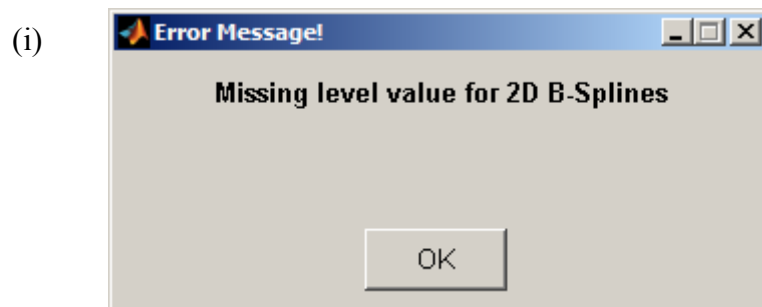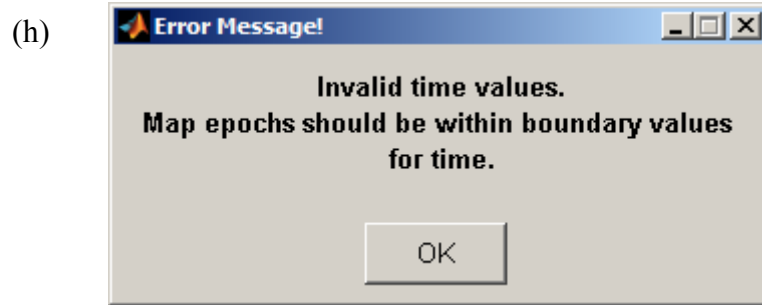
APPENDIX E

FIRST PAGE OF A SAMPLE OUTPUT FILE FOR VTEC VALUES AT SPECIFIED GRID POINTS OF "IONOSPHERE MODELING" FUNCTION

```
TECmapper OUTPUT FILE FOR VTEC VALUES AT SPECIFIED GRID POINTS
                                      03-Aug-2009 13:26:33

METHOD FOR THE MODEL                  : 2D B-SPLINES
     LEVEL FOR LATITUDE               : 2
     LEVEL FOR LONGITUDE              : 2

DATE FOR THE MODEL                    : 26/09/2007
SINGLE LAYER HEIGHT (KM)              : 400
BOUNDARY VALUES FOR LATITUDE (DEG)    : 35, 43
BOUNDARY VALUES FOR LONGITUDE (DEG)   : 25, 46
GRID INTERVAL FOR LATITUDE (DEG)      : 1
GRID INTERVAL FOR LONGITUDE (DEG)     : 1
VTEC VALUES ARE GIVEN FOR EPOCHS (HR:MIN:SEC): 09:30:00 (UT)
                                               09:50:00 (UT)
                                               10:10:00 (UT)
```

LONGITUDE (DEG)	LATITUDE (DEG)	VTEC (TECU) AT 09:30:00	VTEC (TECU) AT 09:50:00	VTEC (TECU) AT 10:10:00
25.00	35.00	12.4401	11.4755	11.6268
25.00	36.00	11.0356	11.0698	11.6945
25.00	37.00	10.3688	10.6385	11.1123
25.00	38.00	10.0124	10.1943	10.3282
25.00	39.00	9.5391	9.7500	9.7906
25.00	40.00	8.8859	9.1673	9.3031
25.00	41.00	7.9901	8.3074	8.6694
25.00	42.00	7.2759	7.5596	8.0501
25.00	43.00	7.1678	7.3127	7.6060
26.00	35.00	12.1300	11.4583	11.6749
26.00	36.00	10.9659	11.1914	11.7684
26.00	37.00	10.3905	10.7407	11.1654
26.00	38.00	10.0521	10.2257	10.3471

APPENDIX F

DATA FOR THE STATIONS USED IN THE STUDY

Table F.1: The receiver types, receiver classes and approximate geodetic coordinates for the stations that are used in the study

Station	Receiver Type	Receiver Class	Geodetic Longitude (deg)	Geodetic Latitude (deg)
ADAN	ASHTECH UZ-12	P1/P2	34.557094	36.808911
AFYN	ASHTECH UZ-12	P1/P2	30.534851	38.808991
AGRI	ASHTECH UZ-12	P1/P2	43.056290	39.719132
ANKA	SEPT POLARX2	P1/P2	32.783726	39.891099
ANTL	ASHTECH UZ-12	P1/P2	30.525661	36.866539
BART	ASHTECH UZ-12	P1/P2	32.359043	41.643751
BDRM	ASHTECH UZ-12	P1/P2	27.257310	37.010205
BURS	ASHTECH UZ-12	P1/P2	29.510074	40.078492
CALT	TRIMBLE NETRS	C1/P2	29.404315	37.991293
ELZT	TRIMBLE NETRS	C1/P2	39.197675	38.687400
ERZI	ASHTECH UZ-12	P1/P2	39.506341	39.745319
ERZU	TPS ODYSSEY_E	P1/P2	41.371395	40.004553
GAZT	TRIMBLE NETRS	C1/P2	37.309321	37.041263
HOPA	ASHTECH UZ-12	P1/P2	41.411394	41.386653
ISTC	ASHTECH UZ-12	P1/P2	29.007584	41.052961
IZMR	ASHTECH UZ-12	P1/P2	27.252227	38.472641
KART	TRIMBLE 4000SSI	C1/X2	28.332572	40.265270
KRDT	TRIMBLE 4000SSI	C1/X2	26.998514	40.950741
KYSR	ASHTECH UZ-12	P1/P2	35.475162	38.722213
KONY	ASHTECH UZ-12	P1/P2	32.484180	37.878651
KTHY	TPS ODYSSEY_E	P1/P2	30.001231	39.426257
MRDN	ASHTECH UZ-12	P1/P2	40.719221	37.324298
SMSN	ASHTECH UZ-12	P1/P2	35.665313	40.968750
TOKT	ASHTECH UZ-12	P1/P2	37.418371	40.440953
TRBZ	ASHTECH UZ-12	P1/P2	39.727044	40.999412
TYF1	TRIMBLE 4000SSI	C1/X2	26.485685	40.384083
VANN	ASHTECH UZ-12	P1/P2	43.395754	38.502698

APPENDIX G

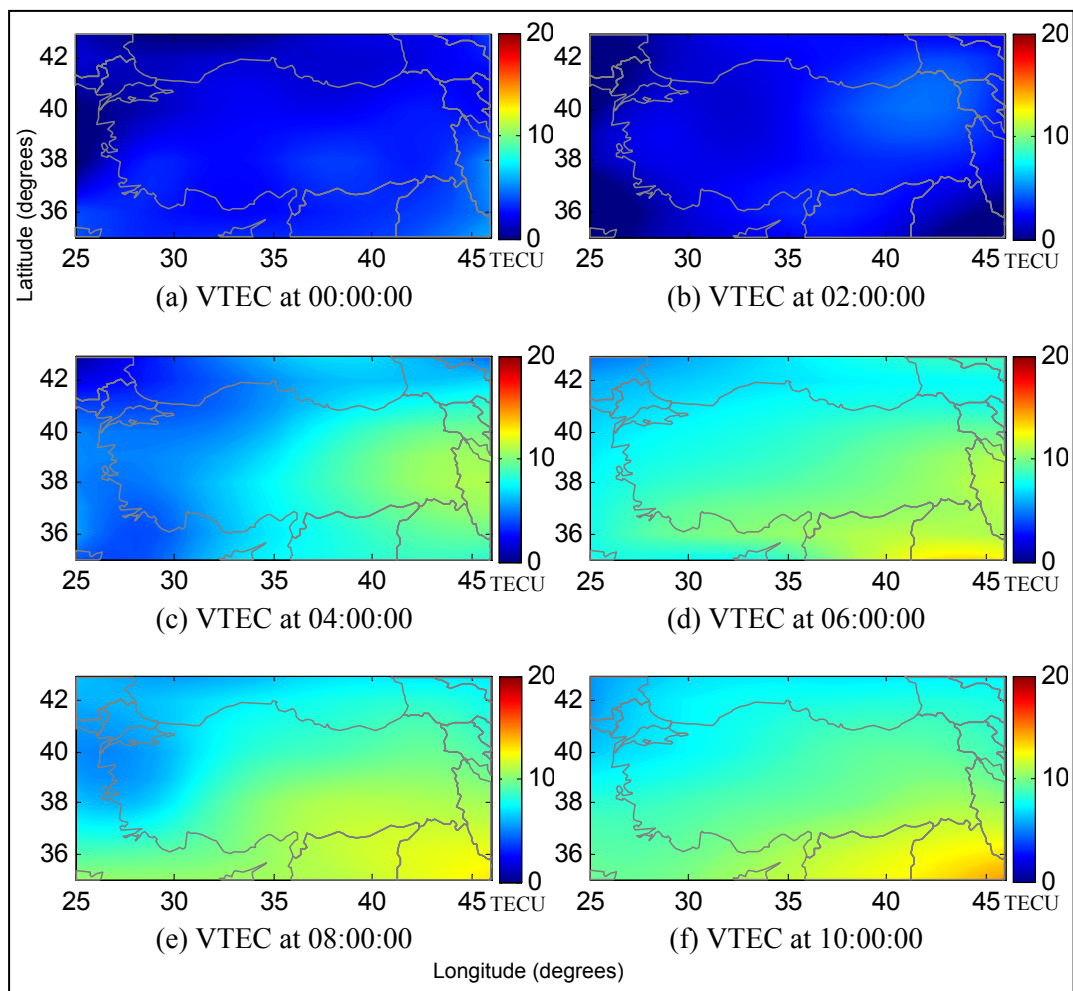# VTEC MAPS OVER TURKEY FOR 26.09.2007

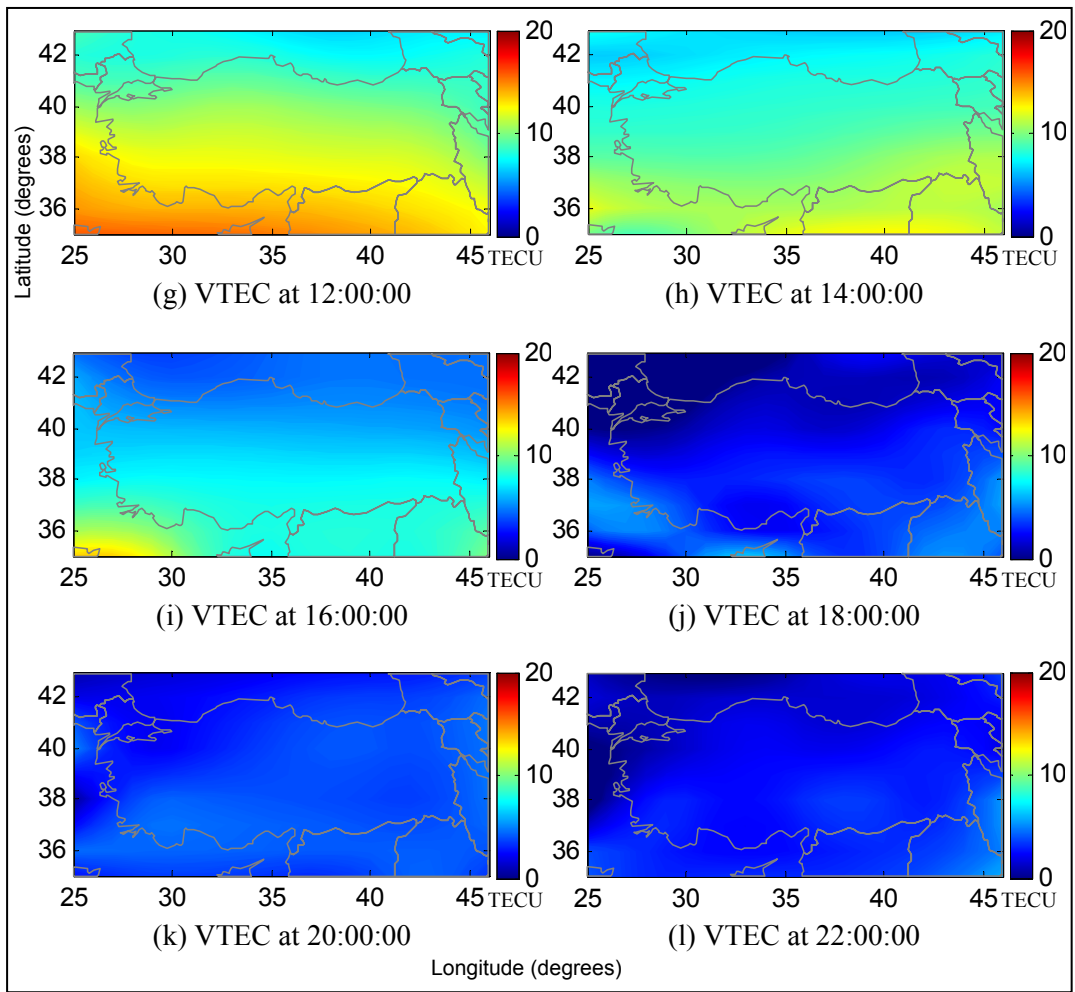**Figure G.1:** VTEC maps over Turkey for 26.09.2007 at every 2 hours

Figure G.1: *Continued*

CURRICULUM VITAE

PERSONAL INFORMATION

Surname, Name: Nohutcu, Metin
Nationality: Turkish (TC)
Date and Place of Birth: 25 July 1976 , Konya
Marital Status: Married
Phone: +90 312 210 54 72
email: metinnohutcu@hotmail.com

EDUCATION

Degree	Institution	Year of Graduation
MS	METU Civil Engineering	2002
BS	METU Civil Engineering	1999
High School	Konya Meram Anatolian High School	1994

WORK EXPERIENCE

Year	Place	Enrollment
1999-2006	METU Department of Civil Eng.	Research Assistant

FOREIGN LANGUAGES

Advanced English

PUBLICATIONS

Nohutcu M, Karslioglu M.O., and Schmidt M.: B-Spline modeling of VTEC over Turkey using GPS observations. *Submitted.*

Karslioglu M. O., Nohutcu M., Gucluer B., Schmidt M., and Zhang Z. (2008): Local modeling of VTEC using GPS observations and B-spline expansions. Poster

presented at: EGU General Assembly, Vienna, Austria, 13-18 April 2008, EGU2008-A-06750.

Nohutcu M., Karslioglu M. O., Gucluer B., Schmidt M., Zeilhofer C., Zhang Z., and Ergintav S. (2008): Local modeling of VTEC using GPS observations. In: Proceedings of the TUJK Annual Scientific Meeting 2007, Monitoring and Modeling of the Ionosphere and Troposphere, 14-16 November 2007, Ankara, Turkey, pp. 33-37.

Yıldız E., Merzi N., and Nohutcu M. (2004): Estimation of Reliability of Water Distribution Networks. 6th International Congress on Advances in Civil Engineering, 6-8 October 2004, Bogazici University, Istanbul, Turkey.

Nohutcu M., Merzi N. and Yıldız E. (2004): A methodology for estimation of reliability of water distribution networks. In: Proceedings of the IMO XVII. Technical Congress, 15-17 April 2004, İstanbul, Turkey, pp. 290-294, (in Turkish).

Merzi N., Nohutcu M., and Yıldız E. (2003): Reliability of Water Distrbution Networks. In: Proceedings of the IWRA XI. World Water Congress, October 2003, Spain.